

**APPLICATIONS OF *STREPTOMYCES* SPP. FOR
SYNTHESIS OF NANOMATERIALS**



**A Thesis Submitted in Partial Fulfillment of the Requirements for the
Degree of Doctor of Philosophy in Biomedical Sciences**

Suranaree University of Technology

Academic Year 2020

การประยุกต์ใช้ *Streptomyces* spp. สำหรับการสังเคราะห์วัสดุนาโน



นางสาวอริยาเทอ โรชิตาห์

วิทยานิพนธ์นี้เป็นส่วนหนึ่งของการศึกษาตามหลักสูตรปริญญาวิทยาศาสตรดุษฎีบัณฑิต

สาขาวิชาชีวเวชศาสตร์

มหาวิทยาลัยเทคโนโลยีสุรนารี

ปีการศึกษา 2563

**APPLICATIONS OF *STRETOMYCES* SPP. FOR SYNTHESIS
OF NANOMATERIALS**

Suranaree University of Technology has approved this thesis submitted in partial fulfillment of the requirements for the Degree of Doctor of Philosophy.

Thesis Examining Committee

Wanwisa Limphirat
(Dr. Wanwisa Limphirat)

Chairperson

[Signature]
(Asst. Prof. Dr. Nawarat Nantapong)

Member (Thesis Advisor)

[Signature]
(Assoc. Prof. Dr. Nuannoi Chudapongse)

Member (Thesis Co-Advisor)

Oratai Weeranantanapan
(Dr. Oratai Weeranantanapan)

Member (Thesis Co-Advisor)

[Signature]
(Asst. Prof. Dr. Duangkamol Maensiri)

Member

[Signature]
(Assoc. Prof. Flt. Lt. Dr. Kontorn Chamniprasart)

Vice Rector for Academic Affairs
and Internationalization

[Signature]
(Assoc. Prof. Dr. Worawat Meevasana)

Dean of Institute of Science

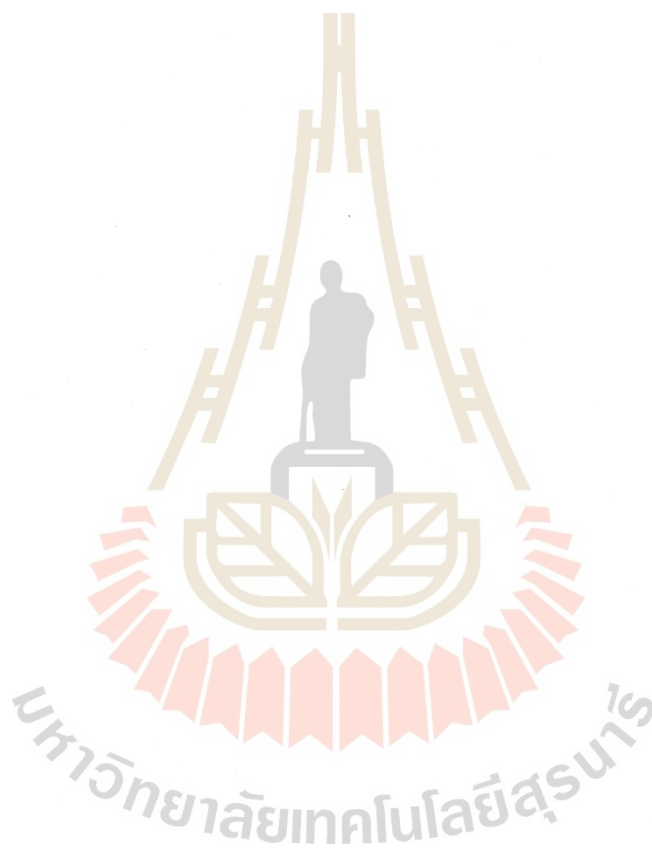
อารียาเทอ โรจีดาห์ : การประยุกต์ใช้ *Streptomyces* spp. สำหรับการสังเคราะห์วัสดุนาโน (APPLICATIONS OF *STREPTOMYCES* SPP. FOR SYNTHESIS OF NANOMATERIALS) อาจารย์ที่ปรึกษา : ผู้ช่วยศาสตราจารย์ ดร.นวรรตน์ นันทพงษ์, 128 หน้า.

Streptomyces เป็นแหล่งของสารต้านจุลชีพ การสังเคราะห์วัสดุนาโนโดยใช้ *Streptomyces* อาจช่วยเพิ่มคุณสมบัติในการต้านจุลชีพของวัสดุนาโนซึ่งสามารถนำไปประยุกต์ใช้ในทางการแพทย์ได้ ในการศึกษานี้ได้ใช้ *Streptomyces* ที่แยกจากดิน 2 สายพันธุ์คือ SSUT88A และ PJ95 ในการสังเคราะห์วัสดุนาโน ยีน 16s rRNA ซึ่งให้เห็นว่า SSUT88A และ PJ95 คือ *Streptomyces chiangmaiensis* TA4-1^T และ *Streptomyces luteosporus* NBRC14657^T ตามลำดับ

Intracellular cell-free supernatant และ extracellular cell-free supernatant ของเชื้อ *Streptomyces* sp. SSUT88A ถูกนำมาใช้ในการสังเคราะห์ AgNPs โดยกำหนดให้เรียก AgNPs ที่สังเคราะห์ขึ้นจาก intracellular cell-free supernatant และ extracellular cell-free supernatant ว่า IS-AgNPs และ ES-AgNPs ตามลำดับ การวิเคราะห์โดยใช้เทคนิค UV-Vis spectroscopy XRD TEM XAS และ EDXRF ใช้ในการยืนยันว่าการผลิต AgNPs ประสบความสำเร็จ และการวิเคราะห์ FTIR แสดงให้เห็นว่าโปรตีนที่เป็นองค์ประกอบของ Intracellular cell-free supernatant และ extracellular cell-free supernatant มีส่วนร่วมในการสังเคราะห์ AgNPs IS-AgNPs แสดงฤทธิ์ต้านจุลชีพต่อเชื้อดื้อยาหลายชนิด คือ *Acinetobacter baumannii* *Klebsiella pneumoniae* 1617 *Pseudomonas aeruginosa* N90PS *Escherichia coli* 8465 และ methicillin-resistant *Staphylococcus aureus* (MRSA) DMST 20654 ส่วน ES-AgNPs จะแสดงฤทธิ์ต้านจุลชีพต่อเชื้อ MRSA DMST 20654 เท่านั้น

เส้นใยนาโนอิเล็กทรอนิกส์ถูกประดิษฐ์ขึ้นโดยใช้พอลิเมอร์ PVDF-HFP 13% ผสมกับสารสกัดหยาบของเชื้อ *Streptomyces* sp. PJ95 ภาพจากกล้องจุลทรรศน์อิเล็กตรอนแบบส่องกราด (SEM) แสดงให้เห็นว่าสัณฐานวิทยาของเส้นใยนาโนอิเล็กทรอนิกส์ที่ประดิษฐ์ขึ้นนั้นมีลักษณะเรียบและไม่เป็นลูกบิด โดยสามารถตรวจพบการมีอยู่ของสารสกัดหยาบจากเชื้อ PJ95 บนเส้นใยนาโนที่บรรจุสารสกัดหยาบด้วยเทคนิค FTIR เส้นใยนาโน PVDF-HFP ที่บรรจุสารสกัดหยาบแสดงฤทธิ์ต้านจุลชีพต่อเชื้อก่อโรคที่ผิวหนัง *S. aureus* TISTR 1466 *Staphylococcus epidermidis* TISTR 518 MRSA DMST 20654 และ *Proteus mirabilis* TISTR 100 และการทดสอบความเป็นพิษต่อเซลล์โดยอ้อมพบว่าเส้นใยนาโน PVDF-HFP ที่บรรจุสารสกัด

หยาบมีความเข้ากันได้ทางชีวภาพกับเซลล์ไฟโบรบลาสต์และสามารถนำไปประยุกต์ใช้เป็น
ผ้าปิดแผล



สาขาวิชาปรีคลินิก

ปีการศึกษา 2563

ลายมือชื่อนักศึกษา

Thian

ลายมือชื่ออาจารย์ที่ปรึกษา

[Signature]

ลายมือชื่ออาจารย์ที่ปรึกษาร่วม

26h

ลายมือชื่ออาจารย์ที่ปรึกษาร่วม

Oratai Weeramanantapan

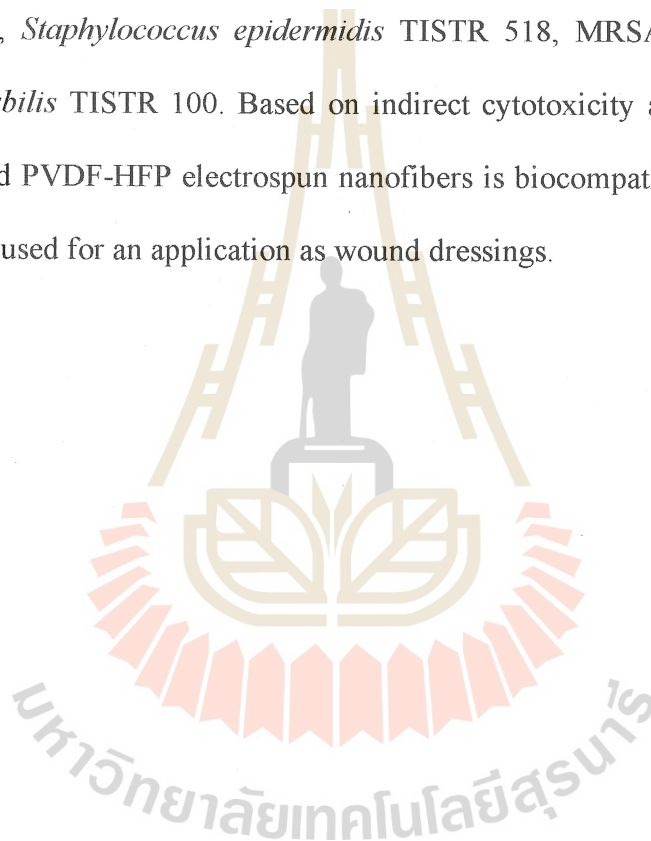
ALIYATUR ROSYIDAH : APPLICATIONS OF *STREPTOMYCES* SPP.
FOR SYNTHESIS OF NANOMATERIALS. THESIS ADVISOR : ASST.
PROF. NAWARAT NANTAPONG, Ph.D. 128 PP.

AgNPs/ANTIMICROBIAL ACTIVITY/ ELECTROSPUN/ NANOFIBERS/
STREPTOMYCES

Streptomyces are known as a source of antimicrobial agents. A synthesis of nanomaterials by using *Streptomyces* may enhance an antimicrobial property of nanomaterials which can be applied for medical uses. In this study, two strains of soil isolate *Streptomyces*, SSUT88A and PJ95, were used for synthesis of nanomaterials. The 16s rRNA gene suggested that SSUT88A and PJ95 were *Streptomyces chiangmaiensis* TA4-1^T and *Streptomyces luteosporeus* NBRC14657^T, respectively.

The intracellular and extracellular cell-free supernatant of *Streptomyces* sp. SSUT88A were used to synthesize silver nanoparticle (AgNPs). The synthesized AgNPs from intracellular and extracellular cell-free supernatant were designated as IS-AgNPs and ES-AgNPs, respectively. The production of AgNPs was successful, as confirmed by UV-Vis spectroscopy, XRD, TEM, XAS, and EDXRF technique. The FTIR analysis revealed an involvement of proteins makeup of cell-free supernatant to the formation of AgNPs. The IS-AgNPs showed antimicrobial activity against several drugs-resistant bacteria, *Acinetobacter baumannii*, *Klebsiella pneumoniae* 1617, *Pseudomonas aeruginosa* N90PS, *Escherichia coli* 8465, and Methicillin-resistant *Staphylococcus aureus* (MRSA) DMST 20654, while the ES-AgNPs was active against MRSA DMST 20654 only.

The electrospun nanofibers were fabricated by using 13% PVDF-HFP polymer incorporated with crude extract of *Streptomyces* sp. PJ95. The SEM revealed that the morphology of the electrospun nanofibers was smooth and bead-free. The presence of crude extract components was detected on PJ95 crude extract-loaded PVDF-HFP nanofibers by using FTIR analysis. The PJ95 crude extract-loaded PVDF-HFP nanofibers showed antimicrobial activity against skin infection pathogens, *S. aureus* TISTR 1466, *Staphylococcus epidermidis* TISTR 518, MRSA DMST 20654, and *Proteus mirabilis* TISTR 100. Based on indirect cytotoxicity assay, the PJ95 crude extract-loaded PVDF-HFP electrospun nanofibers is biocompatible to fibroblast cells and could be used for an application as wound dressings.



School of Preclinic

Academic Year 2020

Student's Signature OrataniAdvisor's Signature [Signature]Co-Advisor's Signature 262Co-Advisor's Signature Oratani Neerananantamajany

ACKNOWLEDGEMENTS

The completion of this thesis could not have been possible without any support and assistance from many people. I want to express my deeply grateful to my advisor, Asst. Prof. Dr. Nawarat Nantapong for the support, guidance, patience, motivation, and immense knowledge. She guided and encouraged me to be a professional student and researcher. I would also like to express my sincere gratitude to my co-advisor, Assoc. Prof. Dr. Nuannoi Chudapongse and Dr. Oratai Weeranantanapan for helping me in all the time of research and writing of this thesis. I could not have imagined having better advisors and mentors for my Ph.D. study. Without their help, the goal of this research would not have been realized. My sincere thanks also go to my thesis committee, Dr. Wanwisa Limphirat and Asst. Prof. Dr. Duangkamol Maensiri for their kindness, encouragement, and suggestion for improving this thesis research.

I am grateful to the SUT-Ph.D Scholarship Program for ASEAN for the financial support of this research and study. And I want to thank the Synchrotron Light Research Institute for the contribution towards the development of this research.

Also, I would like to thanks to my husband Rifana Sobari, my daughter Reashira Aulia Sobari, my parents, my sisters, and my brothers, for their support and unconditional love.

Finally, my thanks go to my lab-mates: Panjamaphon Chanthasena, Supavadee Kerdtoob, Phongsakorn Ganta, Napatsorn Santapan, Wannika Pana, Kenta Wakui,

Hiroyuki Wakui and Jenjuiree Mahittikon for the great discussion and all the fun time we had in the last three years.

Aliyatur Rosyidah



CONTENTS

	Page
ABSTRACT IN THAI.....	I
ABSTRACT IN ENGLISH	III
ACKNOWLEDGEMENTS.....	V
CONTENTS.....	VII
LIST OF TABLES.....	XII
LIST OF FIGURES	XIII
LIST OF ABBREVIATIONS.....	XV
CHAPTER	
I INTRODUCTION.....	1
1.1 Background/Problem	1
1.2 Research objectives.....	4
1.3 Research hypothesis.....	5
1.4 Scope and limitation of the study.....	5
1.5 References.....	6
II BIOSYNTHESIS OF SILVER NANOPARTICLES FROM	
<i>STREPTOMYCES</i> sp. SSUT88A	11
2.1 Introduction.....	11
2.2 Literature review	13

CONTENTS (Continued)

	Page
2.2.1 <i>Streptomyces</i> sp. and their secondary metabolite	13
2.2.2 Synthesis of silver nanoparticles (AgNPs)	16
2.2.3 Antimicrobial and cytotoxicity mechanism of silver nanoparticles	22
2.3 Research methodology	24
2.3.1 Isolation and purification of <i>Streptomyces</i>	24
2.3.2 Identification of <i>Streptomyces</i> based on 16s rRNA gene sequence	25
2.3.3 Preparation of cell-free extract	26
2.3.4 Biosynthesis of silver nanoparticle	27
2.3.5 Characterization of silver nanoparticle	27
2.3.5.1 Ultraviolet-visible (UV-Vis) spectrophotometry	27
2.3.5.2 Determination of particle size and zeta potential	27
2.3.5.3 X-ray diffraction (XRD) evaluation	28
2.3.5.4 Fourier-Transform Infrared (FTIR)	28
2.3.5.5 X-ray absorption spectroscopy (XAS) analysis	28
2.3.5.6 Transmission electron microscopy (TEM) and energy dispersive X-ray fluorescence (EDXRF) analysis	29
2.3.6 Antimicrobial activity assay	29
2.3.7 Cytotoxicity assay	30

CONTENTS (Continued)

	Page
2.3.8 Statistical analysis.....	30
2.4 Results.....	31
2.4.1 Identification of <i>Streptomyces</i> SSUT88A.....	31
2.4.2 Biosynthesis of AgNPs and UV-Vis spectroscopy analysis.....	33
2.4.3 Particle size and zeta potential analysis of synthesized AgNPs.	36
2.4.4 XRD analysis of synthesized AgNPs.....	38
2.4.5 FT-IR analysis of synthesized AgNPs	39
2.4.6 XAS analysis of synthesized AgNPs	41
2.4.7 TEM and EDXRF analysis of synthesized AgNPs.....	42
2.4.8 Antimicrobial activity of AgNPs	44
2.4.9 Cytotoxicity assay of synthesized AgNPs	45
2.5 Discussion.....	46
2.6 References.....	60
III SYNTHESIS OF <i>STREPTOMYCES</i> SP. PJ95 CRUDE EXTRACT- LOADED PVDF-HFP ELECTROSPUN NANOFIBERS	80
3.1 Introduction.....	80
3.2 Literature review	83
3.2.1 Electrospun nanofibers.....	83
3.2.2 Polymers of electrospun nanofibers.....	85
3.2.3 Antimicrobial activity of electrospun nanofibers	86
3.3 Research methodology	87

CONTENTS (Continued)

	Page
3.3.1 Preparation of crude extract of <i>Streptomyces</i> sp PJ95.....	87
3.3.2 Synthesis of PJ95 crude extract-loaded PVDF-HFP electrospun nanofibers	87
3.3.3 Characterization of PJ95 crude extract-loaded PVDF-HFP electrospun nanofibers	88
3.3.3.1 Scanning electron microscopy (SEM) analysis	88
3.3.3.2 Fourier-transform infrared (FTIR)	88
3.3.3.3 Crude extract release study	89
3.3.4 Antimicrobial activity assay	89
3.3.5 Cytotoxicity assay	90
3.3.6 Statistical analysis	90
3.4 Results.....	91
3.4.1 Surface morphology and diameter distribution of electrospun nanofibers.....	91
3.4.2 Chemical composition of crosslinked electrospun nanofibers....	92
3.4.3 Crude extract release study	93
3.4.4 Antimicrobial activity analysis	94
3.4.5 Indirect cytotoxicity analysis	95
3.5 Discussions	96
3.6 References.....	101
IV CONCLUSION	109

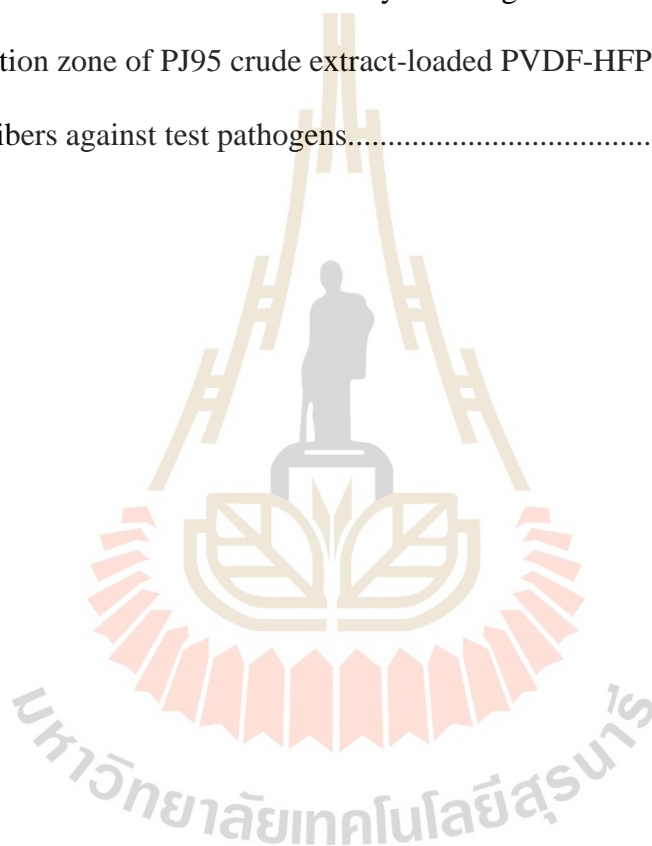
CONTENTS (Continued)

	Page
APPENDIX.....	111
CURRICULUM VITAE.....	128



LIST OF TABLES

Table	Page
2.1 Taxonomy of Actinomycetes	14
2.2 Comparison of antimicrobial activity of IS-AgNPs and ES-AgNPs	45
3.1 Inhibition zone of PJ95 crude extract-loaded PVDF-HFP electrospun nanofibers against test pathogens.....	95



LIST OF FIGURES

Figure	Page
2.1 Antibiotics that produced by Actinomycetes.....	16
2.2 Mechanism of AgNPs synthesis by bacteria mediated via NADH- dependent reductase enzyme.....	20
2.3 Mechanism of antimicrobial action of silver nanoparticles.....	23
2.4 Colony morphology of <i>Streptomyces</i> sp. SSUT88A on ISP2 media.....	31
2.5 Neighbor-joining tree of <i>Streptomyces</i> sp. SSUT88A and closely related species based on 16s rRNA gene sequence.	33
2.6 Visible observation of biosynthesis IS-AgNPs by <i>Streptomyces</i> sp. SSUT88A.....	34
2.7 Visible observation of biosynthesis ES-AgNPs by <i>Streptomyces</i> sp. SSUT88A.	35
2.8 UV-Vis spectra of IS-AgNPs and ES-AgNPs.	36
2.9 The particle size distribution from DLS measurement. (a) IS-AgNPs and (b) ES-AgNPs.....	37
2.10 Zeta potential of (a) IS-AgNPs and (b) ES-AgNPs.	38
2.11 X-ray diffraction pattern of IS-AgNPs.	39
2.12 X-ray diffraction pattern of ES-AgNPs.	39
2.13 FTIR spectra of IS-AgNPs and cell-free supernatant of <i>Streptomyces</i> sp. SUT88A.	40

LIST OF FIGURES (Continued)

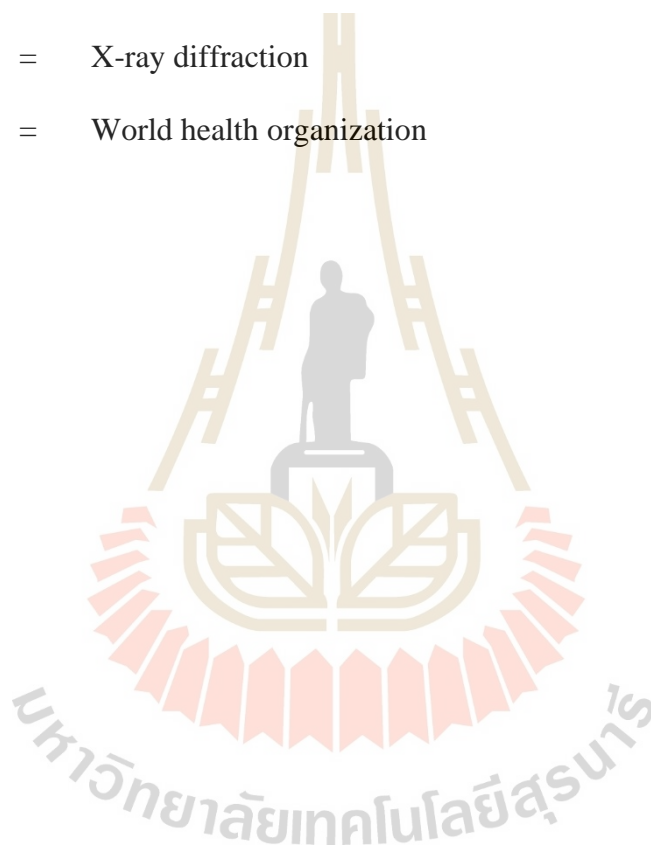
Figure	Page
2.14 FTIR spectra of ES-AgNPs and cell-free supernatant of <i>Streptomyces</i> sp. SUT88A.	41
2.15 XANES spectra of AgNO ₃ , Ag nanopowder, IS-AgNPs and ES-AgNPs.	42
2.16 Morphology and size distribution of the synthesized AgNPs based on TEM imaging.	43
2.17 Energy dispersive spectra of AgNPs obtained from <i>Streptomyces</i> sp. SSUT88A.	44
2.18 Cell viability of NIH-3T3 cell line after treated with AgNPs.	46
3.1 Schematic diagram of the basic setup of electrospinning.	85
3.2 Illustration of electrospun nanofibers fabrication.	88
3.3 The morphology of PVDF-HFP nanofibers and PJ95 crude extract-loaded PVDF-HFP nanofibers.	91
3.4 FTIR spectra of neat PVDF-HFP electrospun nanofibers compared to the PJ95 crude extract-loaded PVDF-HFP electrospun nanofibers.	93
3.6 The cell viability of NIH-3T3 cell lines after treated with PJ95 crude extract-loaded PVDF-HFP electrospun nanofibers in comparison with neat PVDF-HFP.	96

LIST OF ABBREVIATIONS

AgNPs	=	Silver nanoparticles
AIA	=	Actinomycetes isolation agar
CFU	=	Colony forming unit
DI water	=	Deionized water
DLS	=	Dynamic light scattering
DMF	=	Dimethyl foramide
DNA	=	Deoxyribose nucleic acid
EDXRF	=	Energy dispersive X-ray fluorescent
FTIR	=	Fourier transform infra-red
ISP2	=	International <i>Streptomyces</i> Project 2
MDR	=	Multi-drug resistant
MHA	=	Mueller hinton agar
MRSA	=	Methicillin-resistant <i>Staphylococcus aureus</i>
MTT	=	(3-(4,5-Dimethylthiazol-2-yl)-2,5-Diphenyltetrazolium Bromide
PCR	=	Polymerase chain reaction
PVDF-HFP	=	Poly (vinylidene fluoride-co-hexafluoropropylene)
rRNA	=	Ribosomal ribonucleic acid
ROS	=	Reactive oxygen species
SEM	=	Scanning electron microscope
SPR	=	Surface plasmon resonance

LIST OF ABBREVIATIONS (Continued)

TEM	=	Transmission electron microscope
UV-Vis	=	Ultraviolet-visible
VRE	=	Vancomycin-resistant <i>Enterococci</i>
XAS	=	X-ray spectroscopy
XRD	=	X-ray diffraction
WHO	=	World health organization



CHAPTER I

INTRODUCTION

1.1 Background/Problem

Bacterial infections remain a significant public health problem around the world, particularly bacteria that are caused by multidrug-resistant bacteria, so the treatment of antibiotics becomes less effective. The number of infected patients by antibiotic-resistant bacteria is also increasing each year, leading to the death caused by resistant bacterial infection (Michael et al., 2014; Thongkrachang et al., 2016). Nowadays, Methicillin-resistant *Staphylococcus aureus* (MRSA), Vancomycin-resistant *Enterococci* (VRE), *Pseudomonas aeruginosa*, *Acinetobacter baumannii*, and *Enterobacteriaceae* (mostly *Klebsiella pneumoniae*) posed the significant challenges in terms of antibiotic resistance (Rossolini et al., 2014). World Health Organization (WHO) issued a global priority pathogen list (PPL) for antibiotic-resistant bacteria, including *A. baumannii*, *P. aeruginosa*, *S. aureus*, *Enterobacteriaceae*, *Salmonella*, etc., to prioritize the development of new antibiotics (Tacconelli and Magrini, 2017). Therefore, the discovery of a new drug to combat bacterial infection is urgently needed (Panigrahi et al., 2011; Thongkrachang et al., 2016).

Actinomycetes are an essential source of antibiotics, especially the genus of *Streptomyces*. There are around 22500 antimicrobial compounds isolated from

microorganisms, which actinomycetes produce 45% of them (Berdy, 2005; Thongkrachang et al., 2016; Mahajan et al., 2015). Actinomycin was the first antibiotic isolated from *Streptomyces antibioticus* in early 1940. In 1942 and 1944, streptothricin and streptomycin were isolated from *Streptomyces lavendulae* and *Streptomyces griseus*, respectively (Barka et al., 2016; Okami and Hotta, 1988). Therefore, *Streptomyces* are still an exciting source to explore due to their potency to produce active substances against pathogenic bacteria.

The term nanotechnology means designing and making material whose purpose depends on the specific structure at the nanoscale, generally around 100 nm or less (Das et al., 2017). Currently, the application of nanotechnology was used not only in controlling the consumption of available antibiotics but also to combat antibiotic-resistant microorganisms. This technology offers an opportunity for the discovery of novel compounds with antimicrobial activity as well as the use of nanofunctionalization to restore an antimicrobial activity of existing antibiotics (Banin et al., 2017). Nanomaterials are increasingly making a significant impact on human health and are widely used in diagnostic and therapeutic applications (Das et al., 2017).

The most applied nanomaterials in the biomedical field are metal nanoparticles that achieve remarkable attention as novel antimicrobial agents. Several metal nanoparticles, such as silver, gold, zinc, and copper, are reported to be active against pathogenic bacteria and fungi (Bogdanovi et al., 2014; Folorunso et al., 2019; Naqvi et al., 2013; Xie et al., 2011). Silver nanoparticles (AgNPs) are progressively used in various fields due to their unique chemical and physical properties (Zhang et al., 2016). The size of AgNPs is around 1 to 100 nm that makes AgNPs different from bulk materials. The large surface area properties of AgNPs promotes the higher amount of

interaction between AgNPs and bacterial cells that leads to the increase of antibacterial activity (Franci et al., 2015; Liao et al., 2019). Generally, chemical and physical methods were used for the synthesis of AgNPs. However, these methods had several disadvantages, including expensive and hazardous. Currently, green synthesis of AgNPs is applied by using plants and microorganisms, including bacteria, algae, and fungi. Compared to the chemical and physical methods, the biological method is simple, non-toxic, rapid, produce well-defined size and morphology, and eco-friendly (Irvani et al., 2014). In the field of biological and biomedical applications, AgNPs have been used extensively as antibacterial, antifungal, antiviral, anti-inflammatory, anti-cancer, and anti-angiogenic agents (Zhang et al., 2016). Several AgNPs that synthesized by the biological method also have been used to treat multidrug-resistant (MDR) *A. baumannii*, such as AgNPs that synthesized from plant *Mukia scabrella*, bacteria *Xanthomonas* spp., fungi *Penicillium polonicum* and *Aspergillus flavus* (Barros et al., 2018).

Another widely used nanomaterial in the biomedical field is nanofibers prepared by electrospinning. These nanofibers have the potential to be candidates for the formulation of medical fabrics for wound dressing and exhibit several characteristics that provide novel replacement dressing material for wound healing. The electrospinning process is a simple and cost-effective method to produce a drug-containing fiber with small diameters and high surface area (Gizaw et al., 2018; Motealleh et al., 2014; Song et al., 2017). Although human skin is an effective barrier to pathogens, it could be broken by injury. The wound may be infected by any variety of potential pathogens capable of causing systemic or localized diseases (Singleton, 2004). Wound healing is a tissue regeneration process that involving the growth of new

tissue to replace the damage tissue and provide barrier from the outside environment, especially from the infection of pathogenic bacteria. To facilitate wound healing, a sterile dressing material is needed to avoid contamination and promote the healing process. Nowadays, non-healing wounds gels and creams that are used clinically demonstrate slow improvement on the wound (Gizaw et al., 2018). Therefore, it needs a wound dressing that provides wound healing activity with antimicrobial properties to avoid bacterial infections. Electrospun nanofibers not only offer physical protection to the wound but also have the capacity to be incorporated with drugs and can be adjusted the release rate by changing the types and composition of the materials (Chou and Woodrow, 2017). This study was focused on the application of soil isolated *Streptomyces* and used them to synthesize AgNPs and electrospun nanofibers.

1.2 Research objectives

The general purpose of this research was to isolate soil sample *Streptomyces* spp. and use them to synthesize AgNPs and electrospun nanofibers. In meeting its objectives, this research is keyed to two issues described as follow:

- a) To synthesize and characterize AgNPs by a green synthesis method using cell-free supernatant of *Streptomyces* sp. SSUT88A and evaluate their antimicrobial activity against drug-resistant bacteria.
- b) To synthesize and characterize PJ95 crude extract-loaded PVDF-HFP electrospun nanofibers and evaluate their cytotoxicity and antimicrobial activity against pathogenic bacteria.

1.3 Research hypothesis

The main hypothesis of the study was the AgNPs and electrospun nanofibers were successfully synthesized from *Streptomyces* spp. Furthermore, to study the application of *Streptomyces* spp. for the synthesis of AgNPs and electrospun nanofibers, the main hypothesis was divided into two sub-hypotheses, in which they were specified and studied independently as follows:

- a) The AgNPs are successfully synthesized using *Streptomyces* sp. SSUT88A. The synthesized AgNPs were characterized and show antimicrobial activity against clinical drug-resistant bacteria.
- b) The PJ95 crude extract-loaded PVDF-HFP electrospun nanofibers are successfully synthesized and characterized. The synthesized nanofibers show antimicrobial activities against test pathogens.

1.4 Scope and limitation of the study

To explore the application of *Streptomyces* spp. for the synthesis of nanomaterials, this work involves isolation and identification of *Streptomyces*. The *Streptomyces* sp. SSUT88A were isolated from soil sample by using dilution method. The isolated *Streptomyces* were identified based on 16s rRNA gene sequence and used for the synthesis of AgNPs. The synthesized AgNPs were characterized by using UV-Vis Spectrophotometer, TEM (transmission electron microscope), EDXRF (energy-dispersive X-ray fluorescent), FTIR (Fourier transform infrared spectroscopy), XANES (X-ray absorption near edge structure), XRD (X-ray diffraction), and zeta sizer. The synthesized AgNPs were tested for their antimicrobial activity against drug-resistant bacteria and their cytotoxicity to NIH-3T3 mouse fibroblast cell lines. The

electrospun nanofibers were fabricated by mixing PVDF-HFP and *Streptomyces* sp. PJ95 crude extract. The *Streptomyces* sp. PJ95 was obtained from the previous work, which revealed high similarity to *Streptomyces luteosporus* NBRC14657^T. The electrospun nanofibers were characterized using SEM (scanning electron microscope) and FTIR. A release profile of crude extract from the nanofibers were observed. The electrospun nanofibers were tested for their antimicrobial activity against skin infection pathogen bacteria and cytotoxicity to NIH-3T3 mouse fibroblast cell lines.

1.5 References

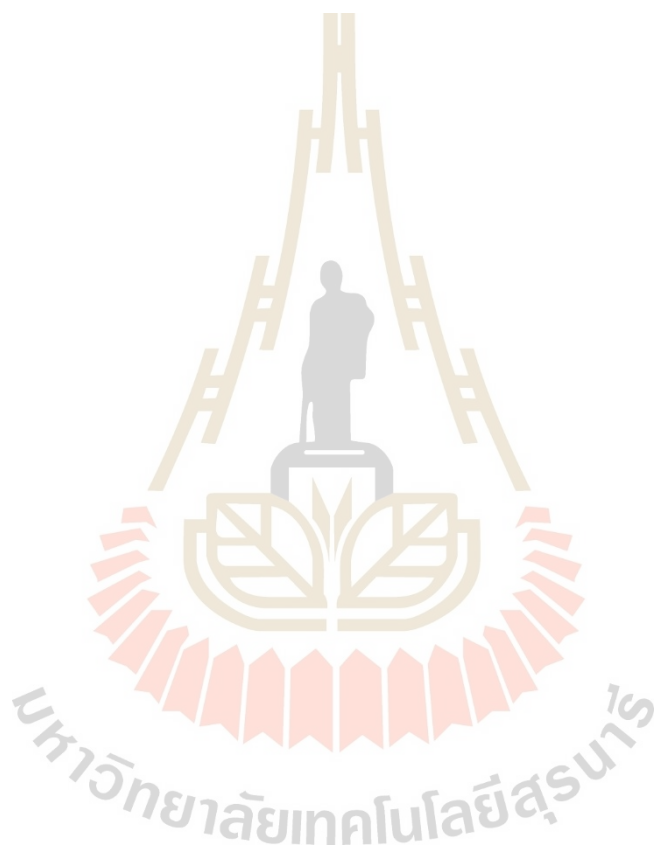
- Banin, E., Hughes, D., and Kuipers, O. P. (2017). Editorial: Bacterial pathogens, antibiotics, and antibiotic resistance. **FEMS Microbiology Reviews**. 41(3): 450–452. <https://doi.org/10.1093/femsre/fux016>.
- Barka, E. A., Vatsa, P., Sanchez, L., Nathalie Gaveau-Vaillant, C. J., Klenk, H.-P., Clément, C., Ouhdouch, Y., and P. van Wezeld, G. (2016). Taxonomy, Physiology, and natural product of Actinobacteria. **American Society for Microbiology**. 80(1): 1–43. <https://doi.org/10.1128/MMBR.00019-15>.
- Barros, C. H. N., Fulaz, S., Stanistic, D., and Tasic, L. (2018). Biogenic nanosilver against multidrug-resistant bacteria (MDRB). **Antibiotics**. 7(3): 1–24. <https://doi.org/10.3390/antibiotics7030069>.
- Berdy, J. (2005). Bioactive microbial metabolites a personal view. **The Journal of Antibiotics**. 58(1): 1–26.
- Bogdanovi, U., Lazi, V., Vodnik, V., Budimir, M., and Markovi, Z. (2014). Copper nanoparticles with high antimicrobial activity. **Material Letters**. 128: 75–78. <https://doi.org/10.1016/j.matlet.2014.04.106>.

- Chou, S. F., and Woodrow, K. A. (2017). Relationships between mechanical properties and drug release from electrospun fibers of PCL and PLGA blends. **Journal of the Mechanical Behavior of Biomedical Materials**. 65: 724–733. <https://doi.org/10.1016/j.jmbbm.2016.09.004>.
- Das, B., Dash, S. K., Mandal, D., Ghosh, T., Chattopadhyay, S., Tripathy, S., Das, S., Dey, S. K., Das, D., and Roy, S. (2017). Green synthesized silver nanoparticles destroy multidrug-resistant bacteria via reactive oxygen species-mediated membrane damage. **Arabian Journal of Chemistry**. 10(6): 862–876. <https://doi.org/10.1016/j.arabjc.2015.08.008>.
- Folorunso, A., Akintelu, S., Kolawole, A., Ajayi, S., and Abiola, B. (2019). Biosynthesis, characterization, and antimicrobial activity of gold nanoparticles from leaf extracts of *Annona muricata*. **Journal of Nanostructure in Chemistry**. 9(2): 121–127. <https://doi.org/10.1007/s40097-019-0301-1>.
- Franci, G., Falanga, A., Galdiero, S., Palomba, L., Rai, M., Morelli, G., and Galdiero, M. (2015). Silver nanoparticles as potential antibacterial agents. **Molecules**. 20(5): 8856–8874. <https://doi.org/10.3390/molecules20058856>.
- Gizaw, M., Thompson, J., Faglie, A., Lee, S. Y., Neuenschwander, P., and Chou, S. F. (2018). Electrospun fibers as a dressing material for drug and biological agent delivery in wound healing applications. **Bioengineering**. 5(1): 1–28. <https://doi.org/10.3390/bioengineering5010009>.
- Iravani, S., Korbekandi, H., Mirmohammadi, S. V., and Zolfaghari, B. (2014). Synthesis of silver nanoparticles: Chemical, physical and biological methods. **Research in Pharmaceutical Sciences**. 9(6): 385–406.

- Liao, S., Zhang, Y., Pan, X., Zhu, F., Jiang, C., Liu, Q., Cheng, Z., Dai, G., Wu, G., Wang, L., and Chen, L. (2019). Antibacterial activity and mechanism of silver nanoparticles against *Pseudomonas aeruginosa*. **International Journal of Nanomedicine**. 14: 1469–1487. <https://doi.org/10.1016/j.micpath.2020.-103980>.
- Michael, C. A., Dominey-Howes, D., and Labbate, M. (2014). The antimicrobial resistance crisis: Causes, consequences, and management. **Frontiers in Public Health**. 2(SEP): 1–8. <https://doi.org/10.3389/fpubh.2014.00145>.
- Motealleh, B., Zahedi, P., Rezaeian, I., Moghimi, M., Abdolghaffari, A. H., and Zarandi, M. A. (2014). Morphology, drug release, antibacterial, cell proliferation, and histology studies of chamomile-loaded wound dressing mats based on electrospun nanofibrous poly(ϵ -caprolactone)/polystyrene blends. **Journal of Biomedical Materials Research - Part B Applied Biomaterials**. 102(5): 977–987. <https://doi.org/10.1002/jbm.b.33078>.
- Naqvi, S. Z. H., Kiran, U., Ali, M. I., Jamal, A., Hameed, A., Ahmed, S., and Ali, N. (2013). Combined efficacy of biologically synthesized silver nanoparticles and different antibiotics against multidrug-resistant bacteria. **International Journal of Nanomedicine**. 8: 3187–3195. <https://doi.org/10.2147/IJN.S49284>
- Okami, Y., and Hotta, K. (1988). Search and discovery of new antibiotics. In M. Goodfellow, M. Mordarski, and S. William (Eds.), *Actinomycetes in biotechnology* (pp. 33–67). Academic Press. <https://doi.org/https://doi.org/10.1016/C2009-0-02828-1>.

- Panigrahi, T., Kumar, G., Karthik, L., Venkat, K., and Rao, B. (2011). Screening of antimicrobial activity of novel *Streptomyces* sp. VITTKGB isolated from agricultural land of Vellore, TN, India. **Journal of Pharmacy Research**. 4(6): 1656–1658.
- Rossolini, G. M., Arena, F., Pecile, P., and Pollini, S. (2014). Update on the antibiotic resistance crisis. **Current Opinion in Pharmacology**. 18: 56–60. <https://doi.org/10.1016/j.coph.2014.09.006>.
- Singleton, P. (2004). *Bacteria in biology, biotechnology and medicine* (6th edition). John Wiley.
- Song, K., Wu, Q., Qi, Y., and Kärki, T. (2017). Electrospun nanofibers with antimicrobial properties. In M. Afshari (Ed.), *Electrospun Nanofibers* (pp. 551–569). Woodheads Publishing. <https://doi.org/10.1016/B978-0-08-100907-9.00020-9>.
- Tacconelli, T., and Magrini, N. (2017). *Global priority list of antibiotic-resistant bacteria to guide research, discovery, and development of new antibiotics*. WHO. https://www.who.int/medicines/publications/WHO-PPL-Short_Summary_25Feb-ET_NM_WHO.pdf.
- Thongkrachang, N., Chanama, S., and Chanama, M. (2016). Inhibitory activity against pathogenic bacteria of *Streptomyces* isolated from natural soil resources. **Journal of Public Health and Development**. 14(3): 59–68.
- Xie, Y., He, Y., Irwin, P. L., Jin, T., and Shi, X. (2011). Antibacterial Activity and Mechanism of Action of Zinc Oxide Nanoparticles against *Campylobacter jejuni*. **Applied and Environmental Microbiology**. 77(7): 2325–2331. <https://doi.org/10.1128/AEM.02149-10>.

Zhang, X. F., Liu, Z. G., Shen, W., and Gurunathan, S. (2016). Silver nanoparticles: Synthesis, characterization, properties, applications, and therapeutic approaches. **International Journal of Molecular Sciences**. 17(9). <https://doi.org/10.3390/ijms17091534>.



CHAPTER II

BIOSYNTHESIS OF SILVER NANOPARTICLES FROM *STREPTOMYCES* SP. SSUT88A

2.1 Introduction

Metal nanoparticles are gaining more attention during the last decade because of their unique characteristics such as physiochemical, antimicrobial, anticancer, optical, magnetic, and electronic properties (Lee and Jun, 2019; Ovais et al., 2018; Rai et al., 2009). Different types of metal nanoparticles like copper, titanium, zinc, gold, magnesium, and silver have been synthesized. However, silver nanoparticles (AgNPs) are the most effective for their antimicrobial properties (Cavassin et al., 2015).

The antimicrobial properties of silver have been documented since 1000 BC. The first medical use of silver for blood purifier and to cure offensive breath was reported in 980 AD. The medical use of silver for eye infection in neonatal was reported in 1881, and the silver was applied for internal antisepsis in 1901. Silver has been widely used to treat superficial and deep dermal burns of the wound in the form of silver nitrate and silver sulfadiazine (Alexander, 2009; Carter et al., 2010; Li et al., 2016; Rai et al., 2009). The silver in nanoscale has different properties compared to the bulk material, such as the surface plasmon resonance, small size with large surface area, and strong toxicity to a wide range of microorganisms (Elechiguerra et al., 2005).

The AgNPs can be synthesized by numerous methods such as physical, chemical, and biological methods. However, the toxic reducing agents such as 2-mercaptoethanol and sodium borohydride are used for the synthesis by chemical method. These toxic substances are negatively impact on environment. While, the physical method produces low yield products and difficult to control the particle size (Gurunathan et al., 2014; Iravani et al., 2014; Ovais et al., 2018; Siddiqi et al., 2018; Zhang et al., 2016). On the other hand, the biological method, known as green synthesis, provides a possible option to synthesize AgNPs due to its simple, cost-effective, producing high-yield, and being eco-friendly processes. AgNPs can be synthesized using plant, bacteria, fungi, and algae (Gurunathan et al., 2014).

Streptomycetes are gram-positive, filamentous soil bacteria and well recognized as antimicrobial producing organisms. Streptomycetes show extensive secondary metabolism and produce two-thirds of all naturally derived antibiotics. Several antibiotics synthesized by Streptomycetes are streptomycin, erythromycin, chloramphenicol, ivermectin, and rifamycin (Barka et al., 2016; Raja and Prabakarana, 2011; van der Meij et al., 2017). The members in the genus *Streptomyces* have been used for the synthesis of AgNPs such as *Streptomyces rochei* MHM13, *Streptomyces coelicolor*, *Streptomyces* sp. LK3, *Streptomyces griseorubens* AU2, and *Streptomyces viridodiastaticus* SSHH-1 (Abd-Elnaby et al., 2016; Karthik et al., 2010; Manikprabhu and Lingappa, 2013; Mohamedin et al., 2015).

The AgNPs have been reported for their antimicrobial properties against Gram-positive and Gram-negative bacteria (Jiang et al., 2004). Morones et al. (2005) reported antimicrobial activity of AgNPs against Gram-negative bacteria, *E. coli*, *Vibrio cholera*, *P. aeruginosa*, and *S. typhi*. They suggested that the antimicrobial action of

AgNPs was to attach and disrupt the cell membrane, penetrate the bacteria, and release silver ions. Interestingly, the antimicrobial activity of AgNPs was also observed on multidrug-resistant bacteria (Cavassin et al., 2015; Scandorieiro et al., 2016; Silva Santos et al., 2016). Several biological synthesis AgNPs reported being effective against multidrug-resistant strains such as multidrug-resistant *A. baumannii*, multidrug-resistant *S. aureus*, and multidrug-resistant *P. aeruginosa* (Wintachai et al., 2019; Yuan et al., 2017). Therefore, the AgNPs provide a potential candidate as an inhibitor for multidrug-resistance microorganisms.

Because of the antimicrobial properties, the AgNPs have been widely used in personal care products, dressing for external wound treatment, surgical instruments, and ointment (Bansod et al., 2015; Eby et al., 2009; Margaret et al., 2006). Furthermore, their application expands to the biological and biomedical fields such as drug and gene delivery, biosensors, diagnostic, medical devices, and implantable materials (Ahamed et al., 2010; Lee and Jun, 2019). In this research, the AgNPs were synthesized by a green method using different cell-free supernatant of *Streptomyces* sp. SSUT88A. The characterization, cytotoxicity against NIH-3T3 cells, and antimicrobial activity against drugs-resistant bacteria were investigated.

2.2 Literature review

2.2.1 *Streptomyces* sp. and their secondary metabolite

Streptomycetes belongs to the class of Actinomycetes. They are Gram-positive, aerobic bacteria, which show branching filament form/hyphae and asexual spores. The actinomycetes are distinguished from other bacteria based on cell morphology, spore arrangement, cell wall chemistry, and type of sugar present in the

cell extract (Purohit et al., 2006). The characteristic of actinomycetes are high content of G+C in their DNA and can be found in both aquatic or marine and terrestrial ecosystems (Barka et al., 2016; van der Meij et al., 2017). Raja and Prabakarana (2011) also reported that actinomycetes are also found in extreme environments, especially in the cryophilic regions. Most of the actinomycetes found in symbiosis with another organism, that gives benefit for their secondary metabolite production. They will exchange the chemicals with the other microbial community or other organisms, which has a major impact on the secondary metabolites and growth (Banin et al., 2017; van der Meij et al., 2017).

Actinomycetes are divided into six orders and 14 suborders (Table 2.1). The genera of this class exhibit enormous diversity in terms of morphology, physiology, and metabolic capabilities (Barka et al., 2016).

Table 2.1 Taxonomy of Actinomycetes (Barka et al., 2016).

Class	Orders	Suborders	
Actinomycetes	Rubrobacterales	Corynebacterineae	
	Acidimicrobiales	Pseudonocardinae	
	Solirubrobacterales	Frankineae	
	Coriobacterales	Streptosporangineae	
	Bifidobacterales	Streptomycineae	
	Actinomycetales		Catenulisporineae
			Micromonosporineae
			Glycomycineae
			Propionibacterineae

Table 2.1 Taxonomy of Actinomycetes (Barka et al., 2016). (Continued)

Class	Orders	Suborders
		Micrococcinae
		Kineosporiineae
		Actinomycineae
		Actinopolysporineae
		Jiangellineae

Actinomycetes are abundant in soil because they play a significant role in the mineralization of organic materials of soil (Purohit et al., 2006). Several factors that affect the growth of actinomycetes are temperature, pH, and soil moisture. Most of the actinomycetes are mesophilic, with optimum growing temperatures between 25 and 37°C. However, some actinomycetes are thermophilic, which can grow at a temperature ranging from 50 to 60°C. The optimum pH of soil for actinomycetes becomes between 6 and 9, with maximum growth around neutrality (Barka et al., 2016).

Actinomycetes also have extensive secondary metabolism and produce two-thirds of all naturally derived antibiotics in current clinical use (Figure 2.1) (Barka et al., 2016; van der Meij et al., 2017). From all of the actinomycetes group, *Streptomyces* possess diverse genus with around 600 species, and they are responsible for the production of half of all known antibiotics (Labeda et al., 2012). They have been recognized as a source of active compounds with antifungals, antibiotics, chemotherapeutic or anticancer activity (Raja and Prabakarana, 2011). Consequently, *Streptomyces* are very important in the fight against emerging multidrug-resistant pathogens (Barka et al., 2016; van der Meij et al., 2017). *Streptomyces* species produce

antibiotics such as tetracyclines, aminoglycosides, macrolides, chloramphenicol, ivermectin, rifamycins, and most other clinically useful antibiotics that are not beta-lactams (Raja and Prabakarana, 2011).



Figure 2.1 Antibiotics that produced by Actinomycetes.

2.2.2 Synthesis of silver nanoparticles (AgNPs)

Nano is a prefix of denoting the minus 9th power of ten. The nanoparticle is an ultrafine particle in the size of nanometer order (Yokoyama et al., 2012). Metal nanoparticles possess a distinctive optical property called Surface Plasmon Resonance

(SPR) due to the collective oscillation of free electron at the interface between negative and positive permittivity of material stimulated by incident light. Due to their small size with large surface area, metal nanoparticles are widely used for hypothermia treatment of malignant cells, magnetic resonance imaging enhancement, cell labeling, cell tracking, *in vivo* imaging, drug delivery system, and some of the biomedical field. Some of the metals that are successfully synthesized as nanoparticles are selenium, tellurium, gold, silver, cadmium, lead, iron, copper, arsenic, chromium, and zinc. Among all of these metals, silver nanoparticles work best for their antimicrobial activity (Sharon et al., 2012; Liao et al., 2019).

Silver has been known to exhibit antibacterial activity. They used for bacterial infection treatment in association with burns, ulcerations, wounds, and to prevent gonococcal ophthalmic infection in newborns (Barros et al., 2018; Franci et al., 2015; Mohammadi et al., 2019; Munteanu et al., 2016; Politano et al., 2013). To treat burns and wounds, the silver has been added to bandages or cream in the form of silver sulfadiazine or silver nitrate (Carter et al., 2010).

There are three different approaches for carrying out the synthesis of AgNPs, chemical method, physical method, and biological method. For chemical methods, they employ three main components, which are precursors, reducing agents, and stabilizing or capping agents. Several techniques were used for chemical synthesis of AgNPs, such as cryochemical synthesis, lithography, electrochemical reduction, laser irradiation, thermal decomposition, and chemical reduction. Toxic and hazardous chemicals used, such as borohydride and 2-mercaptoethanol, are disadvantages of this method. It is also challenging to prepare AgNPs with defined size and need additional steps to prevent particle aggregation. Apart from these disadvantages, the advantages

of the chemical methods are high yield, easy of production, and low cost (Ge et al., 2014; Gurunathan et al., 2014; Siddiqi et al., 2018; Zhang et al., 2016).

In the physical method, evaporation-condensation and laser ablation have been used for AgNPs synthesis. The advantages of physical processes are the absence of solvent contamination in the thin film, no hazardous agents or toxic chemical use, and produce a uniform distribution of nanoparticles. On the other hand, the physical method's disadvantages are low yield, high consuming energy, tube furnace occupies a large space, and requires times to achieve their stability (Ge et al., 2014; Irvani et al., 2014; Siddiqi et al., 2018; Zhang et al., 2016).

Besides chemical and physical methods, biological synthesis or known as green synthesis emerged as a possible option to synthesize AgNPs. Recently, a biologically mediated combination of AgNPs has been gaining more attention. Bacteria, fungi, actinomycetes, algae, and plants have been extensively studied for AgNPs synthesis because it is simple, cost-effective, dependable, and environmentally friendly without using toxic chemicals and gives high yield production with a defined size. Microorganisms, plants, and other small molecules such as amino acid, protein, and vitamin act as reducing and stabilizing agent (Sharon et al., 2012; Ge et al., 2014; Siddiqi et al., 2018; Zhang et al., 2016). Other advantages of using the biological method for the synthesis of AgNPs are short time, high density, stability, and solubility. The biological synthesis of AgNPs depends on three factors, including the solvent, the reducing agent, and the non-toxic materials. The presence of amino acids, proteins, or secondary metabolites in the solvent is the major advantage for the synthesis of AgNPs because they act as stabilizing and capping agent. On the other hand, the use of

biological molecules for synthesis is eco-friendly and pollution-free (Barros et al., 2018; Ge et al., 2014; Zhang et al., 2016).

The overall mechanism of AgNPs synthesis by using bacteria involves entrapment of Ag^+ , reduction, capping, and stabilization processes. This mechanism follows bottom-up approaches (produced from small entities such as atom and molecules via redox reaction) (Figure 2.2). The synthesis of AgNPs using bacteria can occur intracellularly, extracellularly, or both, depending on the location of the reducing agent. Many microorganisms produce inorganic matters inside of the cell and release it. In the case of extracellular synthesis, the reducing agent for reduction Ag^+ to Ag^0 usually comes from small soluble secreted enzymes or proteins that present on the bacterial cell wall. Extracellular compounds are secreted by bacterial cells composed of protein and polysaccharides that capable of adhering and trapping Ag^+ . NADH reductase plays an essential role in some reports related to the reduction of Ag^+ to Ag^0 . Where NADH donates an electron to Ag^+ , then Ag^+ will be reduced to their elemental form and accumulate in the form of AgNPs. The extracellular method for AgNPs synthesis has been suggested because it is cheap, favor for large-scale production, and easy for downstream processing (Barros et al., 2018; Hulkoti and Taranath, 2014; Javaid et al., 2018; Kalishwaralal et al., 2010; Siddiqi et al., 2018). *Streptomyces rochei* MHM13 has been reported for their ability to synthesize AgNPs by an extracellular process in the size of 22-85 nm that showed antibacterial activity against medically important bacteria such as *V. fluvialis*, *P. aeruginosa*, and *S. typhimurium*. (Abd-Elnaby et al., 2016).

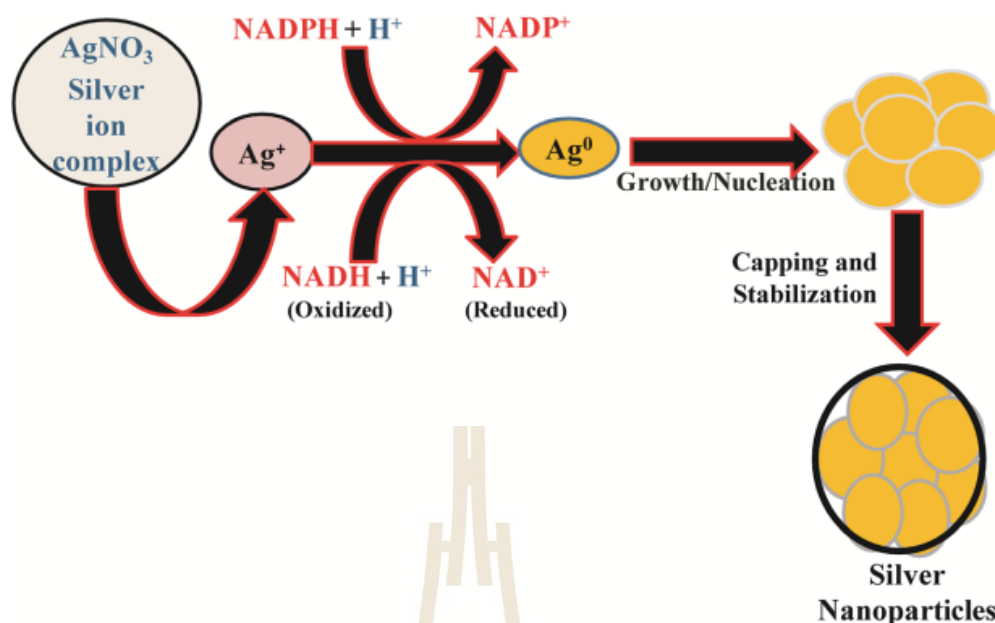


Figure 2.2 Mechanism of AgNPs synthesis by bacteria mediated via NADH-dependent reductase enzyme (Javaid et al., 2018).

Furthermore, the intracellular synthesis of AgNPs involves the transport of Ag⁺ into the cell by a membrane protein. The synthesized AgNPs are reported being accumulated in the cell wall or periplasmic space. The mechanism of intracellular synthesis of AgNPs starts with the trapping of Ag⁺ by the interaction of positively charged Ag⁺ with negatively charged bacterial cell surface due to the presence of the carboxyl group. Several bacteria generate a transmembrane protein that allows Ag⁺ to enter the cell. The silver binding protein attracts an uptake of Ag⁺ inside the cell and initiates the synthesis of AgNPs. However, the additional step required for the intracellular process to collect the synthesized AgNPs, such as lysis of bacterial cells by ultra-sonication, heat treatment, or by the chemical method using salt and detergent. The intracellular synthesis of AgNPs requires metal resistant strains because Ag⁺

should be imported into the cell without causing any damage (Barros et al., 2018; Hulkoti and Taranath, 2014; Javaid et al., 2018). For example, *Corynebacterium* sp. SH09 can synthesize AgNPs by intracellular process and produces AgNPs in the size of 10-15 nm, which form diamine Ag complex on its cell wall (Zhang et al., 2005).

Table 2.2 Green synthesis of AgNPs using Streptomyces.

Microbes name	AgNPs size (nm)	References
<i>Streptomyces rochei</i> MHM13	22-85	(Abd-Elnaby et al., 2016)
<i>Streptomyces coelicolor</i>	28-50	(Manikprabhu and Lingappa, 2013)
<i>Streptomyces</i> sp. LK3	5	(Karthik et al., 2014)
<i>Streptomyces griseorubens</i> AU2	5-20	(Baygar and Ugur, 2017)
<i>Streptomyces</i> sp. PBT 005	198-595	(Kumar et al., 2015)
<i>Streptomyces viridodiastaticus</i> SSHH-1	15-45	(Mohamedin et al., 2015)

Streptomyces can produce secondary metabolites and are considered as an important source for a new product of medical use, such as an antimicrobial agent. Many researchers observe that Streptomyces have an important role in the synthesis of silver nanoparticles. The synthesized AgNPs represent good stability and polydispersity due to the presence of stabilizing and capping agent (Abd-Elnaby et al., 2016; Hulkoti and Taranath, 2014). Table 2.2 show the example of synthesized AgNPs using *Streptomyces*.

AgNPs have attracted considerable attention from many researchers and companies and have been used for manufacturing many products of AgNPs. In the industrial field, AgNPs have been used for paint and household needs such as detergent and healthcare-related products. In the consumer product field, AgNPs have been used for medical devices coating, cosmetics, and optical sensors. Finally, in the pharmaceutical field, AgNPs have been used for drug delivery, antimicrobial agents, anticancer agents, wound dressings, and biomedical equipment (Barros et al., 2018; Carter et al., 2010; Javaid et al., 2018; Naqvi et al., 2013; Zhang et al., 2016).

2.2.3 Antimicrobial and cytotoxicity mechanism of silver nanoparticles

AgNPs exhibit antimicrobial activity against a broad range of pathogenic microorganisms. The activity of AgNPs depends on surface chemistry, size, shape, coating or capping agent, agglomeration, particle reactivity in solution, cell type, and reducing agent. AgNPs synthesized by a biological method is generally more toxic against pathogenic bacteria than those by other methods (Siddiqi et al., 2018; Zhang et al., 2016). Several mechanisms of antimicrobial activity of AgNPs have been reported by many researchers, including the interaction between AgNPs and bacterial cell, generation of ROS that followed by depletion of GSH activity, and DNA and protein damage (Figure 2.3).

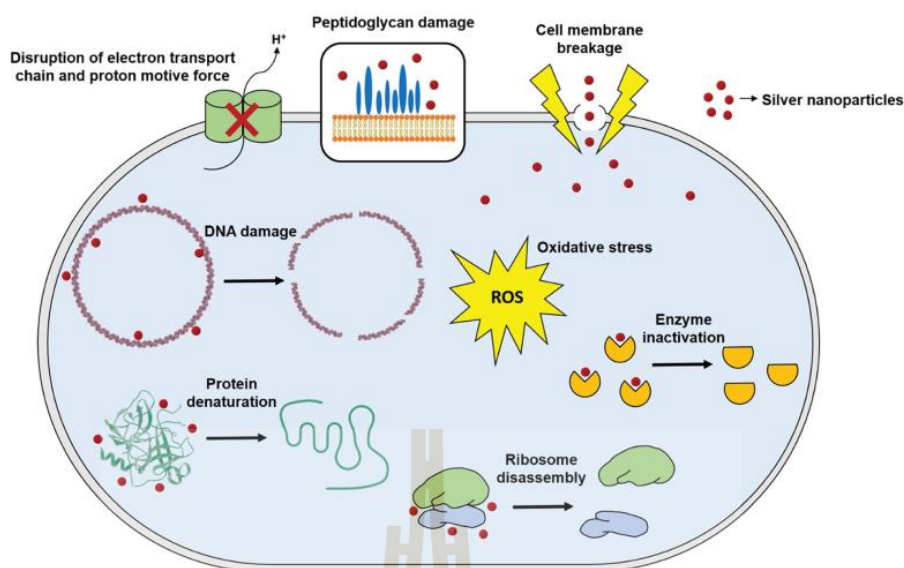


Figure 2.3 Mechanism of antimicrobial action of silver nanoparticles (Roy et al., 2019).

The antimicrobial activity of AgNPs begins with the interaction of AgNPs with bacterial cells. The smaller particle size of AgNPs has been reported being higher toxic compared with the bigger one. The AgNPs will interact with the protein, phospholipids, or thiol-containing groups that appear in the cell wall, leading to proton leakage and disintegration of bacterial cells. The attachment of AgNPs to cell wall also follows by the formation of pits that causes structural cell membrane change, increases cell permeability, and leads to cell death (Barros et al., 2018; Franci et al., 2015; Ge et al., 2014; Siddiqi et al., 2018). The formation of pits on the cell wall was also observed on *E. coli* cells after AgNPs treatment by using SEM and TEM. The AgNPs were found to be accumulated on the bacterial membrane, leading to increased permeability of the membrane and resulted in cell death (Sondi and Salopek-Sondi, 2004).

AgNPs have a higher tendency to interact with phosphorus and sulfur groups of DNA or thiol group of vital enzymes. It causes inhibition of some cell function that

leads to DNA damage and aggregation and disrupts the process of transcription and translation (Barros et al., 2018; Franci et al., 2015; Ge et al., 2014; Liao et al., 2019; Morones et al., 2005; Siddiqi et al., 2018).

AgNPs have reactive redox property, which increases ROS level and causes cell death by DNA or RNA damage that participates in the cell apoptosis process (Jin and Zhao, 2009). Hussain et al. (2005) have observed the cytotoxicity effect of AgNPs at 5-50 $\mu\text{g/mL}$ on the BBL 3A rat liver cells after 24 h incubation. The treatment of AgNPs has caused a decrease in mitochondrial function, membrane leakage of lactate dehydrogenase (LDH), depletion of GSH level, and an increase in ROS level. AgNPs synthesized from branch cyclodextrin has also been reported to cause the cell wall of the *P. aeruginosa* becoming thin, combined with the deformation of cell membrane and release of cell content. Based on the proteomic analysis, the proteins that involved in the ROS metabolism, oxidative stress, and REDOX (superoxide dismutase, catalase, peroxidase) are highly expressed in the AgNPs treated group, followed by the increasing amount of ROS that leads to cell death by apoptosis (Liao et al., 2019).

2.3 Research methodology

2.3.1 Isolation and purification of *Streptomyces*

Soil samples were collected from the Sakaerat Environmental Research Station, Nakhon Ratchasima, Thailand, at depth 10-20 cm and transferred to a clean plastic bag. Soil *Streptomyces* were isolated using a serial dilution method and cultured on the actinomycete isolation agar (AIA, Himedia) medium. Incubation was conducted at 37°C for one week or until the colonies appear. Selected colonies were transferred to

an International *Streptomyces* Project 2 (ISP2) agar medium for purification. The purified isolates were preserved in 20% glycerol and kept at -80°C freezer until used.

2.3.2 Identification of *Streptomyces* based on 16s rRNA gene sequence

Genomic DNA extraction was performed by a method for fungi with modification. *Streptomyces* culture was dispersed in 500 μL of lysis buffer containing 400 mM Tris-HCl (pH 8.0), 60 mM EDTA (pH 8.0), 150 mM NaCl, 1% sodium dodecyl sulfate (SDS) and grinded until fine. The mixture was transferred to a microcentrifuge tube. Then 165 μL of 5 M NaCl was added to the mixture and mixed by inverting the tube. The suspension was centrifuged at 13000 rpm 4°C for 10 minutes. The supernatant was transferred to a new microcentrifuge tube, then added 400 μL chloroform and 400 μL isoamyl alcohol and mixed by inverting the tube. The sample was centrifuged at 13000 rpm 4°C for 10 minutes. The first layer was transferred into a new microcentrifuge tube, added an equal volume of chloroform, and mixed by inverting the tube. The sample was centrifuged at 13000 rpm 4°C for 5 minutes. The supernatant was transferred into a new tube, added two volumes of 95% ethanol, and mixed by inverting the tube. The sample was centrifuged at 13000 rpm 4°C for 5 minutes, and the supernatant was discarded. The pellet was washed three times with 300 μL of 70% ice-cold ethanol and centrifuged at 13000 rpm 4°C for 1 minute. The sample was dried using Mini Dry Bath and dissolved in 50 μL of TE buffer (10 mM Tris-HCL, 0.1 mM EDTA pH 7.8). Extracted DNA was qualitatively checked by using agarose gel electrophoresis.

For PCR amplification, the universal 16s rRNA primers, 27F (5'-AGAGTTTGATCCTGGCTCAG-3') and 1525R (5'-AAGGAGGTGATCCAGCC-3') were used for amplification. The amplification was carried out in a mixture's reaction

containing 10 μL genomic DNA as a template, 2 μL forward (10 pM), 2 μL reverse primer (10 pM), 25 μL master mix (EconoTaq® PLUS 2x Master Mix, Lucigen), and nuclease-free water (Promega) until the final volume of 50 μL reaction mixture. The amplification was performed using thermal cycler machine (THERMO Px2 Thermal Cycler) with the following cycles: 5 minutes initial denaturation at 94°C; 30 second denaturation at 94°C; 30 second annealing at 55°C; 30 second extension at 72°C; for 20 cycles and a final extension of 7 minutes at 72°C. Electrophoresis of amplified products were conducted on 0.7% (w/v) agarose gel in 1X TBE buffer (45 mM Tris-borate, pH 8.3, and 1 mM Na₂ EDTA) at 100 V. The target band that appears in the gel was cut and purified by using FavorPrep™ Gel/PCR Purification Mini Kit (Favorgen™). The purified PCR samples were used for DNA sequencing analysis. The obtained 16s rRNA gene sequence were compared to an online 16s rRNA database, EzBioCloud (<http://www.ezbiocloud.net>). The sequences were aligned with closely related species by using CLUSTAL W. The phylogenetic trees were constructed using Molecular Evolutionary Genetics Analysis software version X (MEGA-X) with a Neighbor-Joining algorithm of 1000 bootstraps.

2.3.3 Preparation of cell-free extract

The *Streptomyces* sp. SSUT88A was inoculated in a 250 mL Erlenmeyer flask containing 100 mL ISP2 medium. A flask was incubated in a rotary shaker at 200 rpm, 37°C for four days. After incubation, the cultures were harvested by centrifugation at 13000 rpm for 5 min. The fermented broth of *Streptomyces* sp. SSUT88A was collected as extracellular cell-free supernatant and used for further experiments. On the other side, the cell pellet was washed three times using sterile deionized water (DI) water to remove traces of medium. The *Streptomyces* sp. SSUT88A biomass was

resuspended in an Erlenmeyer flask containing 100 mL sterile DI water and incubated at 37°C under 200 rpm shaking condition for 24 h. During the incubation, the cells were burst due to the osmotic imbalance caused by the excess water to diffuse into the cells. Thus, the biological molecules were released into the DI water. After incubation, the culture was centrifuged at 13000 rpm for 5 min. The intracellular cell-free supernatant was used for further experiments (Krishnakumar and Bai, 2015).

2.3.4 Biosynthesis of silver nanoparticle

Fifty mL of *Streptomyces* cell-free supernatant was mixed with a 50 mL aqueous solution of 1 mM silver nitrate (AgNO_3) (POCH SA Silver Nitrate 99.9%), and the pH was adjusted to 7. The extracellular and intracellular cell-free supernatant mixture was incubated in a rotary shaker at 200 rpm, 37°C in the dark for 2 and 5 days, respectively. The ISP2, DI, and AgNO_3 were used as a control experiment to check the role of cell-free supernatant in the reduction of silver ion.

2.3.5 Characterization of silver nanoparticle

2.3.5.1 Ultraviolet-visible (UV-Vis) spectrophotometry

The bio reduction of silver ions was monitored by a color change from light yellow to brown. The presence of AgNPs was confirmed by observed their absorption spectrum using a UV-Vis spectrophotometer (Thermo Scientific Multiscan GO, Finland) in the range of 300 to 600 nm from day 0 to day 5 (Abd-Elnaby et al., 2016). The absorbance of AgNPs range from 380 to 450 nm, corresponds to the surface plasmon resonance of silver nanoparticles.

2.3.5.2 Determination of particle size and zeta potential

The particle size distribution and zeta potential measurement of both synthesized AgNPs were measured by Zeta sizer (Malvern Instrument Corp,

Malvern, USA) at 25°C using disposable plastic cuvette (IVWR Cuvettes PMMA) and disposable folded capillary cuvette (DTS1070 Malvern), respectively. The colloidal sample of AgNPs was dispersed in water by dispersing 100 μL of AgNPs in 900 μL of water.

2.3.5.3 X-ray diffraction (XRD) evaluation

The crystallinity of synthesized AgNPs was investigated using X-Ray diffraction (XRD) (D Advance, Bruker, Germany). The AgNPs samples were prepared by freeze-drying for 48 hours. A diffractions pattern was scanned in the range of 2θ from 20° to 80° (Abirami and Kannabiran, 2016).

2.3.5.4 Fourier-Transform Infrared (FTIR)

For FTIR spectroscopy measurement, the AgNPs and cell-free supernatant were previously freeze-dried for 48 h. The possible bioreduction agent of Ag^+ to Ag^0 was evaluated by using Fourier-transform infrared spectroscopy (FTIR) (FTIR, Bruker Hyperion 3000, Germany) in the range 4000-400 cm^{-1} . To identify the functional group in each sample, the spectral data were compared with the database. The FTIR analysis was conducted at beamline 4.1 Synchrotron Light Research Institute (SLRI), Thailand.

2.3.5.5 X-ray absorption near edge structure (XANES) analysis

To determine the local geometric and structure of Ag in the synthesized AgNPs, XANES analysis was used. The samples were placed on the thin polypropylene film (SPEX SampelPrep). The L_3 edge XAS spectra of Ag were measured in fluorescence mode using a Vortex®-EM silicon drift detector. AgNO_3 and Ag nanopowder (Sigma Aldrich Chemicals) was used as a standard. The result of XANES data were averaged and normalized using the Demeter package, version 8.9.26

(Ravel and Newville, 2005). The XAS analysis was conducted at beamline 5.2 Synchrotron Light Research Institute (SLRI), Thailand.

2.3.5.6 Transmission electron microscopy (TEM) and energy dispersive X-ray fluorescence (EDXRF) analysis

The synthesized AgNPs were lyophilized using a freeze-dry machine for 48 h. The powder sample of AgNPs was placed onto carbon tape. TEM (Tecnai G² 20) was used for the analysis of the shape and size of AgNPs. EDXRF (OXFORD Instrument) was used to confirm the presence of elemental silver and chemical composition.

2.3.6 Antimicrobial activity assay

The antibacterial activity of synthesized AgNPs was evaluated against clinical isolate pathogens, including *A. baumannii*, *E. coli* 8465, *K. pneumoniae* 1617, *P. aeruginosa* N90PS, and MRSA TISTR 20654 using an agar well diffusion assay. The test pathogens were obtained from Suranaree university of technology hospital and Thailand Institute of Scientific and Technological Research (TISTR). The AgNPs samples were adjusted the concentration to be the same based on the data obtained from EDXRF by diluting it in water. The 5×10^5 CFU/mL of mid-log phase test pathogens were seeded onto MHA plates. Then, a hole with a diameter of 6-8 mm was punched aseptically with a sterile cork borer, and a volume of 100 μ L of 0.2 mg/mL AgNPs samples was introduced into the well. The plates were incubated at 37°C. After 24 h, antibacterial activity was recorded by measuring the diameter of the zone of inhibition (Abirami and Kannabiran, 2016).

2.3.7 Cytotoxicity assay

The cytotoxicity evaluation of synthesized AgNPs was evaluated against NIH-3T3 mouse embryonic fibroblast cell lines. The 10^4 cells were cultured using DMEM supplemented with 10% fetal bovine serum (FBS) and 1% antibiotics (Penicillin, Streptomycin) in a 96 culture well plate for 24 h to allow attachment of the cells onto the well surface. After 24 h, the medium was substituted with serum-free medium containing synthesized AgNPs and incubate it at 37°C, 5% CO₂ for 24 h. The Ag nanopowder (Sigma) was used as a control. The MTT assay was used to determine the viability of the treated cells. The medium in wells was removed and 10 μ L of 5 mg/ml of 3-(4,5-dimethylthiazol-2-yl)-2,5-diphenyltetrazolium bromide (MTT, Invitrogen™) on phosphate buffer saline (PBS) was added, followed by adding 100 μ L of sterile PBS. The cells were incubated for 4 h at 37°C, 5% CO, the formazan crystals formed were solubilized by remove MTT solution and adding 50 μ L DMSO to the wells. The absorbance was determined at 540 nm using spectrophotometer (Thermo Scientific Multiscan GO, Finland).

2.3.8 Statistical analysis

The statistical analysis of the data was executed using independent sample t-test and one-way analysis of variance (ANOVA) using IBM SPSS Statistics Version 23. To determine the significant difference between groups on ANOVA analysis, Tukey's test was applied with $p < 0.05$.

2.4 Results

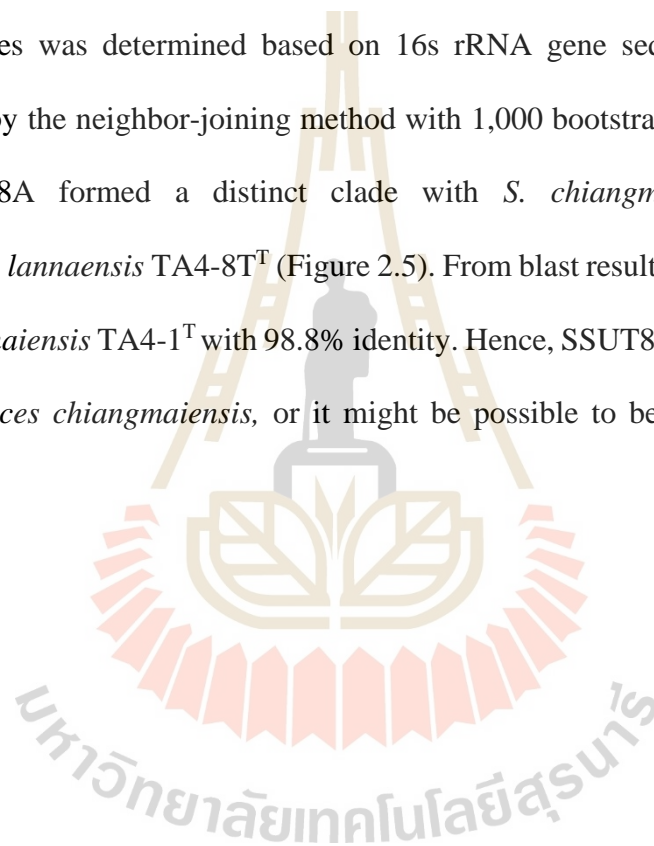
2.4.1 Identification of *Streptomyces* SSUT88A

A total of 112 *Streptomyces* isolates were successfully isolated from soil samples of Sekaerat Environmental Research Station and screened for their antimicrobial activity. Five isolates showed the antimicrobial activity and two of them were chosen for the synthesis of AgNPs. The *Streptomyces* sp. SSUT88A showed an ability for the synthesis of AgNPs and used for further experiment. The colony morphology of *Streptomyces* sp. SSUT88A was velvety with white substrate mycelium. The grey spore was produced from aerial mycelium after 9 days of incubation (Figure 2.4). Strain SSUT88A also released diffusible yellowish pigment on ISP2, MHA, and starch casein agar (SCA) media.



Figure 2.4 Colony morphology of *Streptomyces* sp. SSUT88A on ISP2 media.

The *Streptomyces* sp. SSUT88A's 16s rRNA gene sequence was amplified using 27F and 1525R primers. The 16s rRNA PCR product was purified and submitted for sequencing. The obtained 16s rRNA gene sequence was blasted and aligned with the online 16s rRNA sequence database from EzBioCloud. The 16s rRNA gene sequence of *Streptomyces* sp. SSUT88A shows 98.8% similarity to *Streptomyces chiangmaiensis* TA4-1^T. The phylogenetic relationship between SSUT88A and closely related species was determined based on 16s rRNA gene sequence. The tree was constructed by the neighbor-joining method with 1,000 bootstraps. The result showed that SSUT88A formed a distinct clade with *S. chiangmaiensis* TA4-1^T and *Streptomyces lannaensis* TA4-8T^T (Figure 2.5). From blast result, it was closely related to *S. chiangmaiensis* TA4-1^T with 98.8% identity. Hence, SSUT88A could be identified as *Streptomyces chiangmaiensis*, or it might be possible to be a candidate for new species.



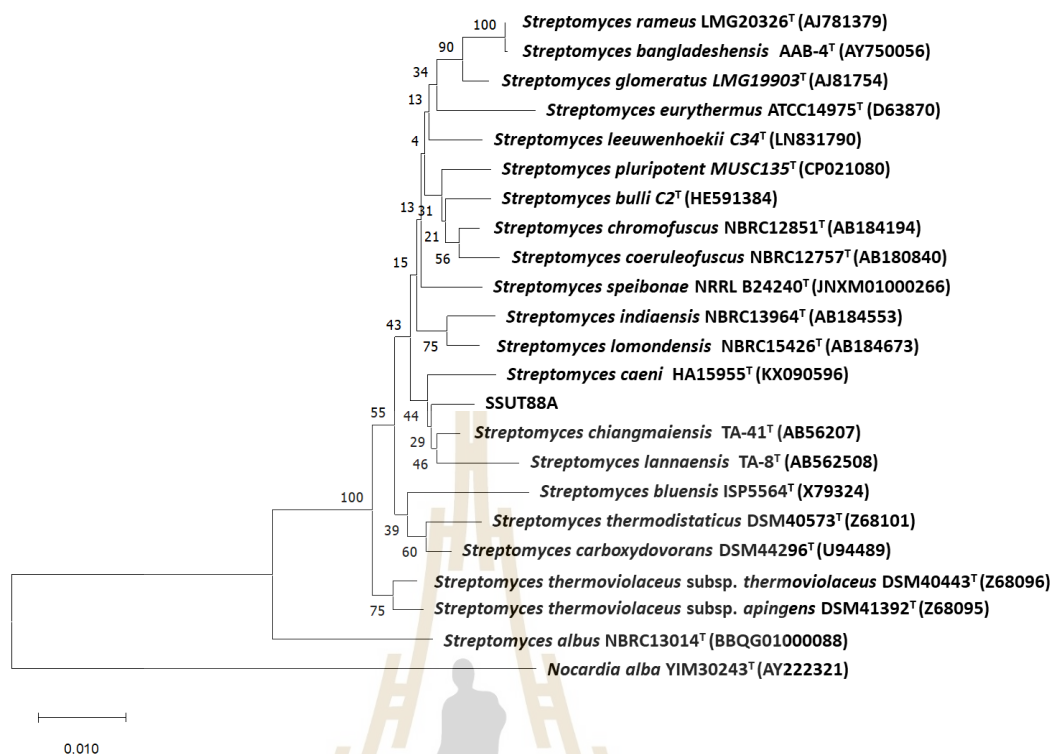


Figure 2.5 Neighbor-joining tree of *Streptomyces* sp. SSUT88A and closely related species based on 16s rRNA gene sequence. The 16s rRNA region was aligned by using ClustalW. The neighbor-joining tree was generated using MEGAX software. The number at the nodes indicate levels of a bootstrap based on 1,000 resampling. The scale bar indicates 0.010 substitutions per nucleotide position. *Nocardia alba* YM 30243^T was used as an outgroup.

2.4.2 Biosynthesis of AgNPs and UV-Vis spectroscopy analysis

The current study focused on the synthesis of AgNPs using intracellular and extracellular cell-free supernatant of *Streptomyces* sp. SSUT88A as reducing agents. The synthesis of AgNPs was done by mixing either intracellular or extracellular cell-free supernatant with 1 mM AgNO₃ and incubate it at 37°C under 200 rpm shaking

condition for 2 and 5 days, respectively. The synthesized AgNPs from intracellular cell-free supernatant and extracellular cell-free supernatant were designated as IS-AgNPs and ES-AgNPs, respectively. After incubation, the color of a mixture was changed from light yellow to brown, as shown in Figure 2.6 and Figure 2.7 number 2. No color change was observed from negative control where cell-free supernatant was substituted with either DI (Figure 2.6, number 3) or ISP2 (Figure 2.7, number 3).

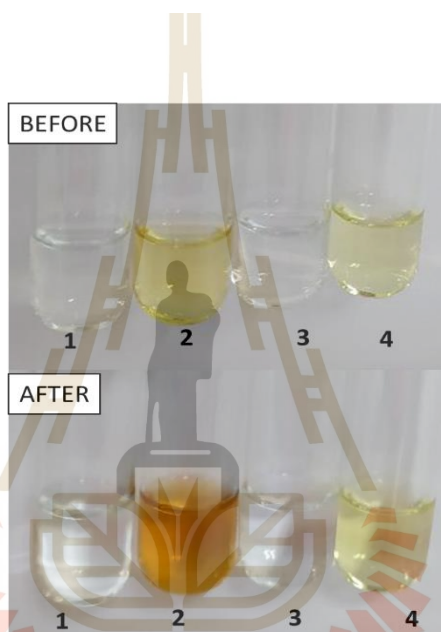


Figure 2.6 Visible observation of biosynthesis IS-AgNPs by *Streptomyces* sp. SSUT88A. (1). AgNO_3 ; (2). Cell-free supernatant+ AgNO_3 (IS-AgNPs); (3). DI+ AgNO_3 ; (4). Cell-free supernatant.

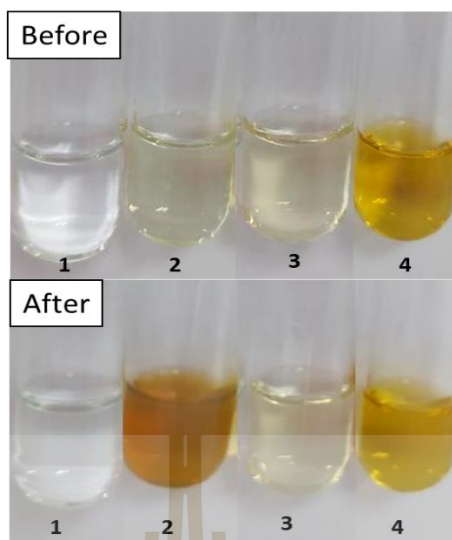


Figure 2.7 Visible observation of biosynthesis ES-AgNPs by *Streptomyces* sp. SSUT88A. (1). AgNO_3 ; (2) Cell-free supernatant+ AgNO_3 (ES-AgNPs); (3). ISP2+ AgNO_3 ; (4). Cell-free supernatant.

The synthesized AgNPs, cell-free supernatant, and AgNO_3 were scanned with UV-Vis spectroscopy, and the spectra showed in Figure 2.8. The UV-Vis spectroscopy analysis indicated the maximum absorbance at 418 nm and 422 nm for IS-AgNPs and ES-AgNPs, respectively, correspond to the AgNPs absorption spectrum. No AgNPs absorption spectrum from only cell-free supernatant or AgNO_3 was observed after incubation, as shown in Figure 2.8.

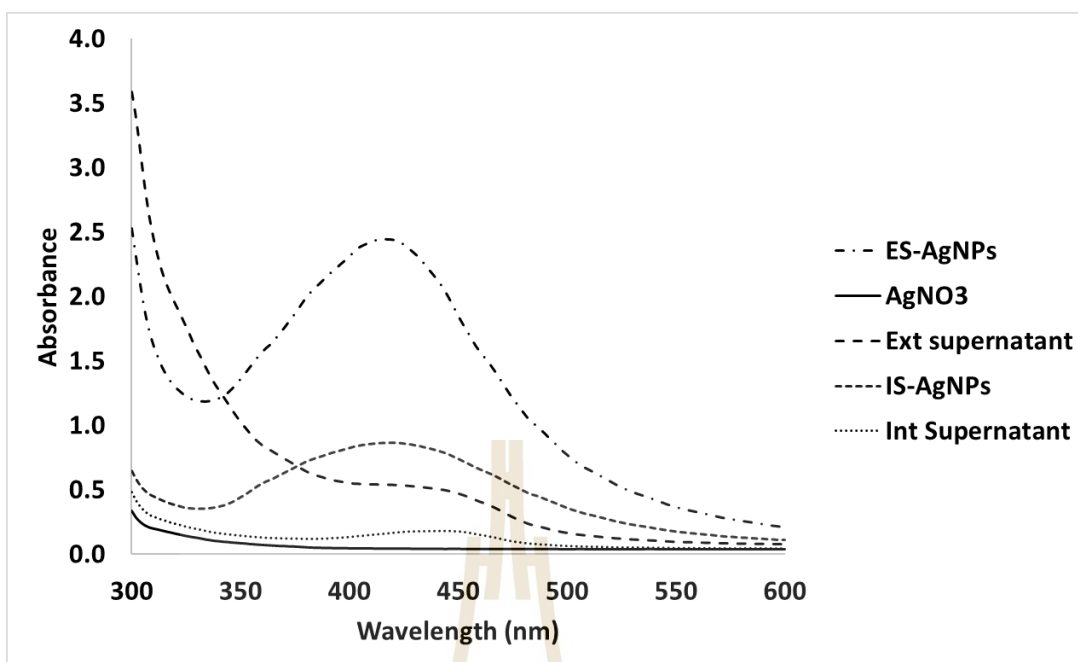


Figure 2.8 UV-Vis spectra of IS-AgNPs and ES-AgNPs.

2.4.3 Particle size and zeta potential analysis of synthesized AgNPs.

The size distribution of IS-AgNPs and ES-AgNPs were determined using dynamic light scattering (DLS). The colloidal samples were measured by dispersing the AgNPs sample in water. For IS-AgNPs, DLS analysis showed nanoparticles with an average size of 77.03 nm, while the ES-AgNPs was higher (82.44 nm) (Figure 2.9).

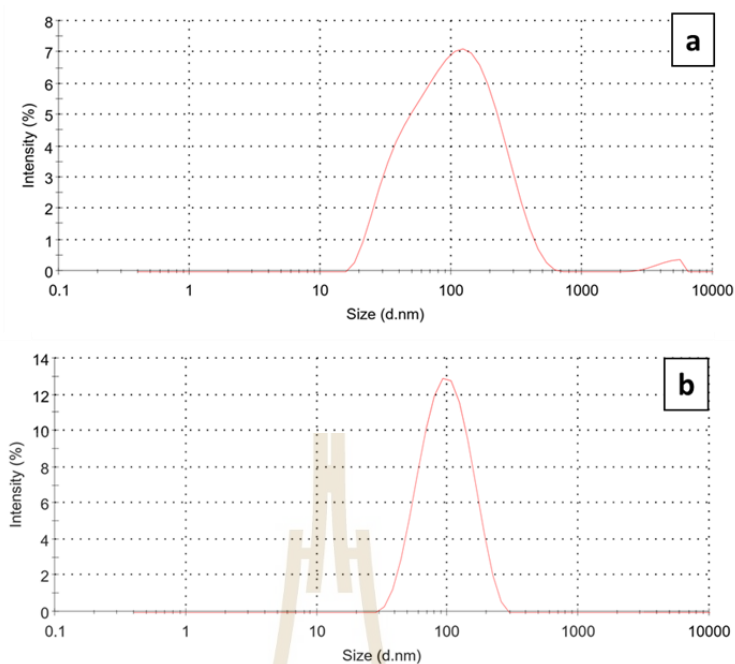


Figure 22.9 The particle size distribution from DLS measurement. (a) IS-AgNPs and (b) ES-AgNPs.

The stabilization of synthesized AgNPs was confirmed by measuring its zeta potential. The zeta potential value of the IS-AgNPs and ES-AgNPs were -32 mV and -27.9 mV, respectively, indicating the presence of negative repulsion among the nanoparticles, as shown in Figure 2.10.

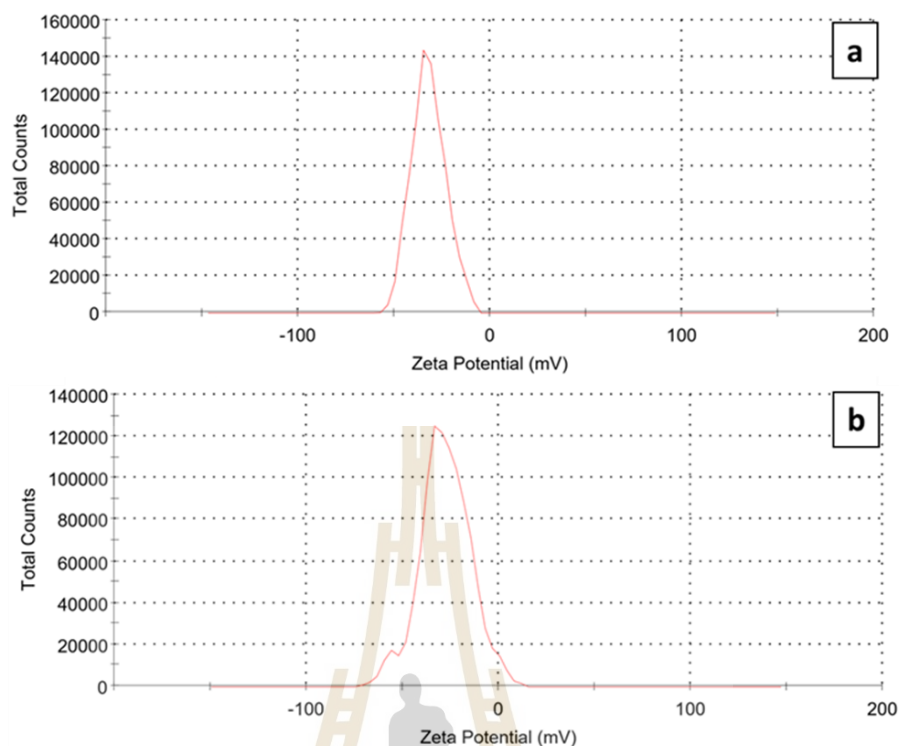


Figure 2.10 Zeta potential of (a) IS-AgNPs and (b) ES-AgNPs.

2.4.4 XRD analysis of synthesized AgNPs

The X-ray diffraction spectra profile of synthesized AgNPs were obtained by XRD, as seen in Figures 2.10 and 2.11. Both synthesized AgNPs express the intense peaks of AgNPs at 38.11° , 44.27° , 64.42° , and 77.47° that corresponding to (111), (200), (220), and (311) planes of face-centered cubic (fcc) of metallic silver based on the Standard Joint Committee for Powder Diffraction Set (JCPDS files).

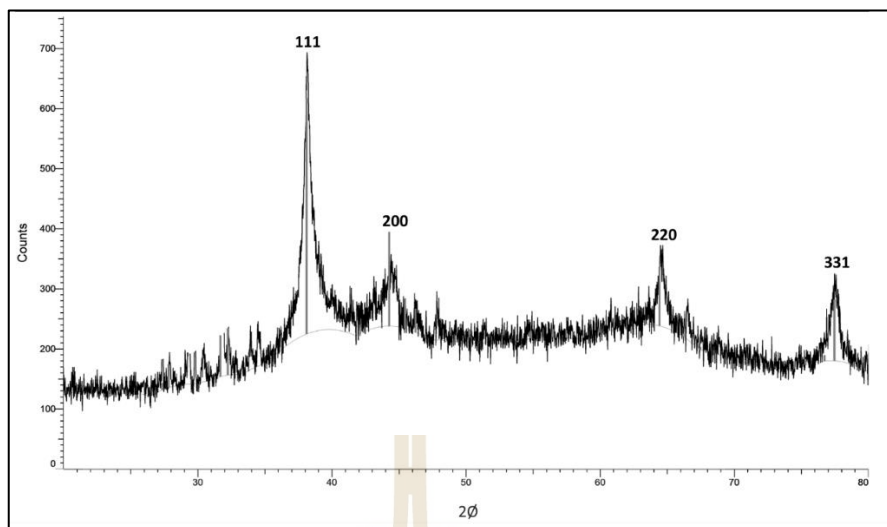


Figure 2.11 X-ray diffraction pattern of IS-AgNPs.

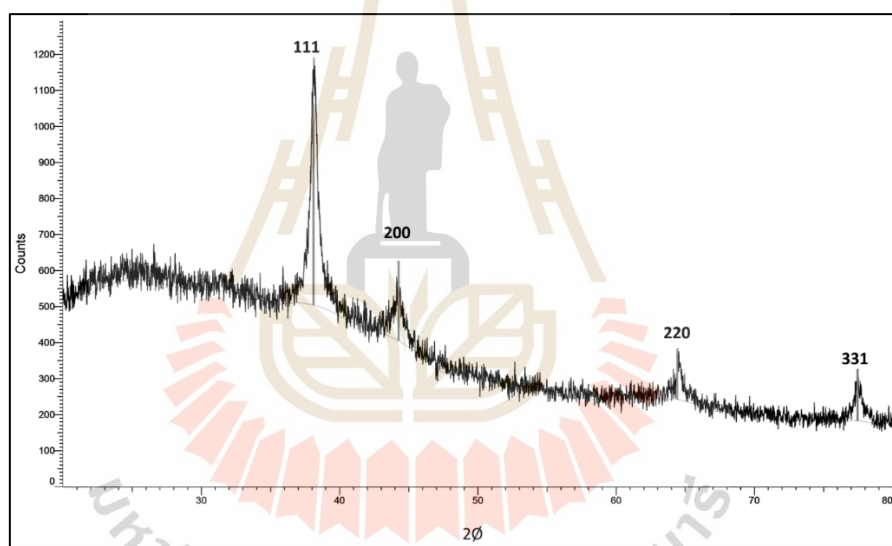


Figure 2.12 X-ray diffraction pattern of ES-AgNPs.

2.4.5 FT-IR analysis of synthesized AgNPs

The FTIR was carried out to determine the possible biomolecules responsible for reducing and capping AgNPs. The intracellular cell-free supernatant of *Streptomyces* sp. SSUT88A showed a maximum peak at 3371.7 cm^{-1} , correspond to the O-H stretching. The peak at 1594.98 cm^{-1} was a broad peak that correspond to O-H scissors which contain C-N stretching and N-H stretching. The C-H bending peak was

observed at 1405.92 cm^{-1} . Also, the C-O-C stretching was observed at 1082.14 cm^{-1} (Figure 2.13). In contrast, the IS-AgNPs showed maximum absorption peaks at 3476.01 that correspond to the O-H stretching, 1668.86 and 1629.75 correspond to the C=O stretching of amide I, 1382.02 cm^{-1} correspond to the C-N stretching of amide III, and 834.41 cm^{-1} correspond to the C-N stretching.

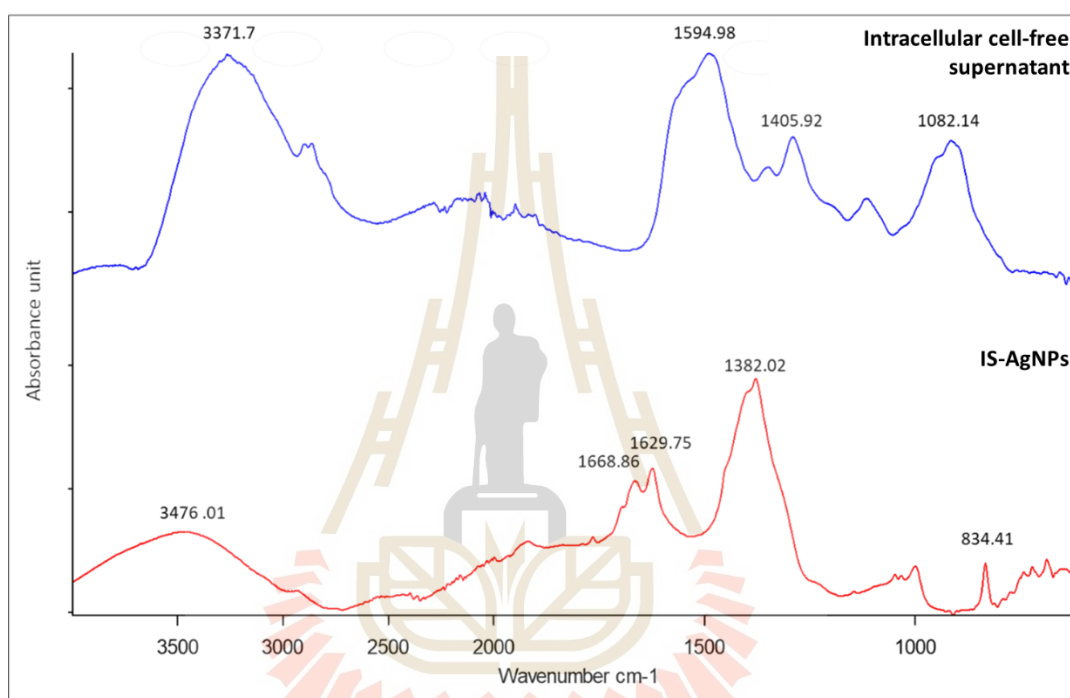


Figure 2.13 FTIR spectra of intracellular cell-free supernatant and IS-AgNPs of *Streptomyces* sp. SUT88A.

The FTIR spectra of extracellular cell-free supernatant of *Streptomyces* sp. SSUT88A and ES-AgNPs showed in Figure 2.14. In the extracellular cell-free supernatant, the absorption peaks at 3315.2 cm^{-1} correspond to the O-H stretching, 1592.8 cm^{-1} was a broad peak that correspond to O-H scissoring which contain C-N stretching and N-H stretching. The peak at 1408.1 cm^{-1} correspond to the C-H and

1073.4 cm^{-1} correspond to the C-O-C stretching were observed. On the other hand, the ES-AgNPs showed maximum absorption peaks at 3384.7, 1594.8, 1405.9, and 1079.9 cm^{-1} , which represent O-H stretching, O-H scissors, N-H stretching and C-O-C stretching, respectively.

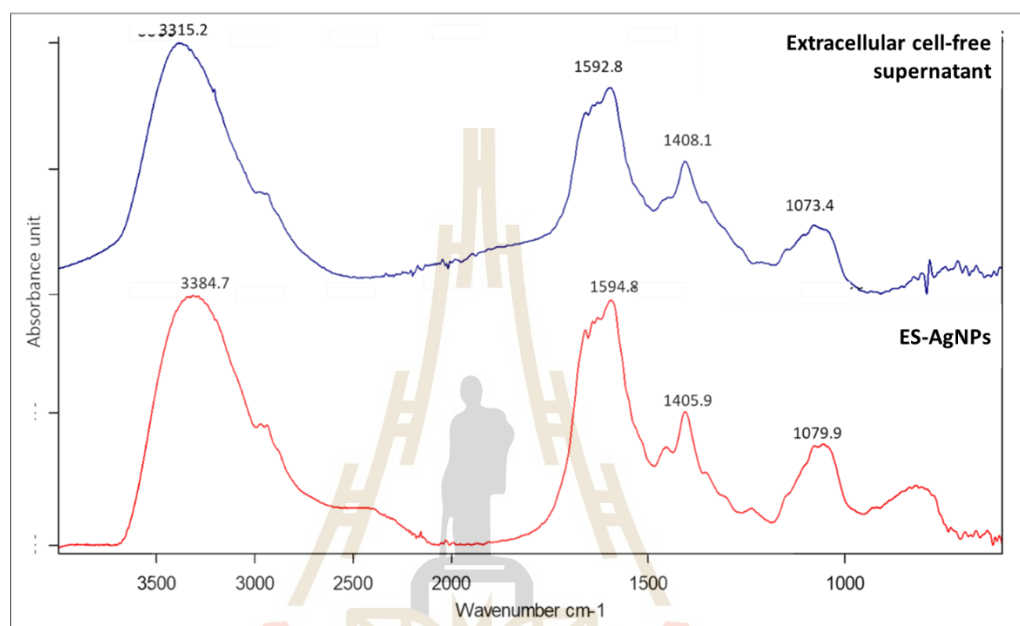


Figure 2.14 FTIR spectra of extracellular cell-free supernatant and ES-AgNPs of *Streptomyces* sp. SUT88A.

2.4.6 XANES analysis of synthesized AgNPs

The XANES was conducted to investigate the oxidation state of different synthesized AgNPs. The colloidal AgNPs sample was placed on thin-film for XAS investigation. AgNO_3 and Ag nanopowder (Sigma) was used as a standard for Ag^+ and Ag^0 , respectively. Different L_3 edge of XANES spectra profiles of AgNO_3 and Ag nanopowder obtained from the XANES measurement (Figure 2.15). This result proved that the silver in the AgNO_3 and Ag nanopowder was in a different state. The spectra

of IS-AgNPs and ES-AgNPs show a clear profile of similar spectrum to Ag nanopowder instead of AgNO₃. This XANES spectrum revealed that the silver in both synthesized AgNPs was in the form of nanoparticle. Therefore, the Ag⁺ was completely reduced into Ag⁰ during the synthesis process.

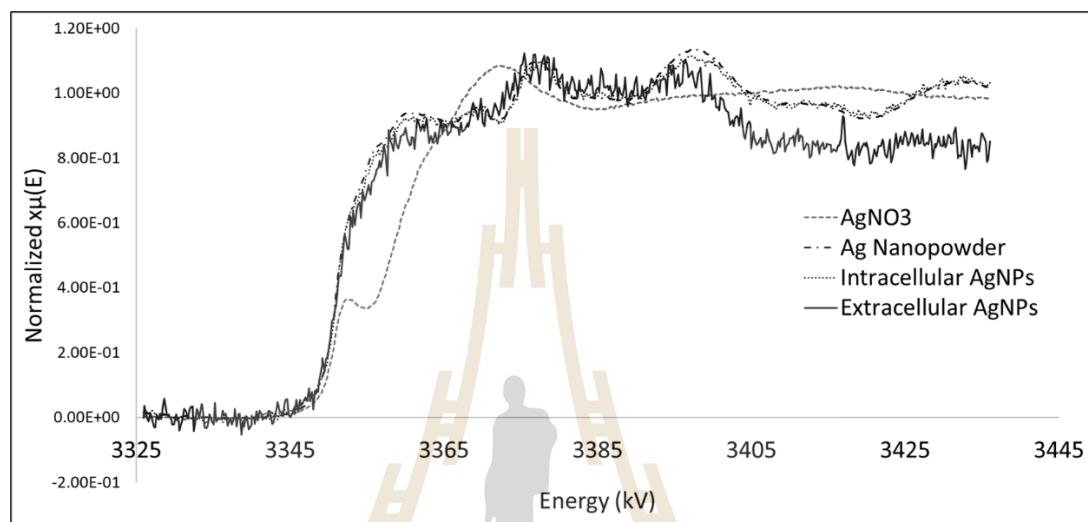


Figure 2.15 XANES spectra of L₃ edge of AgNO₃, Ag nanopowder, IS-AgNPs and ES-AgNPs photon energy.

2.4.7 TEM and EDXRF analysis of synthesized AgNPs

TEM was applied to determine the size and shape of synthesized AgNPs.

The TEM image of synthesized AgNPs from cell-free supernatant of *Streptomyces* sp. SSUT88A showed a spherical form. The size of the IS-AgNPs was varied, ranging from 6.1 to 23.75 nm, with an average size around 13.57 nm. While the size of the ES-AgNPs was significantly larger than intracellular AgNPs ($p < 0.05$). It was varying between 15.35 and 47.68 nm, with 30.47 nm on average, as shown in Figure 2.16. The obtained particle size was smaller than the obtained particle size from DLS.

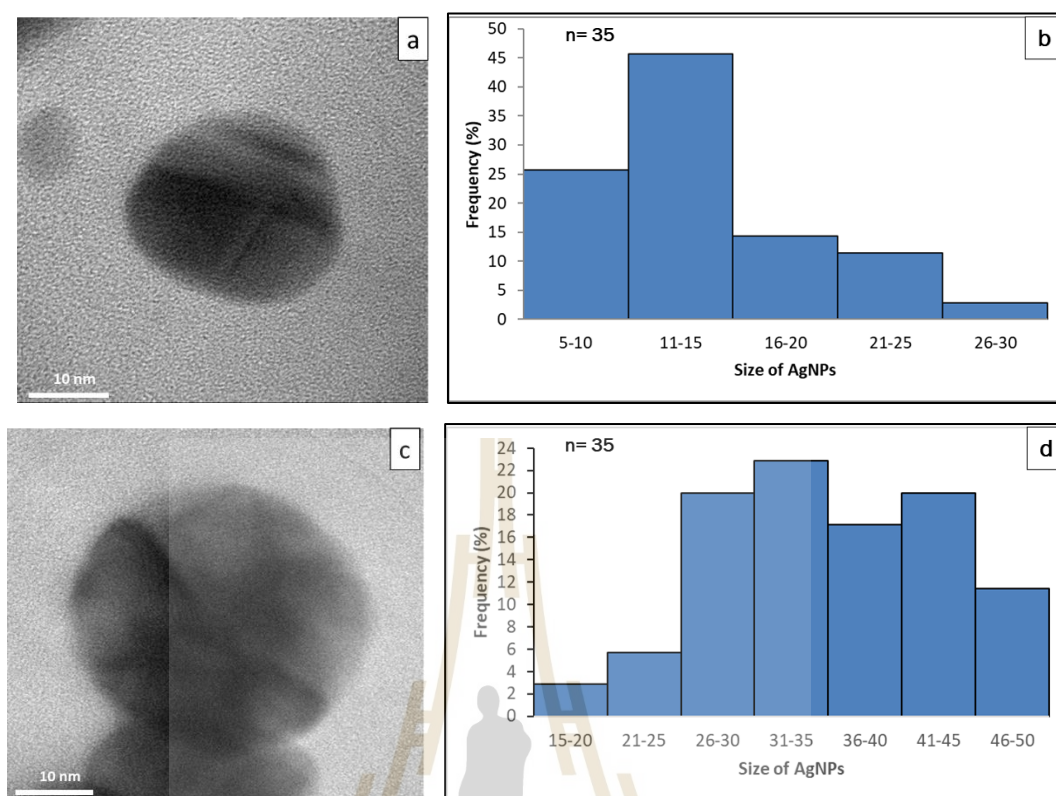


Figure 2.16 Morphology and size distribution of the synthesized AgNPs based on TEM imaging. a) morphology of IS-AgNPs; b) size distribution of IS-AgNPs; c) morphology of ES-AgNPs; and d) size distribution of ES-AgNPs. Scale bar = 10 nm, n = 35.

The dispersive energy of XRF was used to determine the elemental composition within the sample. The result exhibits clear identification of the elemental composition of Ag at 3 kV in both IS-AgNPs and ES-AgNPs. The amount of Ag in the IS-AgNPs was lower than ES-AgNPs. According to the EDXRF observation, the amount of Ag in the IS-AgNPs and ES-AgNPs was 21.93% and 49.09%, respectively. The signal of carbon (C), nitrogen (N), oxygen (O), silicon (Si), and phosphorus (P) was able to detect from both IS-AgNPs and ES-AgNPs (Figure 2.17). These elements

in the synthesized AgNPs due to a signal of enzymes or protein in the cell-free supernatant.

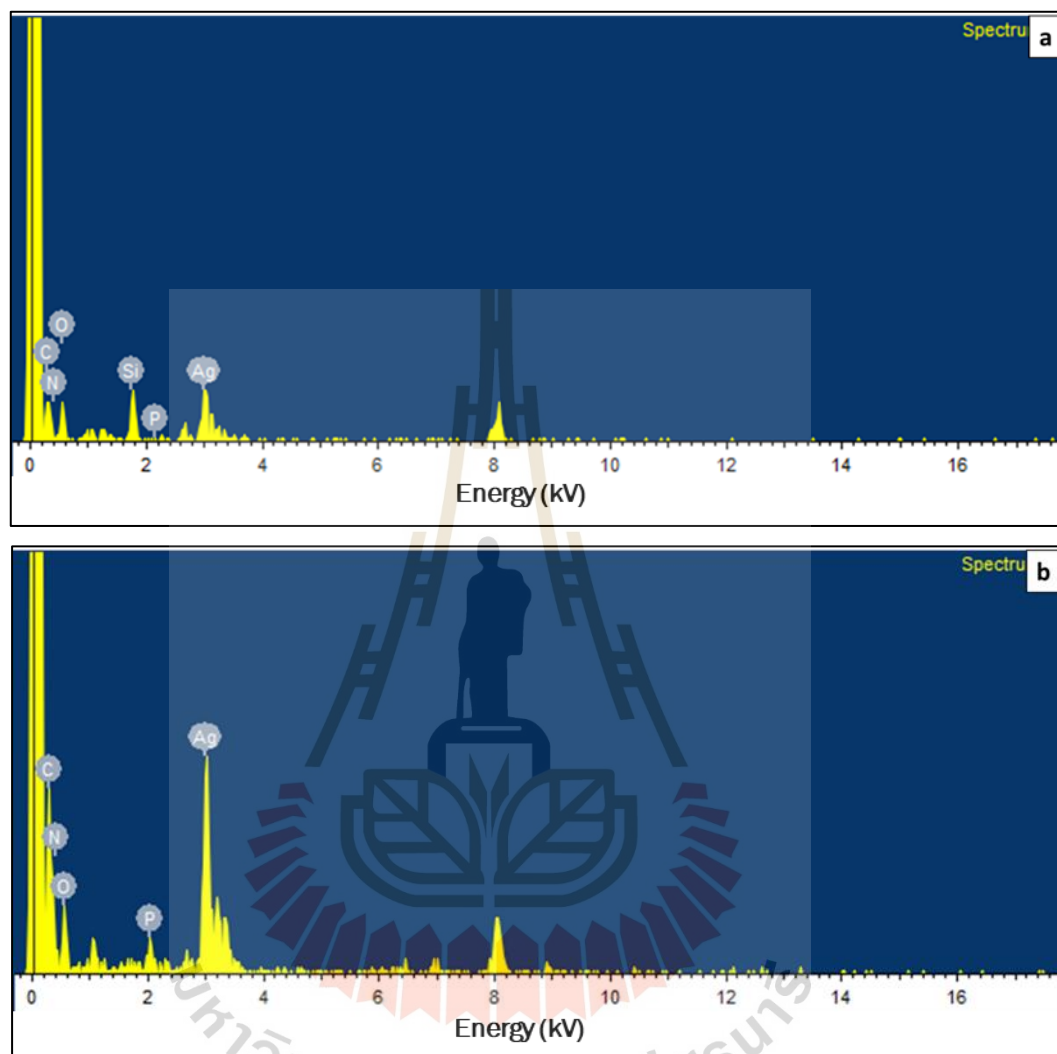


Figure 2.17 Energy dispersive spectra of AgNPs obtained from *Streptomyces* sp. SSUT88A. (a). IS-AgNPs and (b). ES-AgNPs.

2.4.8 Antimicrobial activity of AgNPs

The antibacterial activities of synthesized AgNPs from cell-free supernatant of *Streptomyces* sp. SSUT88A against selected bacterial showed in Table 2.3. The antimicrobial activity of synthesized AgNPs was performed using the agar well diffusion method. According to the EDXRF result, the amount of Ag in the IS-

AgNPs and ES-AgNPs was 21.93% and 49.09%, respectively. This data was used to prepare AgNPs samples for antimicrobial activity assay by adjusting each sample in the same concentration of AgNPs. The different fraction of the cell-free supernatant was not only producing the distinct character of AgNPs but also exhibit different antimicrobial activity. The inhibition zone of IS-AgNPs against clinical drug-resistant isolates *A. baumannii*, *K. pneumoniae* 1617, *P. aeruginosa* N90PS, *E. coli* 8465, and MRSA DMST 20654 was 20.3 ± 1.7 mm, 12.6 ± 1.5 mm, 20.3 ± 0.5 mm, 22 ± 1.7 mm, and 18.6 ± 0.5 mm, respectively. However, ES-AgNPs was active only against Gram-positive bacterium, MRSA DMST 20654, with an inhibition zone of 9.1 ± 1 mm. This antimicrobial activity against MRSA 20654 was similar to the antimicrobial activity of extracellular cell-free supernatant. Thus, the exerted antimicrobial activity of ES-AgNPs might derived from the supernatant.

Table 2.2 Comparison of antimicrobial activity of IS-AgNPs and ES-AgNPs

Drugs-resistant pathogen	Inhibition zone (mm)			
	Intracellular		Extracellular	
	AgNPs	Supernatant	AgNPs	Supernatant
<i>A. baumannii</i>	20.3 ± 1.7	0	0	0
<i>K. pneumoniae</i> 1617	12.6 ± 1.5	0	0	0
<i>P. aeruginosa</i> N90PS	20.3 ± 0.5	0	0	0
<i>E. coli</i> 8465	22 ± 1.7	0	0	0
MRSA DMST 20654	18.6 ± 0.5	0	9.1 ± 1	8.7 ± 0.5

2.4.9 Cytotoxicity assay of synthesized AgNPs

The cytotoxicity activity of synthesized AgNPs on NIH-3T3 mouse embryonic fibroblast cell lines was examined by the MTT assay method. After 24 hours of incubation, the result demonstrated that IS-AgNPs and ES-AgNPs significantly

reduced the viability of NIH-3T3 cells. There was no reduction in cell viability in the treatment of Ag nanopowder (Figure 2.18). However, the decrease of cell viability was much higher when cultivated in the presence of IS-AgNPs than ES-AgNPs. The result also revealed that the IS-AgNPs and ES-AgNPs were toxic to the NIH-3T3 cells.

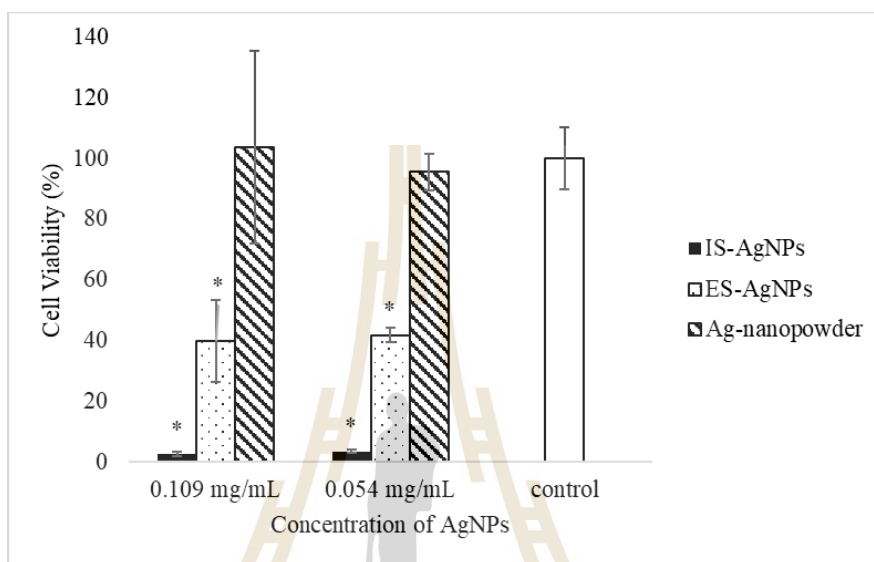


Figure 2.18 Cell viability of NIH-3T3 cell line after treated with AgNPs (n=3, p<0.05).

2.5 Discussion

Streptomyces species belong to the *Streptomycetaceae* family. They are abundant in soil habitat, especially in alkaline soil and the soil rich in organic matter. The members of this genus have been subjected to extensive isolation and screening due to their ability to produce a variety of bioactive metabolite such as antibacterial, antifungal, antiviral, anticancer, as well as several industrial important enzymes (Barka et al., 2016; Berdy, 2005; Labeda et al., 2012; Mehling et al., 1995). The presence of *Streptomyces* on the soil depends on the climate, surrounding area condition, and soil

quality (Harir et al., 2018). In this study, the *Streptomyces* sp. SSUT88A was isolated from a soil sample collected at Sekaerat Environmental Research Station, Thailand.

The rapid and accurate identification of bacterial isolate is needed. The use of phenotypic characteristics of bacteria for identification was not as precise as molecular identification. Thus, a 16s rRNA gene has been served as an essential tool to classify unknown bacterial isolate since this gene is highly conserved (Patel, 2001; Woo et al., 2008). There are several features of the 16s rRNA gene as a phylogenetic marker that used for the study of bacterial phylogeny and taxonomy, including the presence of 16s rRNA gene in almost all bacteria, the function of this gene has not easily changed over the time, and the length of 16s rRNA gene is large enough to provide distinctive and statistically valid measurements. The 16s rRNA gene consists of conserved and variable regions. The variable regions are applied to classify the group of bacteria (Clarridge, 2004; Janda and Abbott, 2007). Several unusual phenotypic bacteria, rare bacteria, and uncultured bacteria have been identified based on 16s rRNA gene sequence. In the past recent years, the PCR technique has been used to amplify the 16s rRNA gene sequence. The overall steps included DNA extraction, PCR amplification, purification of PCR product, DNA sequencing, and sequence analysis (Woo et al., 2008).

In the current study, the soil isolates *Streptomyces* sp. SSUT88A was identified based on the 16s rRNA gene. The assembly of 16s rRNA gene sequences produced 1419 nucleotides. *Streptomyces* sp. SSUT88A shows 98.8% similarity to *S. Chiangmaiensis* TA4-1^T. The phylogenetic tree of SSUT88A was constructed by using the neighbor-joining method. The neighbor-joining method was proposed for phylogenetic tree construction from evolutionary distance data. This method's principle

was to find the operational taxonomy unit (OTU) with minimum evolution. This method is also applicable to any evolutionary distance data (Saitou and Nei, 1987).

The increasing phenomena of antibiotic-resistant bacteria happen due to the continuous use of antibiotics throughout the world. With the emerge of this infection, it is essential to look for a novel alternative antimicrobial agent (Gurunathan et al., 2014; Thongkrachang et al., 2016). Currently, the application of nanotechnology is used not only in controlling the consumption of available antibiotics but also to combat antibiotic-resistant microorganisms (Banin et al., 2017). The most applied nanomaterials in the biomedical field are AgNPs that achieve remarkable attention as novel antimicrobial agents (Naqvi et al., 2013).

Nowadays, the preparation of AgNPs gaining significant interest due to their unique properties. There are three available approaches for the AgNPs synthesis, e.g., chemical, physical, and biological synthesis. Among these known methods, biological synthesis provides an eco-friendly approach without using hazardous substances (Iravani et al., 2014; Manikprabhu and Lingappa, 2013). *Streptomyces* have been proved as nano factories for developing non-toxic and clean procedures to synthesis of silver and gold nanoparticles (Harir et al., 2018). Due to the surface plasmon resonance of metal nanoparticle, the AgNPs exhibit striking colors from light yellow to brown during the synthesis. The appearance color change is a clear indicator of the reduction of Ag^+ to Ag^0 (Sastry et al., 2014). Abd-Elnaby et al. reported the color changes from yellow to brown on the biosynthesis of AgNPs using *S. rochei* MHM13 cell-free supernatant after 5 days incubation. Mohamedin et al. had also shown a similar observation in the extracellular mechanism synthesis of AgNPs by *S. viridodiatisticus* SSHH-1. In the current study, the UV-Vis absorbance was used to indicate the synthesis

process (Data in appendix). The different incubation time was observed for the synthesis of AgNPs between intracellular and extracellular cell-free supernatant. The synthesis of AgNPs from intracellular cell-free supernatant require 5 days incubation. While 2 days of incubation was required for the synthesis of AgNPs using extracellular cell-free supernatant. This process tends to take longer than the biosynthesis of silver nanoparticles using other reducing agents such as using cell-free supernatant of *Streptomyces* sp. BU3, which only takes 30 minutes for the synthesis of AgNPs (Krishnakumar and Bai, 2015). After the incubation of cell-free supernatant of *Streptomyces* sp. SSUT88A with 1 mM AgNO₃ showed a change of the solution color from light-yellow to brown. This evidence was a clear indicator of reduction Ag⁺ to Ag⁰ through reducing agents that contain in the cell-free supernatants of *Streptomyces* sp. SSUT88A. The exact mechanism of Ag⁺ reduction into Ag⁰ remains unclear. Several researchers proposed nicotinamide adenine dinucleotide (NADH) and reduced form of nicotinamide adenine dinucleotide phosphate (NADPH) that released from bacterial cells play a significant role as reducing agent (Kumar et al., 2007; Mukherjee et al., 2018; Ovais et al., 2018; Talekar et al., 2016).

For the primary characterization of synthesized AgNPs, UV-Vis spectroscopy was used because it is an easy and reliable technique to monitor the synthesis and stability of AgNPs. The absorbance of AgNPs ranges from 380 to 450 nm, which corresponds to the SPR absorbance of AgNPs (Coronado et al., 2011; Zhang et al., 2016). Abd-Elnaby et al. mentioned that the synthesis of AgNPs using *S. rochei* MHM13 shows the maximum absorbance at 410 nm. Similar results were also shown by Faghri Zonooz and Salouti (2011) and Abirami and Kannabiran (2016). In the current study, both IS-AgNPs and ES-AgNPs exhibit a sharp peak at 418 and 422 nm,

respectively, which confirm the presence of AgNPs. The increase of absorbance in the ES-AgNPs indicated an increase in the number of particles that absorb the UV-Vis. The λ_{\max} of the samples reflects an alteration of size, shape, and the scattering color of AgNPs. As diameter increases, the peak plasmon resonance of AgNPs is broader and shifted to longer wavelengths (Brause et al., 2002; Coronado et al., 2011; Evanoff and Chumanov, 2004; Lee and Jun, 2019; Paramelle et al., 2014).

Zeta potential analysis was used to determine the long-term stability of nanoparticles and surface charge of the nanoparticles. The value of nanoparticles zeta potential ranges from +100 mV to -100 mV. A stable nanoparticle shows the zeta potential value of more than +30 mV or less than -30 mV (Honary and Zahir, 2013; Saeb et al., 2014; Zhang et al., 2008). The negative or positive value of zeta potential was determined by the capping or stabilizing agent used during the synthesis. Tamiyakul et al. reported that the use of poly(4-styrene sulfonic acid-co-maleic acid) (PSSMA) as a capping agent for the chemical synthesis AgNPs gives a higher zeta potential value than uncapping AgNPs. A higher value of zeta potential leads to an increase in stability due to the electrostatic interaction (El Badawy et al., 2011; Tamiyakul et al., 2015). In the biological synthesis of AgNPs using red algae *Poryphyraa vietnamensis*, the presence of polysaccharide was not only involved in the reduction of AgNO₃, but also contributed to the electrostatic stability of the particles. The stability of the AgNPs from red algae was indicated by the presence of anionic polysaccharide as a capping agent and zeta potential value -35.05 mV (Venkatpurwar and Pokharkat, 2011). The negative zeta potential value was also reported by Scandorieiro et al. (2016) on the biosynthesis of AgNPs using *Fusarium oxysporum* and Ningnanagouda et al. (2014) on the biosynthesis AgNPs using *Aspergillus niger*. In

the current study, the zeta potential value of IS-AgNPs and ES-AgNPs was -32 mV and -27.9 mV, respectively. The zeta potential measurement suggested that the surface charge of both AgNPs are negative and well dispersed in the water. Thus, the different cell-free supernatant used for the synthesis of AgNPs also reflected the changes in zeta potential value due to the presence of the biological molecules that involved in the capping and stabilizing agents. The presence of stabilizing agents from the cell-free supernatant was one of the advantages of using the biological method to synthesize AgNPs since it can prevent the AgNPs from aggregation. the result of this study indicated the ES-AgNPs were less stable since their zeta potential value was lower than IS-AgNPs.

XRD analysis was used to identify the crystalline structure at the atomic scale of nanomaterials. The principle of XRD is when X-ray light reflects on any crystal, it will lead to the formations of several diffraction patterns. This pattern indicates a reflection of the physio-chemicals characteristics of the materials (Zhang et al., 2016). The crystalline structure of both synthesized AgNPs was further confirmed using XRD. The result revealed the formation of AgNPs in both of the AgNPs samples by the expression of diffraction peak of AgNPs that correspond to reflection (111), (200), (220), and (331) of face-centered cubic (FCC) structure of metallic silver. This finding was in similar to the report of synthesized AgNPs by biological method (Anandalakshmi et al., 2016; Chauhan et al., 2013; de Barros et al., 2018; Naqvi et al., 2013; Néilly et al., 2017; Syed et al., 2016).

In the synthesis of AgNPs, it is important to understand the kinetics of the reaction and know the nature of the metal form present in the synthesized AgNPs. XAS was useful in revealing the chemical state of an element by determining the local atomic

coordination and oxidation state of materials. This method gives information on the relative structure to a known atomic type and type of the surrounding atom by measuring the dependence energy of their electron scattering factors. The principle of XAS, the x-ray will hit an atom in the sample that causing excitation or ejection of a core electron. Then, the absorption can be qualified by measuring the fluorescent emitted by the excited electron. The XAS includes two main components, which are extended absorption fine structure (EXAFS) and X-ray absorption near-edge spectroscopy (XANES). The EXAFS provides more structural information of neighboring an element, whereas XANES reveals the chemical state of the element (Calvin, 2013; Koningsberger and Prins, 1988; Parra Berumen et al., 2009). Therefore, XANES spectroscopy is a powerful tool for probing the oxidation state and coordination environment of a chosen element. The result of XANES showed that the synthesized AgNPs are in the metallic nanoparticle states, without any AgNO₃ component. The Ag⁺ from AgNO₃ was successfully reduced to Ag⁰ in both IS-AgNPs and ES-AgNPs. Because both of AgNPs have a similar pattern of energy as Ag nanopowder (SIGMA). The different profile energy of XANES spectra between AgNO₃ and AgNPs was also reported by Godfrey et al. (2020) on reducing AgNO₃ by citrate. Therefore, the XAS is a useful tool for the analysis of nanoparticle structure.

The potential biomolecules present in the synthesized AgNPs that responsible for reducing Ag⁺ to Ag⁰ was analyzed using FT-IR. The functional group that appears in the AgNPs might act simultaneously as a reducing, stabilizing, and capping agents (Gurunathan et al., 2014). The biomolecules that present in the cell-free supernatant of bacteria, such as protein, enzymes, inorganic complexes, and bio-surfactants, serve as reducing agents and capping or stabilizing agents (Abdelghany et al., 2018; Siddiqi et

al., 2018). Mohamedin et al. (2014) reported that the presence of an amine group from the FTIR spectra of synthesized AgNPs using *Streptomyces viridodiastaticus* SSHH-1 indicated the presence of proteins that released into the cell-free supernatant involved in the reduction agent and acts simultaneously as a capping agent. The presence of a capping agent gives an advantage to AgNPs because it can prevent the particles from aggregation or agglomeration (Abirami and Kannabiran, 2016). Based on the FTIR results, it was known that the protein involves in the synthesis of IS-AgNPs. However, a shift in several peaks after the formation of IS-AgNPs was observed. The O-H and C-O-C stretching peaks at 3371 and 1082 cm^{-1} region which have been found to appear at 3476 and 841 cm^{-1} in the IS-AgNPs. The broad peak at 1594 cm^{-1} was changed to amide I form at 1668 and 1629 cm^{-1} . A band at 1405 cm^{-1} has been assigned to C-N stretching of amide III was to 1382 cm^{-1} . On the other hand, O-H stretching, O-H scissors containing C-H and N-H stretching, and C-O-C stretching were observed from extracellular cell free supernatant and ES-AgNPs. The band of each functional groups of ES-AgNPs were appeared in the same region of spectrum as extracellular cell-free supernatant. These spectral results suggest that protein involved in the reduction and stabilization of AgNPs in aqueous conditions.

TEM is the most valuable tool to study the size and morphology of nanoparticle (Gurunathan et al., 2014). The result showed that the shape of both synthesized AgNPs were spherical. A spherical shape is a common form of biological synthesis AgNPs by microbes (Mohamedin et al., 2015; Shivaji et al., 2011). A spherical shape of synthesized AgNPs was similar to the report of Abirami and Kanabiran (2017), Abd-Elnaby et al. (2016), and Karthik et al. (2014), who synthesis AgNPs via *S. ghanaensis* VITHM1, *S. rochei* MHM13, and *Streptomyces* sp. LK3, respectively. Our result also

indicated that different cell-free supernatant used for a synthesis produces different sizes of AgNPs. The size of the ES-AgNPs was larger than IS-AgNPs from the TEM image. This result was correlated to the size obtained from the DLS: 77.03 nm for IS-AgNPs and 82.44 nm for ES-AgNPs. However, the average size of the AgNPs obtained in DLS was larger than the calculated size from TEM. Anandhalakshmi et al. (2006) had shown a similar observation on the determination particle size of AgNPs synthesized from *Pedarium murex* leaf extract using TEM and DLS. The particles size measured by DLS was larger than measured by TEM. It is probably due to the size of particles that measured by DLS includes the hydrodynamic size of the particle. The hydrodynamic sized measured by DLS defined as the size of hypothetical sphere with the same translational diffusion coefficient as the measured particle, assuming a hydration layer surrounding the particle (de Barros et al., 2018). The factors that affect the size and shape of nanoparticles are the type of reducing agent, the concentration of reducing agents, and temperature during the synthesis (Kim et al., 2016; Pillai and Kamat, 2004). Therefore, the different sizes between IS-AgNPs and ES-AgNPs might be caused by different reducing agents present in the cell-free supernatant.

To analyze the chemical composition of synthesized AgNPs, the EDXRF was used. This technique was used to determine the relative element composition of the sample, where calibration and samples of known concentrations do not exist. Both of synthesized AgNPs generated the Ag spectrum on 3 kV. The Ag spectrum between 3-4 kV indicates a signal for metallic silver (Mohamedin et al., 2015). The presence of Ag in the ES-AgNPs was two times higher than IS-AgNPs. Other components, such as carbon, nitrogen, sodium, and silica detected in the colloidal sample of AgNPs, might come from cell-free supernatant.

The nanoparticles are known as relatively toxic than larger material. The surface properties of AgNPs including size, shape, surface charge, stability and capping or stabilizing agents play an important role to the interaction with a microorganism or other cell that give an effect to the antimicrobial and toxicity properties (Niska et al., 2016; Mohanty et al., 2012; Siddiqi et al., 2018). It has been known that the smaller nanoparticles the higher bactericidal effect. Since the smaller nanoparticles have a large surface area for interaction with bacterial cells and they can easily adhere to the bacterial cell components (Gurunathan et al., 2014; Prabhu and Poulose, 2012; Siddiqi et al., 2018). In the current study, the ES-AgNPs only inhibit the MRSA DMST 20654, while IS-AgNPs inhibit *A. baumannii*, *K. pneumoniae* 1617, *P. aeruginosa* N90PS, *E. coli* 8465, and MRSA DMST 20654. No antimicrobial activity was observed from intracellular cell-free supernatant. On the other hand, the extracellular cell-free supernatant only showed antimicrobial activity against MRSA DMST 20654. This antimicrobial activity was possibly due to the antimicrobial activity of *Streptomyces* sp. SSUT88A against Gram-positive bacteria as shown on the appendix page. The different antimicrobial activity of the synthesized AgNPs could be due to the different size, capping agent, surface charge, stability of materials and type of pathogens. The particle size of IS-AgNPs is smaller than ES-AgNPs, in consequence the IS-AgNPs might provide better antimicrobial activity compared to the ES-AgNPs. The presence of biological molecules in the cell-free supernatant used for the synthesis play role as capping and stabilization agents and gave a difference in the zeta potential value which led to the stability of the AgNPs. The IS-AgNPs were more stable than ES-AgNPs based on zeta potential value. Hence, different capping or stabilizing agents, surface charge, and stability on the synthesized IS-AgNPs and ES-AgNPs serve different

antimicrobial activity. The antimicrobial activity of AgNPs against resistant pathogens was previously reported by Yuan and co-workers (2017). They synthesized AgNPs using quercetin showed excellent antimicrobial activities against the MDR *S. aureus* and *P. aeruginosa*. Recently, spherical AgNPs were produced using *Penicillium polonicum* and present antimicrobial activity against MDR *A. baumannii* (Neethu et al., 2018). Therefore, the AgNPs can be used as a promising antimicrobial agent against multidrug resistant bacteria.

Several studies have proposed that the mechanism of the bactericidal effect of AgNPs is due to the binding of AgNPs to the surface of the bacterial cell membrane, thus disrupting the cell permeability. The binding of AgNPs to the cell membrane also impair bacterial respiration leading to an increase in ROS generation (Gurunathan et al., 2014; Manikprabhu and Lingappa, 2013; Prabhu and Poulose, 2012; Siddiqi et al., 2018). Several investigations have reported that the surface charge of AgNPs affects to the bactericidal properties, especially in the interaction with bacterial cells. The positive charge of AgNPs was most effective, while the negative charge of AgNPs was least effective (Abbaszadegan et al., 2015; El Badawy et al., 2011). Related to the negative zeta potential of AgNPs, Maillard et al. (2018) reported that the zeta potential of the *E. coli* membrane became more negative by the interaction with negative zeta potential AgNPs. The increase of negative charge indicating interfacial interaction where AgNPs keep absorbed to the membrane via the insertion of capping agents of AgNPs into the bilayer lipid of bacteria. The interaction of AgNPs with the bacterial cell membranes might also inhibit bacterial cell proliferation by damaging the cell structure, including cell envelope, cytoplasmic membrane, and the membrane's content. When AgNPs enter the cell, they could bind to cellular structures and biomolecules such as DNA, proteins,

and lipids. The interaction of AgNPs with DNA leads to DNA condensation and loss of their replication abilities. Additionally, the interaction of AgNPs with ribosomes may cause denaturation of ribosomes leading to the inhibition of translation and protein synthesis (Dakal et al., 2016; Feng et al., 2000; Mohamed et al., 2020a; Woo et al., 2008). Mohamed et al. (2020) reported that the penetration of AgNPs to the *E. coli* cells could cause cell damage. Wintachai et al. (2019) reported that the AgNPs synthesized from *Eucalyptus citriodora* triggered DNA condensation and bacterial cell death on MDR *A. baumannii*. The biosynthesis of AgNPs from quercetin cause an increase in the production of ROS and leakage of protein and sugar on multidrug-resistant *P. aeruginosa* and *S. aureus* (Yuan et al., 2017).

Cytotoxicity study of AgNPs was conducted using NIH-3T3 mouse embryonic fibroblast cell lines and examined by MTT assay. MTT is a common method used for in vitro cytotoxicity evaluation of nanoparticles. Therefore, this result could provide information on the potential risk of AgNPs to humans, especially in the development of safe practices for the application of AgNPs. The result revealed that synthesized AgNPs produced toxicity by significantly reducing the cell viability of NIH-3T3 cells. While the treatment of Ag nanopowder was not toxic as the percentages of cell viability were not significantly different compared to the negative control. The treatment of IS-AgNPs reduces almost 100% of NIH-3T3 cell viability in both concentrations used. While 50.4% and 51.7% of cell viability were observed after treated with 0.109 mg/mL and 0.054 mg/mL of ES-AgNPs, respectively. Thus, the IS-AgNPs provide higher cytotoxicity to the NIH-3T3 cell lines than ES-AgNPs. The cytotoxic activity of biosynthesized AgNPs using myricetin on NIH-3T3 cells was reported before by Gurunathan et al. (2018). The treatment of AgNPs induced loss in cell proliferation and

cell viability in a dose-dependent manner. Lee et al. (2014) and Sambale et al. (2015) were also shown similar observations on the cytotoxic activity of AgNPs against NIH-3T3 cell lines. Carlson et al. (2008) had also reported that smaller particle (15 nm) exhibited higher toxicity than bigger size (55 nm). The toxicity was indicated by the decreased cell viability of alveolar macrophage which also followed by the increase of ROS generation. The toxicity was also reported in a dose-dependent manner. Furthermore, Kim et al. (2012) found that 10 nm AgNPs were more toxic to the MC3T3-E1 mouse osteoblast cell lines than 50 nm and 100 nm AgNPs. The toxicity of AgNPs into mammalian cell lines was depended on the capping agents and cell type. Netchareonsirisuk et al. (2016) reported that alginate-capped AgNPs provide higher toxicity to A375 human melanoma cell lines than CCD-986SK human normal skin fibroblast cells. In the current study, low toxicity of Ag nanopowder compared to the synthesized AgNPs can be explained in the term of different size and capping agent. It was known that the size of Ag nanopowder, IS-AgNPs, and ES-AgNPs was around 100 nm, 13.57 nm, and 30.47 nm, respectively with different capping agents. Thus, the differences in the cytotoxic activity of both AgNPs and Ag nanopowder could be due to the different size, capping and stabilizing agent of each.

Liao et al. (2019) mentioned that the cellular uptake of AgNPs might occur via translocation, endocytosis, or phagocytosis. When the cell was exposed to AgNPs, the AgNPs will attach to the cell membrane and internalized into cells. The AgNPs were reported to be accumulated in the cytoplasm and gathered in the perinucleus of human embryonic stem cell-derived fibroblast and L-929 cells (Peng et al., 2012). Another report mentioned that the treatment of AgNPs to NIH-3T3 cells caused alteration in cell morphology, including shrinkage, few cellular extensions, and accumulation of AgNPs

in the cytoplasm (Lee et al., 2014). The internalization of AgNPs into the cytoplasm can generate ROS, leading to DNA damage, protein denaturation, and apoptosis. The accumulation of AgNPs in mitochondria induces mitochondrial dysfunction by reducing mitochondrial membrane potential and ROS generation (Liao et al., 2019). Usually, the increase of cellular ROS level are followed by the depletion of glutathione (GSH), mitochondrial dysfunction, increased malondialdehyde (MDA) levels, decreased antioxidants levels, and release of lactate dehydrogenase (LDH) that lead to the protein and DNA damage (Carlson et al., 2008; Gurunathan et al., 2018; Hsin et al., 2008; Hussain et al., 2005; Liao et al., 2019). Moreover, the interaction of AgNPs with membrane protein caused activation of signalling pathways which led to the cell proliferation inhibition (Liao et al., 2019). In NIH-3T3 cells, the treatment of AgNPs induced apoptosis, indicated by the release of cytochrome *c* into the cytosol and translocation of Bax to mitochondria (Hsin et al., 2008). The cytotoxicity of AgNPs was also reported against several cancer cells, such as human cervical cancer cell (HeLa), MCF-7 human breast cancer, HCT116 colon cancer cells, and A549 lung cancer cell (Al-Sheddi et al., 2018; Al Sufyani et al., 2019; Gomathi et al., 2020; Mfouo-Tynga et al., 2014). Hence, the cytotoxicity of AgNPs could be due to the size-, dose-, and time-dependent caused by ROS generation, oxidative stress, and DNA damage. Moreover, due to the cytotoxic activity of IS-AgNPs, it gives an opportunity to be used as promising anticancer agents. Therefore, it suggested to test the cytotoxic activity of IS-AgNPs against several cancer cells for the future work.

In conclusion, the soil sample *Streptomyces* were successfully isolated and identified based on molecular technique using the 16s rRNA gene sequence. The *Streptomyces* sp. SSUT88A exhibits 98.8% similarity to *S. Chiangmaiensis* TA4-1^T.

Streptomyces sp. SSUT88A has been exploited for the synthesis of AgNPs. The ES-AgNPs show a larger size compared to the IS-AgNPs in both TEM and zeta sizer analysis. The IS-AgNPs showed antimicrobial activity against clinical isolate *A. baumannii*, *K. pneumoniae* 1617, *P. aeruginosa* N90PS, *E. coli* 8465, and MRSA DMST 20654. While the ES-AgNPs only show antimicrobial activity against MRSA DMST 20654. Furthermore, the IS-AgNPs produce higher cytotoxicity to NIH-3T3 cell lines than ES-AgNPs.

2.6 References

- Abbaszadegan, A., Ghahramani, Y., Gholami, A., Hemmateenejad, B., Dorostkar, S., Nabavizadeh, M., and Sharghi, H. (2015). The effect of charge at the surface of silver nanoparticles on antimicrobial activity against gram-positive and gram-negative bacteria: A preliminary study. **Journal of Nanomaterials**. 2015(September 2014). <https://doi.org/10.1155/2015/720654>.
- Abd-Elnaby, H. M., Abo-Elala, G. M., Abdel-Raouf, U. M., and Hamed, M. M. (2016). Antibacterial and anticancer activity of extracellular synthesized silver nanoparticles from marine *Streptomyces rochei* MHM13. **Egyptian Journal of Aquatic Research**. 42(3): 301–312. <https://doi.org/10.1016/j.ejar.2016.05.004>.
- Abdelghany, T. M., Al-Rajhi, A. M. H., Al Abboud, M. A., Alawlaqi, M. M., Ganash Magdah, A., Helmy, E. A. M., and Mabrouk, A. S. (2018). Recent advances in green synthesis of silver nanoparticles and their applications: about future directions. A Review. **BioNanoScience**. 8(1): 5–16. <https://doi.org/10.1007/s12668-017-0413-3>.

- Abirami, M., and Kannabiran, K. (2016). *Streptomyces ghanaensis* VITHM1 mediated green synthesis of silver nanoparticles: Mechanism and biological applications. **Frontiers of Chemical Science and Engineering**. 10(4): 542–551. <https://doi.org/10.1007/s11705-016-1599-6>.
- Ahamed, M., AlSalhi, M. S., and Siddiqui, M. K. J. (2010). Silver nanoparticle applications and human health. **Clinica Chimica Acta**. 411(23–24): 1841–1848. <https://doi.org/10.1016/j.cca.2010.08.016>.
- Alexander, J. W. (2009). History of the medical use of silver. **Surgical Infections**. 10(3): 289–292. <https://doi.org/10.1089/sur.2008.9941>.
- Al-Sheddi, E. S., Farshori, N. N., Al-Oqail, M. M., Al-Massarani, S. M., Saquib, Q., Wahab, R., Musarrat, J., Al-Khedhairi, A. A., and Siddiqui, M. A. (2018). Anticancer potential of green synthesized silver nanoparticles using extract of *Nepeta deflersiana* against human cervical cancer cells (HeLA). **Bioinorganic Chemistry and Applications**. 2018: 1–12. <https://doi.org/10.1155/2018/9390-784>.
- Al Sufyani, N. M., Hussien, N. A., and Hawsawi, Y. M. (2019). Characterization and anticancer potential of silver nanoparticles biosynthesized from *Olea chrysophylla* and *Lavandula dentata* leaf extracts on HCT116 colon cancer cells. **Journal of Nanomaterials**. 2019: 1–9. <https://doi.org/10.1155/2019-7361695>.
- Anandalakshmi, K., Venugobal, J., and Ramasamy, V. (2016). Characterization of silver nanoparticles by green synthesis method using *Pedaliium murex* leaf extract and their antibacterial activity. **Applied Nanoscience (Switzerland)**. 6(3): 399–408. <https://doi.org/10.1007/s13204-015-0449-z>.

- Banin, E., Hughes, D., and Kuipers, O. P. (2017). Editorial: Bacterial pathogens, antibiotics and antibiotic resistance. **FEMS Microbiology Reviews**. 41(3): 450–452. <https://doi.org/10.1093/femsre/fux016>.
- Bansod, S. D., Bawaskar, M. S., Gade, A. K., and Rai, M. K. (2015). Development of shampoo, soap and ointment formulated by green synthesised silver nanoparticles functionalised with antimicrobial plants oils in veterinary dermatology: Treatment and prevention strategies. **IET Nanobiotechnology**. 9(4): 165–171. <https://doi.org/10.1049/iet-nbt.2014.0042>.
- Barka, E. A., Vatsa, P., Sanchez, L., Nathalie Gaveau-Vaillant, C. J., Klenk, H.-P., Clément, C., Ouhdouch, Y., and P. van Wezeld, G. (2016). Taxonomy, Physiology and natural product of Actinobacteria. **American Society for Microbiology**. 80(1): 1–43. <https://doi.org/10.1128/MMBR.00019-15>.Address.
- Barros, Caio H.N., Fulaz, S., Stanisc, D., and Tasic, L. (2018). Biogenic nanosilver against multidrug-resistant bacteria (MDRB). **Antibiotics**. 7(3): 1–24. <https://doi.org/10.3390/antibiotics7030069>.
- Berdy, J. (2005). Bioactive microbial metabolites a personal view. **The Journal of Antibiotics**. 58(1): 1–26.
- Brause, R., Moltgen, H., and Kleinermanns, K. (2002). Characterization of laser-ablated and chemically reduced silver colloids in aqueous solution by UV/VIS spectroscopy and STM/SEM microscopy. **Applied Physics B**. 75: 711–716. <https://doi.org/10.1007/s00340-002-1024-3>.
- Calvin, S. (2013). XAFS for everyone. CRC Press.

- Carlson, C., Hussein, S. M., Schrand, A. M., Braydich-Stolle, L. K., Hess, K. L., Jones, R. L., and Schlager, J. J. (2008). Unique cellular interaction of silver nanoparticles: Size-dependent generation of reactive oxygen species. **Journal of Physical Chemistry B**. 112(43): 13608–13619. <https://doi.org/10.1021/jp7-12087m>.
- Carter, M. J., Tingley-Kelley, K., and Warriner, R. A. (2010). Silver treatments and silver-impregnated dressings for the healing of leg wounds and ulcers: A systematic review and meta-analysis. **Journal of the American Academy of Dermatology**. 63(4): 668–679. <https://doi.org/10.1016/j.jaad.2009.09.007>.
- Cavassin, E. D., de Figueiredo, L. F. P., Otoch, J. P., Seckler, M. M., de Oliveira, R. A., Franco, F. F., Marangoni, V. S., Zucolotto, V., Levin, A. S. S., and Costa, S. F. (2015). Comparison of methods to detect the in vitro activity of silver nanoparticles (AgNP) against multidrug resistant bacteria. **Journal of Nanobiotechnology**. 13(1): 1–16. <https://doi.org/10.1186/s12951-015-0120-6>.
- Chauhan, R., Kumar, A., and Abraham, J. (2013). A biological approach to the synthesis of silver nanoparticles with *Streptomyces* sp. JAR1 and its antimicrobial activity. **Scientia Pharmaceutica**. 81(2): 607–621. <https://doi.org/10.3797/scipharm.1302-02>.
- Clarridge, J. E. (2004). Impact of 16S rRNA gene sequence analysis for identification of bacteria on clinical microbiology and infectious diseases. **Clinical Microbiology Reviews**. 17(4): 840–862. <https://doi.org/10.1128/CMR.-17.4.840-862.2004>.

- Coronado, E. A., Encina, E. R., and Stefani, F. D. (2011). Optical properties of metallic nanoparticles: Manipulating light, heat and forces at the nanoscale. **Nanoscale**. 3(10): 4042–4059. <https://doi.org/10.1039/c1nr10788g>.
- Dakal, T. C., Kumar, A., Majumdar, R. S., and Yadav, V. (2016). Mechanistic basis of antimicrobial actions of silver nanoparticles. **Frontiers in Microbiology**. 7(NOV): 1–17. <https://doi.org/10.3389/fmicb.2016.01831>.
- de Barros, Caio Henrique Nasi, Cruz, G. C. F., Mayrink, W., and Tasic, L. (2018). Bio-based synthesis of silver nanoparticles from orange waste: Effects of distinct biomolecule coatings on size, morphology, and antimicrobial activity. **Nanotechnology, Science and Applications**. 11: 1–14. <https://doi.org/10.2147-/NSA.S156115>.
- Eby, D. M., Luckarift, H. R., and Johnson, G. R. (2009). Hybrid antimicrobial enzyme and silver nanoparticle coatings for medical Instruments. **ACS Applied Materials and Interfaces**. 1(7): 1553–1560. <https://doi.org/10.1021/am900-2155>.
- El Badawy, A. M., Silva, R. G., Morris, B., Scheckel, K. G., Suidan, M. T., and Tolaymat, T. M. (2011). Surface charge-dependent toxicity of silver nanoparticles. **Environmental Science and Technology**. 45(1): 283–287. <https://doi.org/10.1021/es1034188>.
- Elechiguerra, J. L., Burt, J. L., Morones, J. R., Camacho-Bragado, A., Gao, X., Lara, H. H., and Yacaman, M. J. (2005). Interaction of silver nanoparticles with HIV-1. **Journal of Nanobiotechnology**. 3: 1–10. <https://doi.org/10.1186/1477-3155-3-6>.

- Evanoff, D. D., and Chumanov, G. (2004). Size-Controlled Synthesis of Nanoparticles. 2. Measurement of Extinction, Scattering, and Absorption Cross Sections. *The Journal of Physical Chemistry B*. 108(37): 13957–13962. <https://doi.org/10.1021/jp0475640>.
- Faghri Zonooz, N., and Salouti, M. (2011). Extracellular biosynthesis of silver nanoparticles using cell filtrate of *Streptomyces* sp. ERI-3. *Scientia Iranica*. 18(6): 1631–1635. <https://doi.org/10.1016/j.scient.2011.11.029>.
- Feng, Q., Wu, J., Chen, G., Kim, T., and Kim, J. (2000). A mechanistic study of the antibacterial effect of silver ions on *Escherichia coli* and *Staphylococcus aureus*. *Journal of Biomedical Materials Research*. 52(4): 662–668. [https://doi.org/10.1002/1097-4636\(20001215\)52:4<662::aid-jbm10>3.0.co;2-3](https://doi.org/10.1002/1097-4636(20001215)52:4<662::aid-jbm10>3.0.co;2-3).
- Franci, G., Falanga, A., Galdiero, S., Palomba, L., Rai, M., Morelli, G., and Galdiero, M. (2015). Silver nanoparticles as potential antibacterial agents. *Molecules*. 20(5): 8856–8874. <https://doi.org/10.3390/molecules20058856>.
- Ge, L., Li, Q., Wang, M., Ouyang, J., Li, X., and Xing, M. M. Q. (2014). Nanosilver particles in medical applications: Synthesis, performance, and toxicity. *International Journal of Nanomedicine*. 9(1): 2399–2407. <https://doi.org/10.2147/IJN.S55015>.
- Godfrey, I. J., Godfrey, I. J., Dent, A. J., Parkin, I. P., Maenosono, S., and Sankar, G. (2020). Following the formation of silver nanoparticles using in situ X-ray absorption spectroscopy. *ACS Omega*. 5(23): 13664–13671. <https://doi.org/10.1021/acsomega.0c00697>.

- Gomathi, A. C., Xavier Rajarathinam, S. R., Mohammed Sadiq, A., and Rajeshkumar, S. (2020). Anticancer activity of silver nanoparticles synthesized using aqueous fruit shell extract of *Tamarindus indica* on MCF-7 human breast cancer cell line. **Journal of Drug Delivery Science and Technology**. 55(101376): 1–8. <https://doi.org/10.1016/j.jddst.2019.101376>.
- Gurunathan, S., Han, J. W., Kwon, D. N., and Kim, J. H. (2014). Enhanced antibacterial and anti-biofilm activities of silver nanoparticles against Gram-negative and Gram-positive bacteria. **Nanoscale Research Letters**. 9(1): 1–17. <https://doi.org/10.1186/1556-276X-9-373>.
- Gurunathan, S., Qasim, M., Park, C., Yoo, H., Choi, D. Y., Song, H., Park, C., Kim, J. H., and Hong, K. (2018). Cytotoxicity and transcriptomic analysis of silver nanoparticles in mouse embryonic fibroblast cells. **International Journal of Molecular Sciences**. 19(11): 1–23. <https://doi.org/10.3390/ijms19113618>.
- Harir, M., Bendif, H., Bellahcene, M., Fortas, Z., and Pogni, R. (2018). Streptomyces secondary metabolites. In S. Enany (Ed.), *Basic Biology and Application of Actinobacteria* (pp. 99–122). IntechOpen. <https://doi.org/10.1016/j.colsurfa.2011.12.014>.
- Honary, S., and Zahir, F. (2013). Effect of zeta potential on the properties of nano-drug delivery systems - A review (Part 2). **Tropical Journal of Pharmaceutical Research**. 12(2): 265–273. <https://doi.org/10.4314/tjpr.v12i2.20>.
- Hsin, Y. H., Chen, C. F., Huang, S., Shih, T. S., Lai, P. S., and Chueh, P. J. (2008). The apoptotic effect of nanosilver is mediated by a ROS- and JNK-dependent mechanism involving the mitochondrial pathway in NIH3T3 cells. **Toxicology Letters**. 179(3): 130–139. <https://doi.org/10.1016/j.toxlet.2008.04.015>.

- Hulkoti, N. I., and Taranath, T. C. (2014). Biosynthesis of nanoparticles using microbes-A review. **Colloids and Surfaces B: Biointerfaces**. 121: 474–483. <https://doi.org/10.1016/j.colsurfb.2014.05.027>.
- Hussain, S. M., Hess, K. L., Gearhart, J. M., Geiss, K. T., and Schlager, J. J. (2005). In vitro toxicity of nanoparticles in BRL 3A rat liver cells. **Toxicology in Vitro**. 19(7): 975–983. <https://doi.org/10.1016/j.tiv.2005.06.034>.
- Iravani, S., Korbekandi, H., Mirmohammadi, S. V., and Zolfaghari, B. (2014). Synthesis of silver nanoparticles: Chemical, physical and biological methods. **Research in Pharmaceutical Sciences**. 9(6): 385–406.
- Janda, J. M., and Abbott, S. L. (2007). 16S rRNA gene sequencing for bacterial identification in the diagnostic laboratory: Pluses, perils, and pitfalls. **Journal of Clinical Microbiology**. 45(9): 2761–2764. <https://doi.org/10.1128/JCM.01228-07>.
- Javaid, A., Oloketuyi, S. F., Khan, M. M., and Khan, F. (2018). Diversity of Bacterial Synthesis of Silver Nanoparticles. **BioNanoScience**. 8(1): 43–59. <https://doi.org/10.1007/s12668-017-0496-x>.
- Jiang, H., Manolache, S., Wong, A. C. L., and Denes, F. S. (2004). Plasma-enhanced deposition of silver nanoparticles onto polymer and metal surfaces for the generation of antimicrobial characteristics. **Journal of Applied Polymer Science**. 93(3): 1411–1422. <https://doi.org/10.1002/app.20561>.
- Jin, Y., and Zhao, X. (2009). Cytotoxicity of photoactive nanoparticle. In T. J. Webster (Ed.), *Safety of nanoparticle from manufacturing to medical application* (pp. 19–31). Springer.

- Kalishwaralal, K., BarathManiKanth, S., Pandian, S. R. K., Deepak, V., and Gurunathan, S. (2010). Silver nanoparticles impede the biofilm formation by *Pseudomonas aeruginosa* and *Staphylococcus epidermidis*. **Colloids and Surfaces B: Biointerfaces**. 79(2): 340–344. [https://doi.org/10.1016-j.colsurfb.2010.04.014](https://doi.org/10.1016/j.colsurfb.2010.04.014).
- Karthik, L., Kumar, G., and Bhaskara Rao, K. V. (2010). Diversity of marine actinomycetes from Nicobar marine sediments and its antifungal activity. **International Journal of Pharmacy and Pharmaceutical Sciences**. 2(1): 199–203.
- Karthik, L., Kumar, G., Kirthi, A. V., Rahuman, A. A., and Bhaskara Rao, K. V. (2014). *Streptomyces* sp. LK3 mediated synthesis of silver nanoparticles and its biomedical application. **Bioprocess and Biosystems Engineering**. 37(2): 261–267. <https://doi.org/10.1007/s00449-013-0994-3>.
- Kim, H. seok, Seo, Y. S., Kim, K., Han, J. W., Park, Y., and Cho, S. (2016). Concentration effect of reducing agents on green synthesis of gold nanoparticles: Size, morphology, and growth mechanism. **Nanoscale Research Letters**. 11(1). <https://doi.org/10.1186/s11671-016-1393-x>.
- Kim, T. H., Kim, M., Park, H. S., Shin, U. S., Gong, M. S., and Kim, H. W. (2012). Size-dependent cellular toxicity of silver nanoparticles. **Journal of Biomedical Materials Research - Part A**. 100 A(4): 1033–1043. <https://doi.org/10.1002/jbm.a.34053>.
- Koningsberger, D., and Prins, R. (1988). X-ray absorption: principles, applications, techniques of EXAFS, SEXAFS, and XANES. Wiley.

- Krishnakumar, S., and Bai, V. D. M. (2015). Extracellular biosynthesis of silver nanoparticles using terrestrial *Streptomyces* sp. SBU3 and its antimicrobial efficiency against plant pathogens. **International Journal of TechnoChem Research**. 1(02): 112–118.
- Kumar, S., Abyaneh, M., SW, G., Kulkarni, S., Pasricha, R., Ahmad, A., and Khan, M. (2007). Nitrate reductase-mediated synthesis of silver nanoparticles from AgNO₃. **Biotechnology Letters**. 29(3): 439–445. <https://doi.org/DOI:10.1007/s10529-006-9256-7>.
- Labeda, D. P., Goodfellow, M., Brown, R., Ward, A. C., Lanoot, B., Vannanneyt, M., Swings, J., Kim, S. B., Liu, Z., Chun, J., Tamura, T., Oguchi, A., Kikuchi, T., Kikuchi, H., Nishii, T., Tsuji, K., Yamaguchi, Y., Tase, A., Takahashi, M., and Hatano, K. (2012). Phylogenetic study of the species within the family Streptomycetaceae. **Antonie van Leeuwenhoek, International Journal of General and Molecular Microbiology**. 101(1): 73–104. <https://doi.org/10.1007/s10482-011-9656-0>.
- Lee, S. H., and Jun, B. (2019). Silver Nanoparticles : Synthesis and Application for Nanomedicine. **International Journal of Molecular Sciences**. 20: 1–24. <https://doi.org/10.3390/ijms20040865>.
- Lee, Y. H., Cheng, F. Y., Chiu, H. W., Tsai, J. C., Fang, C. Y., Chen, C. W., and Wang, Y. J. (2014). Cytotoxicity, oxidative stress, apoptosis and the autophagic effects of silver nanoparticles in mouse embryonic fibroblasts. **Biomaterials**. 35(16): 4706–4715. <https://doi.org/10.1016/j.biomaterials.2014.02.021>.

- Li, R., Chen, J., Cesario, T. C., Wang, X., Yuan, J. S., and Rentzepis, P. M. (2016). Synergistic reaction of silver nitrate, silver nanoparticles, and methylene blue against bacteria. **Proceedings of the National Academy of Sciences of the United States of America**. 113(48): 13612–13617. <https://doi.org/10.1073/pnas.1611193113>.
- Liao, S., Zhang, Y., Pan, X., Zhu, F., Jiang, C., Liu, Q., Cheng, Z., Dai, G., Wu, G., Wang, L., and Chen, L. (2019). Antibacterial activity and mechanism of silver nanoparticles against *Pseudomonas aeruginosa*. **International Journal of Nanomedicine**. 14: 1469–1487. <https://doi.org/10.1016/j.micpath.2020.103980>.
- Liao, C., Li, Y., and Tjong, S. C. (2019). Bactericidal and cytotoxic properties of silver nanoparticles. **International Journal of Molecular Sciences**. 20(2): 2–47. <https://doi.org/10.3390/ijms20020449>.
- Maillard, A. P. V., Dalmasso, P. R., López de Mishima, B. A., and Hollmann, A. (2018). Interaction of green silver nanoparticles with model membranes: possible role in the antibacterial activity. **Colloids and Surfaces B: Biointerfaces**. 171: 320–326. <https://doi.org/10.1016/j.colsurfb.2018.07.044>.
- Manikprabhu, D., and Lingappa, K. (2013). Antibacterial activity of silver nanoparticles against methicillin-resistant *Staphylococcus aureus* synthesized using model *Streptomyces* sp. pigment by photo-irradiation method. **Journal of Pharmacy Research**. 6(2): 255–260. <https://doi.org/10.1016/j.jopr.2013.01.022>.
- Margaret, I., Lui, S. L., Poon, V. K. M., Lung, I., and Burd, A. (2006). Antimicrobial activities of silver dressings: An in vitro comparison. **Journal of Medical Microbiology**. 55(1): 59–63. <https://doi.org/10.1099/jmm.0.46124-0>.

- Mehling, A., Wehmeier, U. F., and Piepersberg, W. (1995). Nucleotide sequences of streptomycete 16S ribosomal DNA: Towards a specific identification system for streptomycetes using PCR. **Microbiology**. 141(9): 2139–2147. <https://doi.org/10.1099/13500872-141-9-2139>.
- Mfouo-Tynga, I., El-Hussein, A., Abdel-Harith, M., and Abrahamse, H. (2014). Photodynamic ability of silver nanoparticles in inducing cytotoxic effects in breast and lung cancer cell lines. **International Journal of Nanomedicine**. 9(1): 3771–3780. <https://doi.org/10.2147/IJN.S63371>.
- Mohamed, D. S., El-Baky, R. M. A., Sandle, T., Mandour, S. A., and Ahmed, E. F. (2020). Antimicrobial activity of silver-treated bacteria against other multi-drug resistant pathogens in their environment. **Antibiotics**. 9(4): 2–14. <https://doi.org/10.3390/antibiotics9040181>.
- Mohamedin, A., El-Naggar, N. E.-A., Shawqi Hamza, S., and Sherief, A. A. (2015). Green synthesis, characterization and antimicrobial activities of silver nanoparticles by *Streptomyces viridodiastaticus* SSHH-1 as a living nanofactory: Statistical optimization of process variables. **Current Nanoscience**. 11(5): 640–654. <https://doi.org/10.2174/157341371166615030-9233939>.
- Mohanty, S., Mishra, S., Jena, P., Jacob, B., Sarkar, B., and Sonawane, A. (2012). An investigation on the antibacterial, cytotoxic, and antibiofilm efficacy of starch-stabilized silver nanoparticles. **Nanomedicine: Nanotechnology, Biology, and Medicine**. 8(6): 916–924. <https://doi.org/10.1016/j.nano.2011.11.007>.

- Morones, J. R., Elechiguerra, J. L., Camacho, A., Holt, K., Kouri, J. B., Ramírez, J. T., and Yacaman, M. J. (2005). The bactericidal effect of silver nanoparticles. **Nanotechnology**. 16(10): 2346–2353. <https://doi.org/10.1088/0957-4484/16/10/059>.
- Mukherjee, K., Gupta, R., Kumar, G., Kumari, S., Biswas, S., and Padmanabhan, P. (2018). Synthesis of silver nanoparticles by *Bacillus clausii* and computational profiling of nitrate reductase enzyme involved in production. **Journal of Genetic Engineering and Biotechnology**. 16(2): 527–536. <https://doi.org/10.1016-/j.jgeb.2018.04.004>.
- Munteanu, A., Florescu, I. P., and Nitescu, C. (2016). A modern method of treatment: The role of silver dressings in promoting healing and preventing pathological scarring in patients with burn wounds. **Journal of Medicine and Life**. 9(3): 306–315.
- Naqvi, S. Z. H., Kiran, U., Ali, M. I., Jamal, A., Hameed, A., Ahmed, S., and Ali, N. (2013). Combined efficacy of biologically synthesized silver nanoparticles and different antibiotics against multidrug-resistant bacteria. **International Journal of Nanomedicine**. 8: 3187–3195. <https://doi.org/10.2147/IJN.S49284>.
- Nélly, M. S.-V., Nelson, E. D. C., Taciana, de A. S., Patrick, V. Q., Alyne, R. de A., Ana, C. M. de M., Ana, L. dos S. C., João, P. F. L., Ricardo, B. A., Durcilene, A. da S., José, R. de S. de A. L., and Maria, F. S. T. (2017). Extracellular biogenic synthesis of silver nanoparticles by Actinomycetes from amazonic biome and its antimicrobial efficiency. **African Journal of Biotechnology**. 16(43): 2072–2082. <https://doi.org/10.5897/ajb2017.16148>.

- Netchareonsirisuk, P., Puthong, S., Dubas, S., Palaga, T., and Komolpis, K. (2016). Effect of capping agents on the cytotoxicity of silver nanoparticles in human normal and cancer skin cell lines. **Journal of Nanoparticle Research**. 18(11): 322. <https://doi.org/10.1007/s11051-016-3624-6>.
- Ninganagouda, S., Rathod, V., Singh, D., Hiremath, J., Singh, A. K., Mathew, J., and Ul-Haq, M. (2014). Growth kinetics and mechanistic action of reactive oxygen species released by silver nanoparticles from *Aspergillus niger* on *Escherichia coli*. **BioMed Research International**. 2014. <https://doi.org/10.1155/2014/753419>.
- Niska, K., Knap, N., Kędzia, A., Jaskiewicz, M., Kamysz, W., and Inkielewicz-Stepniak, I. (2016). Capping agent-dependent toxicity and antimicrobial activity of silver nanoparticles: An in vitro study. concerns about potential application in dental practice. **International Journal of Medical Sciences**. 13(10): 772–782. <https://doi.org/10.7150/ijms.16011>.
- Ovais, M., Khalil, A. T., Ayaz, M., Ahmad, I., Nethi, S. K., and Mukherjee, S. (2018). Biosynthesis of metal nanoparticles via microbial enzymes: A mechanistic approach. **International Journal of Molecular Sciences**. 19(12): 1–20. <https://doi.org/10.3390/ijms19124100>.
- Paramelle, D., Sadovoy, A., Gorelik, S., Free, P., Hobley, J., and Fernig, D. G. (2014). A rapid method to estimate the concentration of citrate capped silver nanoparticles from UV-visible light spectra. **Analyst**. 139(19): 4855–4861. <https://doi.org/10.1039/c4an00978a>.

- Parra Berumen, J., Gallegos-Loya, E., Esparza-Ponce, H., Gonzalez-Valenzuela, R., Gonzalez-Valenzuela, C., and Duarte-Moller, A. (2009). XAS Study of silver nanoparticles formed in *Phaseolus vulgaris*. **Proceedings of the 8th International Conference on Applications of Electrical Engineering/8th International Conference on Applied Electromagnetics, Wireless and Optical Communications**. 211–215.
- Peng, H., Zhang, X., Wei, Y., Liu, W., Li, S., Yu, G., Fu, X., Cao, T., and Deng, X. (2012). Cytotoxicity of silver nanoparticles in human embryonic stem cell-derived fibroblasts and an L-929 cell line. **Journal of Nanomaterials**, 2012: 1–9. <https://doi.org/10.1155/2012/160145>.
- Pillai, Z. S., and Kamat, P. V. (2004). What factors control the size and shape of silver nanoparticles in the citrate ion reduction method? **Journal of Physical Chemistry B**. 108(3): 945–951. <https://doi.org/10.1021/jp037018r>.
- Politano, A. D., Campbell, K. T., Rosenberger, L. H., and Sawyer, R. G. (2013). Use of silver in the prevention and treatment of infections: Silver review. **Surgical Infections**. 14(1): 8–20. <https://doi.org/10.1089/sur.2011.097>.
- Prabhu, S., and Poulouse, E. K. (2012). Silver nanoparticles: mechanism of antimicrobial. **International Nano Letters**. 2: 32–41.
- Purohit, S. S., Saluja, A. K., and Kakrani, H. N. (2006). Pharmaceutical microbiology. Agrobios.
- Rai, M., Yadav, A., and Gade, A. (2009). Silver nanoparticles as a new generation of antimicrobials. **Biotechnology Advances**. 27(1): 76–83. <https://doi.org/10.1016/j.biotechadv.2008.09.002>.

- Raja, A., and Prabakarana, P. (2011). Actinomycetes and drug-an overview. **American Journal of Drug Discovery and Development**. 1(2): 75–84. <https://doi.org/10.3923/ajdd.2011.75.84>.
- Ravel, B., and Newville, M. (2005). ATHENA, ARTEMIS, HEPHAESTUS: data analysis for X-ray absorption spectroscopy using IFEFFIT. **J Synchrotron Rad**. 12: 537–541. <https://doi.org/10.1107/S0909049505012719>.
- Saeb, A. T. M., Alshammari, A. S., Al-Brahim, H., and Al-Rubeaan, K. A. (2014). Production of silver nanoparticles with strong and stable antimicrobial activity against highly pathogenic and multidrug resistant bacteria. **Scientific World Journal**. 2014(Article ID 704708), 9. <https://doi.org/10.1155/2014/704708>.
- Saitou, N., and Nei, M. (1987). The neighbor-joining method: a new method for reconstructing phylogenetic trees. **Molecular Biology and Evolution**. 4(4), 406–425.
- Sambale, F., Wagner, S., Stahl, F., Khaydarov, R. R., Scheper, T., and Bahnemann, D. (2015). Investigations of the toxic effect of silver nanoparticles on mammalian cell lines. **Journal of Nanomaterials**. 2015: 1–9. <https://doi.org/10.1155/2015/136765>.
- Saravana Kumar, P., Balachandran, C., Duraipandiyar, V., Ramasamy, D., Ignacimuthu, S., and Al-Dhabi, N. A. (2015). Extracellular biosynthesis of silver nanoparticle using *Streptomyces* sp. 09 PBT 005 and its antibacterial and cytotoxic properties. **Applied Nanoscience (Switzerland)**. 5(2): 169–180. <https://doi.org/10.1007/s13204-014-0304-7>.
- Sastry, M., Ahmad, A., Khan, M. I., and Kumar, R. (2014). Biosynthesis of metal nanoparticles using fungi and actinomycete. **Current Science**. 85(2): 162–170.

- Scandorieiro, S., de Camargo, L. C., Lancheros, C. A. C., Yamada-Ogatta, S. F., Nakamura, C. V., de Oliveira, A. G., Andrade, C. G. T. J., Duran, N., Nakazato, G., and Kobayashi, R. K. T. (2016). Synergistic and additive effect of oregano essential oil and biological silver nanoparticles against multidrug-resistant bacterial strains. **Frontiers in Microbiology**. 7(MAY): 1–14. <https://doi.org/10.3389/fmicb.2016.00760>.
- Shivaji, S., Madhu, S., and Singh, S. (2011). Extracellular synthesis of antibacterial silver nanoparticles using psychrophilic bacteria. **Process Biochemistry**. 46(9): 1800–1807. <https://doi.org/10.1016/j.procbio.2011.06.008>.
- Siddiqi, K. S., Husen, A., and Rao, R. A. K. (2018). A review on biosynthesis of silver nanoparticles and their biocidal properties. **Journal of Nanobiotechnology**. 16(1). <https://doi.org/10.1186/s12951-018-0334-5>.
- Silva Santos, K., Barbosa, A. M., Da Costa, L. P., Pinheiro, M. S., Oliveira, M. B. P., and Ferreira Padilha, F. (2016). Silver nanocomposite biosynthesis: Antibacterial activity against multidrug-resistant strains of *Pseudomonas aeruginosa* and *Acinetobacter baumannii*. **Molecules**. 21(9): 1–7. <https://doi.org/10.3390/molecules21091255>.
- Sondi, I., and Salopek-Sondi, B. (2004). Silver nanoparticles as antimicrobial agent: A case study on *E. coli* as a model for Gram-negative bacteria. **Journal of Colloid and Interface Science**. <https://doi.org/10.1016/j.jcis.2004.02.012>.
- Syed, B., Nagendra, N. P., B.L., D., Mohan Kumar, K., Yallappa, S., and Satish, S. (2016). Synthesis of silver nanoparticles by endosymbiont *Pseudomonas fluorescens* CA 417 and their bactericidal activity. **Enzyme and Microbial Technology**. 95(May 2018): 128–136. <https://doi.org/10.1016/j.enzmictec.2016.10.004>.

- Talekar, S., Joshi, A., Chougale, R., Nakhe, A., and Bhojwani, R. (2016). Immobilized enzyme mediated synthesis of silver nanoparticles using cross-linked enzyme aggregates (CLEAs) of NADH-dependent nitrate reductase. **Nano-Structures and Nano-Objects**. 6: 23–33. [https://doi.org/https://doi.org/10.1016/j.nanoso.-2016.03.002](https://doi.org/10.1016/j.nanoso.-2016.03.002).
- Tamiyakul, H., Tanasupawat, S., Dubas, S. T., and Warisnoicharoen, W. (2015). Antibacterial Potential of Silver Nanoparticles Capped with Poly(4-styrenesulfonic acid-co-maleic acid) Polymer. **Advanced Materials Research**. 1088: 64–68. <https://doi.org/10.4028/www.scientific.net/amr.1088.64>.
- Thongkrachang, N., Chanama, S., and Chanama, M. (2016). Inhibitory activity against pathogenic bacteria of streptomycetes isolated from natural soil resources. **Journal of Public Health and Development**. 14(3): 59–68.
- van der Meij, A., Worsley, S. F., Hutchings, M. I., and van Wezel, G. P. (2017). Chemical ecology of antibiotic production by actinomycetes. **FEMS Microbiology Reviews**. 41(3): 392–416. <https://doi.org/10.1093/femsre/fux005>.
- Venkatpurwar, V., and Pokharkar, V. (2011). Green synthesis of silver nanoparticles using marine polysaccharide: Study of in-vitro antibacterial activity. **Materials Letters**. 65(6): 999–1002. <https://doi.org/10.1016/j.matlet.2010.12.057>.
- Wintachai, P., Paosen, S., Yupanqui, C. T., and Voravuthikunchai, S. P. (2019). Silver nanoparticles synthesized with *Eucalyptus citriodora* ethanol leaf extract stimulate antibacterial activity against clinically multidrug-resistant *Acinetobacter baumannii* isolated from pneumonia patients. **Microbial Pathogenesis**. 126 (May 2018): 245–257. <https://doi.org/10.1016/j.micpath.-2018.11.018>.

- Woo, P. C. Y., Lau, S. K. P., Teng, J. L. L., Tse, H., and Yuen, K. Y. (2008). Then and now: Use of 16S rDNA gene sequencing for bacterial identification and discovery of novel bacteria in clinical microbiology laboratories. **Clinical Microbiology and Infection**. 14(10): 908–934. <https://doi.org/10.1111/j.1469-0691.2008.02070.x>.
- Yokoyama, T., Masuda, H., Suzuki, M., Ehara, K., Nogi, K., Fuji, M., Fukui, T., Suzuki, H., Tata, i, J., Hayashi, K., and Tada, K. (2012). Basic properties and measuring method of nanoparticle. In M. Hosokawa, M. Naito, K. Nogi, and T. Yokoyama (Eds.), *Nanoparticle technology handbook* 2nd edition, pp. 3–48. Elsevier. <https://doi.org/https://doi.org/10.1016/C2010-0-69564-2>.
- Yuan, Y. G., Peng, Q. L., and Gurunathan, S. (2017). Effects of silver nanoparticles on multiple drug-resistant strains of *Staphylococcus aureus* and *Pseudomonas aeruginosa* from mastitis-infected goats: An alternative approach for antimicrobial therapy. **International Journal of Molecular Sciences**. 18(3): <https://doi.org/10.3390/ijms18030569>.
- Zhang, H., Li, Q., Lu, Y., Sun, D., Lin, X., Deng, X., He, N., and Zheng, S. (2005). Biosorption and bioreduction of diamine silver complex by *Corynebacterium*. **Journal of Chemical Technology and Biotechnology**. <https://doi.org/10.1002/jctb.1191>.
- Zhang, X., Liu, Z. G., Shen, W., and Gurunathan, S. (2016). Silver nanoparticles: Synthesis, characterization, properties, applications, and therapeutic approaches. **International Journal of Molecular Sciences**. 17(9). <https://doi.org/10.3390-ijms17091534>.

Zhang, Y., Yang, M., Portney, N. G., Cui, D., Budak, G., Ozbay, E., Ozkan, M., and Ozkan, C. S. (2008). Zeta potential: A surface electrical characteristic to probe the interaction of nanoparticles with normal and cancer human breast epithelial cells. **Biomedical Microdevices**. 10(2): 321–328. <https://doi.org/10.1007/s10544-007-9139-2>.



CHAPTER III

SYNTHESIS OF *STREPTOMYCES* SP. PJ95 CRUDE EXTRACT-LOADED PVDF-HFP ELECTROSPUN NANOFIBERS

3.1 Introduction

The human skin provides an effective barrier to the environment, prevents the pathogen invasion, and protects the body from the chemical and physical attacks. On the other hand, the skin can also be injured because of wounding, surgery, or insect bites. The open wound might be easily infected by pathogens capable of causing systemic disease or localized disease (Jensen and Proksch, 2009; Singleton, 2004). To facilitate wound healing, the sterile dressing material is needed to avoid bacterial infection, promote the healing process, and provide a suitable environment for wound healing (Gizaw et al., 2018; Martins et al., 2008; Unalan et al., 2019). Therefore, a wound dressing that has antimicrobial activity and provides wound healing activity is needed.

Nanofibers are potential candidate for the formulation of medical fabrics for wound healing and exhibit several characteristics that provide novel replacement dressing material. Electrospinning is a versatile method in which electrostatic forces are used to fabricate polymeric nanofibers. It is a simple and cost-effective method to produce a drug-containing fiber with small diameters and high surface area. Thus, the

electrospun nanofibers have been studied extensively for their application, advantages, and future developments (Gizaw et al., 2018; Song et al., 2017; Motealleh et al., 2014; Beachley and Wen, 2009; Ditaranto et al., 2018). Electrospun nanofibers provide physical protection to the wound and can be incorporated with drugs. The release rate from nanofibers can also be adjusted by changing the types and composition of the materials (Chou and Woodrow, 2017). The incorporation of natural and synthetic polymers gives advantages in the chemical structure's stability and enhances the biological properties on the electrospinning method (Unalan et al., 2019; Martins et al., 2008). The biocompatible and non-toxic natural polymers have been used to fabricate the electrospun nanofibers, such as chitosan, gelatin, cellulose, collagen, hyaluronic acid, keratin, and silk fibroin. In some cases, the natural polymers are difficult to spin due to their molecular structure (Gizaw et al., 2018; Khan et al., 2018; Chou et al., 2015). The introduction of synthetic polymers, such as poly(l-lactide) (PLA), poly(glycolide) (PGA), and poly(lactide-co-glycolide) (PLGA), poly(ϵ -caprolactone) (PCL), polyurethane (PU), poly(vinylidene fluoride) (PVDF), polyvinyl alcohol (PVA), poly(ethylene oxide) (PEO), and polyvinyl pyrrolidone (PVP) provide a possible option for the fabrication of electrospun nanofibers (Xu et al., 2006, Gizaw et al., 2018). The fabrication of electrospun PVDF mats containing silver nanoparticles was firstly reported by Yuan et al. (2010) and showed good antibacterial activity against *S. aureus* and *K. pneumoniae*. The copolymer of PVDF with HFP provides excellent mechanical strength, outstanding chemical resistance, good thermal stability, and high hydrophobicity compared to the PVDF. PVDF-HFP has been successfully fabricated into electrospun nanofibers and used as membrane distillation (Fadhil et al., 2016; Gao et al., 2014; Lalia et al., 2012; Wang et al., 2018). The fabrication of electrospun

nanofibers using poly (vinylidene fluoride-co-hexafluoropropylene) (PVDF-HFP) copolymers for antimicrobial wound dressing application has never been carried out. Therefore, in this study, the fabrication of electrospun nanofibers was carried out by using PVDF-HFP copolymer as a candidate for wound dressing material.

Streptomycetes are an essential source of secondary metabolite with antibacterial, antifungal, anticancer, and anti-inflammation properties. (Thongkrachang et al., 2016; Berdy 2005; Mahajan et al., 2015). Streptomycetes belongs to the *Streptomycetaceae* family. They are Gram-positive, aerobic, and spore-producing bacteria. Streptomycetes are widely distributed in nature, especially soil habitat (Sripreechasak et al., 2014; Barka et al., 2016). *Streptomyces* sp. PJ95 reported to have antimicrobial activity against gram-positive and gram-negative pathogenic bacteria. This isolate revealed high similarity to *Streptomyces luteosporus* NBRC14657^T (Chanthasena and Nantapong, 2016).

Many reports have been issued on the fabrication of electrospun nanofibers incorporated with antibiotics, nanoparticles, essential oils, and plant extract (Khan et al., 2019; Mohammadi et al., 2019; Pisani et al., 2019; Unalan et al., 2019; Vatankhah, 2018; Yuan et al., 2010). However, the fabrication of PVDF-HFP electrospun nanofibers containing crude extract of *Streptomyces* with antimicrobial properties is still new. Therefore, this study aimed to fabricate antimicrobial electrospun nanofiber containing crude extract of *Streptomyces* sp. PJ95 by using PVDF-HFP as a polymer. The characterization of synthesized nanofibers and their antimicrobial and cytotoxicity activity were also investigated.

3.2 Literature review

3.2.1 Electrospun nanofibers

The development of a potential nontoxic polymer that has an antimicrobial activity is needed. For this reason, researchers are looking for the structural parameters to determine the activity, structures, or mechanism of action to tune the polymer's potency and toxicity (Álvarez-Paino et al., 2017). Three approaches were used to render biomaterials with antibacterial properties, including anti-adhesive, biocide release, and contact active antimicrobial modification (Xu et al., 2006). In the case of wound bandage or wound dressing, it is necessary to consider some of the properties, including the characteristic of wound type and wound healing time, as well as the physical, mechanical, and chemical properties of the bandages to achieve better aesthetic repair and higher healing rates of the wound. A common and simple method to manufacture nanoscale polymer fibers for wound dressing is electrospinning (Álvarez-Paino et al., 2017). Electrospinning is a fiber production process using electrostatic forces from the polymer solution to produce a fiber with 10 to 500 nm in diameter (Kurečić, 2013; Xu et al., 2006). The electrospun nanofibers are a suitable platform to fabricate new antimicrobial materials due to small size, high specific surface area, multi-scale porosity, high flexibility of surface functionalization, excellent fluid drainage, and gradual drug release rate (Motealleh et al., 2014; Song et al., 2017). Other advantages of electrospinning are low cost and relatively high production rate (Ramakrisna et al., 2006).

Electrospinning has been successfully applied to synthesis nanofibers with diameters ten nanometers from various materials such as polymers, ceramics, small molecules, and their combination. They have broad-spectrum applications including

surface coating, energy harvesting, encapsulation of bioactive species, drug delivery, tissue engineering, regenerative medicine, environmental engineering (membrane and filters), and defense (chemical and biological protection sensors) (Gao et al., 2014; Khan et al., 2018; Ramakrishna et al., 2006; Song et al., 2017; Xue et al., 2017; Martins et al., 2008).

The principle of electrospinning is accessible and simple. The electrospinning machine consists of four major components (figure 3.1): a syringe pump to inject the fluid, high voltage power supply, spinneret or needle, and a collector to collect the fibers (Gao et al., 2014; Xue et al., 2017). Before running the sample into electrospinning, polymers are dissolved in appropriate solvents completely. The polymer fluid is then introduced into a syringe or capillary tube for electrospinning (Kurečić, 2013). The method of electrospinning begins when a small amount of polymer is slowly pumped out through the spinneret/needle. The products from the needle tend to be spherical droplet form. Still, in this case, a high voltage power supply is applied, so the electrostatic repulsion among the surface charges that the feature the same sign deforms the droplet into solid fibers (Gao et al., 2014; Xue et al., 2017; Martins et al., 2008). Several parameters that affect the nanofiber properties are solution properties, applied voltage, distance from the needle tip to the collector plate, and feeding rate of polymeric solution (Gizaw et al., 2018; Khan et al., 2018).

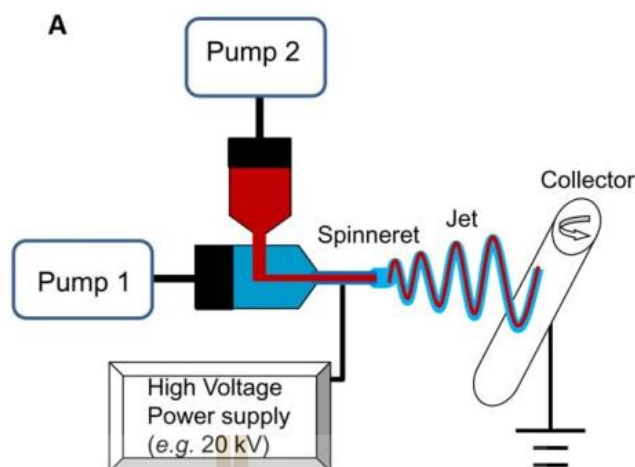


Figure 3.1 Schematic diagram of the basic setup of electrospinning (Gao et al., 2014).

3.2.2 Polymers of electrospun nanofibers

Two types of polymers can be used for electrospinning, divided into natural and synthetic polymers. The benefits of natural polymers are that they are abundant, accessible, biocompatible, biodegradable, and non-toxic in most cases. But these natural polymers are difficult to spin due to their molecular structures. Examples of natural polymers are chitosan, gelatin, cellulose, collagen, hyaluronic acid, keratin, and silk fibroin (Gizaw et al., 2018; Khan et al., 2018). Nowadays, there are biodegradable synthetic polymers used in biomedical applications, which have been approved by US Food and Drug Administration (FDA), such as poly (l-lactide) (PLA), poly(glycolide) (PGA), and poly(lactide-co-glycolide) (PLGA) (Xu et al., 2006). Other examples of synthetic polymers are poly(ϵ -caprolactone) (PCL), polyurethane (PU), poly(vinylidene fluoride) (PVDF), polyvinyl alcohol (PVA), poly(ethylene oxide) (PEO), and polyvinyl pyrrolidone (PVP) (Gizaw et al., 2018). These synthetic polymers show biocompatible properties, suitable in most of the solvent and provide good

mechanical property. Several disadvantages of using synthetic polymers are hydrophobic, slowly degrading, and less cytocompatible (Sundaramurthi and Sethuraman, 2014).

3.2.3 Antimicrobial activity of electrospun nanofibers

Many researchers have fabricated electrospun nanofibers incorporated with a functional agent such as an antibacterial agent and showed an increase in their antimicrobial properties compared to single antimicrobial material to prevent bacterial growth or infection. The carboxymethyl chitosan/polyethylene oxide containing AgNPs nanofibers shows better antimicrobial activity against *E. coli*, *S. aureus*, and *P. aeruginosa* compared to the single AgNPs (Fouda et al., 2013; Gao et al., 2014; Song et al., 2017). Besides, PVDF nanofibers containing silver nanoparticles have antimicrobial activity against *S. aureus* and *K. pneumoniae*. PVDF shows excellent mechanical properties, resistance to severe environmental stress, and good chemical resistance (Gao et al., 2014). Fabricated PLA containing silver nanoparticles show antibacterial activity against *S. aureus* and *E. coli* with the reduction of microorganisms 98.5% and 94.2%, respectively (Xu et al., 2006).

Moreover, plant extract has been used for nanofiber synthesis by electrospinning for antibacterial and wound healing applications. Motealleh and co-workers (2014) have fabricated poly(ϵ -caprolactone)/polystyrene (PCL/PS) nanofibers containing chamomile that have antibacterial and antifungal activities. These nanofibers can heal the wound up to 99% after 14 days of treatment studied by *in vivo* method. They also have high efficiency for the wound closure and healing process than the PCL/PS nanofibers.

3.3 Research methodology

3.3.1 Preparation of crude extract of *Streptomyces* sp PJ95.

Streptomyces sp. PJ95 was obtained from a previous study (Chanhasena and Nantapong, 2016), cultured on 10 mL ISP2 broth, and incubated at 37°C with 200 shaking conditions for 3 days. The suspension was transferred into 100 mL ISP2 broth and incubated at 37°C under 200 rpm shaking condition for 6 days. After incubation, the cells were filtered using Whatman No.1 filter paper (Whatman™, GE Healthcare, UK). The crude compound was extracted from the fermented broth using ethyl acetate (RCI, Labscan). The organic layer containing the active compound was collected and evaporated using a rotary evaporator (BUCHI Rotavapor® R-300).

3.3.2 Synthesis of PJ95 crude extract-loaded PVDF-HFP electrospun nanofibers

The preparation of electrospinning solutions was illustrated in figure 3.2. The poly(vinylidene fluoride-co-hexafluoro propylene) (PVDF-HFP) (Sigma-Aldrich) polymer was dissolved in dimethylformamide (DMF): acetone (1:1). For the PJ95 crude extract-loaded PVDF-HFP nanofibers, 1.25% w/w of crude extract were added into the polymer solution. The prepared solutions were continuously stirred at room temperature until homogeneity occurs. Each electrospinning solution was loaded into 5 mL syringe equipped with a needle. An aluminum sheet wrapped on the collector plate was placed at a distance 10 cm from the needle tip. The nanofibers were electrospinning by applying a voltage at ± 15 kV in the needle and -1 kV in the target. Further, the obtained samples were stored at 4°C in the dark until further use.

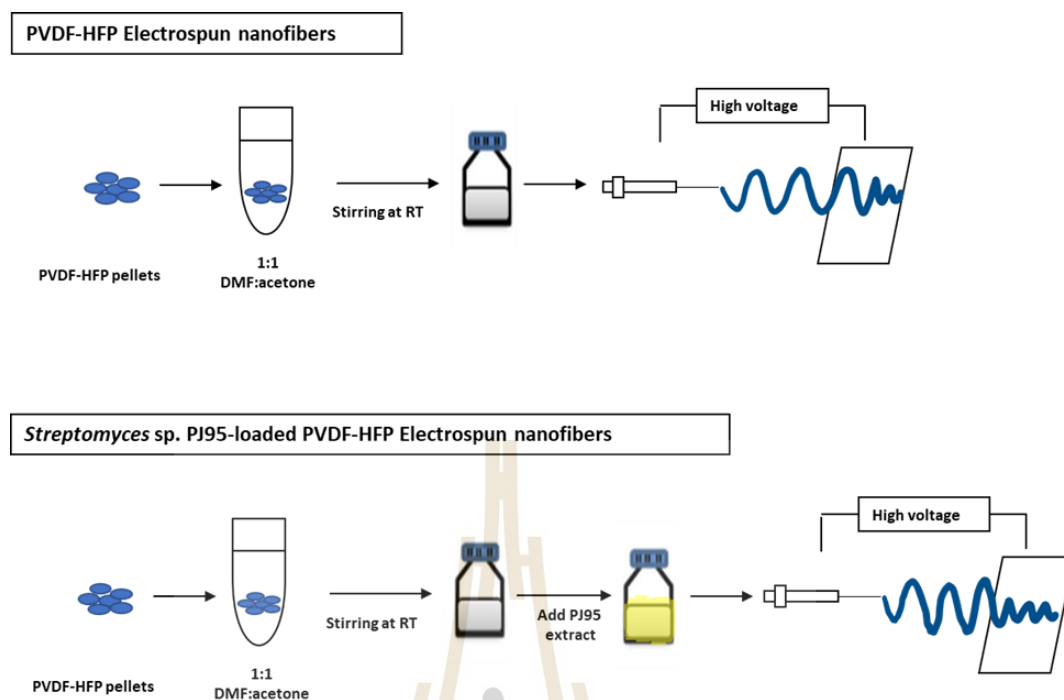


Figure 3.2 Illustration of electrospun nanofibers fabrication.

3.3.3 Characterization of PJ95 crude extract-loaded PVDF-HFP electrospun nanofibers

3.3.3.1 Scanning electron microscopy (SEM) analysis

The diameter and morphology of the electrospun nanofibers were observed under scanning electron microscope (SEM JEOL model JSM800F, Japan). The samples were prepared by cutting the nanofiber and placed on carbon tape. The samples were then gold sputtering coated using Neo Coater MP19020NCTR for 5 min before SEM observations. The average diameter was measured randomly at 35 different points of each sample.

3.3.3.2 Fourier-transform infrared (FTIR)

The interaction between the polymer nanofibers and crude extract of PJ95 was evaluated using Fourier-transform infrared spectroscopy (FTIR

Bruker, Hyperion 3000 Germany). Spectra were recorded between wavenumber 4000 to 400 cm^{-1} . The FTIR analysis was conducted at beamline 4.1 Synchrotron Light Research Institute (SLRI), Thailand.

3.3.3.3 Crude extract release study

The crude extract release study was adapted from Wongkanya et al (2017) with some modification. PJ95 crude extract-loaded PVDF-HFP nanofibers were cut into a circular shape with a diameter of 5 mm. Each nanofiber was immersed in 200 μL of phosphate buffer saline (PBS, pH 7.4) solution at 96 well plates. The plate was incubated at 37°C incubator for 48 h. To determine the amount of crude extract release, the optical density of the sample was measured every 6 h for 48 h period. The UV-Vis spectrophotometer (Thermo Scientific Multiscan GO, Finland) was used to determine the amount of crude compound release. The maximum wavelength for PJ95 crude extract was about 230 nm.

3.3.4 Antimicrobial activity assay

To evaluate the antibacterial properties of electrospun nanofibers with/without PJ95 crude extract, the disk diffusion test was performed against *S. aureus* TISTR 1466, *S. epidermidis* TISTR 518, MRSA DMST 20654, and *P. mirabilis* TISTR 100. The 10^6 CFU/mL of mid-log phase test pathogens were seeded onto the muller hinton agar (MHA, Himedia) plate. The nanofibers sample were cut as circular disks with a diameter of 5 mm, sterilized under UV light for 30 minutes, and placed on the MHA plate seeded with test pathogen. The plates were incubated at 37°C for 24 h. After incubation, an inhibitory zone around the sample disks was determined. Three replicates were tested for each sample.

3.3.5 Cytotoxicity assay

The indirect cytotoxicity evaluation of PJ95 crude extract-loaded PVDF-HFP electrospun nanofibers was conducted based on ISO 10993-5:2009 standard (Wongkanya et al., 2017). Nanofibers sample (5 mm diameter of circular disks) were sterilized under UV light for 30 minutes and immersed in DMEM supplemented with 10% fetal bovine serum (FBS) and 1% antibiotics (Penicillin, Streptomycin) in a 96 culture well plate. The plate was incubated at 37°C incubator under 5% CO₂ for 48 h. During the incubation, the crude extract was released from the nanofibers to the cultured media designated as the extracted medium. NIH-3T3 cells were cultured separately at 10⁴ cells/well using DMEM supplemented with 10% fetal bovine serum (FBS) and 1% antibiotics (Penicillin, Streptomycin) in a 96 culture well plate for 24 h to allow attachment of the cells onto the well surface. After that, the medium was replaced with an extracted medium and incubated for 24 h. The MTT was used to determine the viability of the treated cells. The medium in the wells was removed, and 10 µL of 5 mg/ml of 3-(4,5-dimethylthiazol-2-yl)-2,5-diphenyltetrazolium bromide (MTT, Invitrogen™) was added, followed by adding 100 µL of PBS. The cells were incubated for 4 h at 37°C under 5% CO₂. A reducing yellow tetrazole to purple formazan in the living cell was solubilized by remove MTT solution and adding 50 µL DMSO to the wells. The absorbance of each sample was determined at 540 nm by using spectrophotometer (Thermo Scientific Multiscan GO, Finland).

3.3.6 Statistical analysis

The obtained data were analysed using statistical analysis independent sample t-test and one-way analysis of variance (ANOVA) using IBM SPSS Statistics

Version 23. To determine the significant difference between groups, Tukey's test was applied with $p < 0,05$.

3.4 Results

3.4.1 Surface morphology and diameter distribution of electrospun nanofibers

Electrospun nanofibers of PVDF-HFP and PJ95 crude extract-loaded PVDF-HFP electrospun nanofibers were fabricated by electrospinning method. To fabricate the nanofiber, the final concentration of 1.25% w/w of PJ95 crude extract was added into the polymer solution. The process of electrospinning was optimized at 15 kV and 10 cm distance to produce homogenous and smooth fibers. The nanofibers had smooth, bead-free, and uniform morphology from the SEM observation. The average of nanofibers diameters of PVDF-HFP nanofibers and PJ95 crude extract loaded PVDF-HFP electrospun nanofibers were $0.54 \pm 0.05 \mu\text{m}$ and $0.33 \pm 0.06 \mu\text{m}$, respectively. It was known that the addition of PJ95 crude extract did not significantly decrease the distribution of the nanofiber diameter compared to the PVDF-HFP nanofibers ($p > 0.05$) (Figure 3.3).

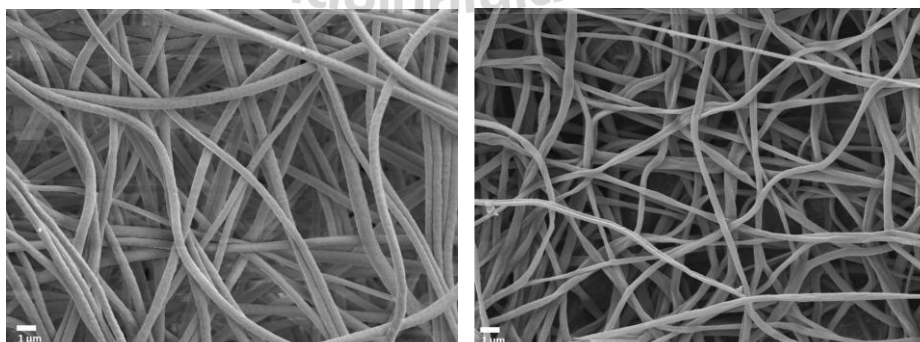


Figure 3.3 The morphology of PVDF-HFP nanofibers (left) and PJ95 crude extract-loaded PVDF-HFP nanofibers (right). Scale bar= $1\mu\text{m}$.

3.4.2 Chemical composition of crosslinked electrospun nanofibers

In order to identify the presence of crude extract on the electrospun nanofibers, FTIR analysis was performed on PVDF-HFP, PJ95 crude extract-loaded PVDF-HFP electrospun nanofibers, and PJ95 crude extract (Figure 3.4). The spectra of neat PVDF-HFP electrospun nanofibers presented peaks in the region 974 and 764 cm^{-1} , which attributed to the α -phase of PVDF, a peak in the region of 875 cm^{-1} attributed to the β -phase of PVDF, and peaks in the region of 1175 and 1401 cm^{-1} attributed to the $-\text{CF}_3$ symmetrical stretching and C-F stretching, respectively. The peaks at 2958 and 1671 cm^{-1} of PJ95 crude extract corresponded to the C-H stretching of lipid and C=O stretching of amide I, respectively. Compared to the PJ95 crude extract-loaded PVDF-HFP electrospun nanofibers, the absorption bands of C-H and C=O of crude extract were shifted to a higher number at 2958 and 1671 cm^{-1} , respectively. The absorption band of CF_3 symmetrical stretching, C-F stretching, and β -phase were also shifted to 1182, 1399, and 877 cm^{-1} , respectively. The shifted peaks might be due to the incorporation of PJ95 crude extract with the polymer. Similar to the PVDF-HFP nanofibers, the absorption band of α -phase of PVDF remains in the same region at 974 and 764 cm^{-1} .

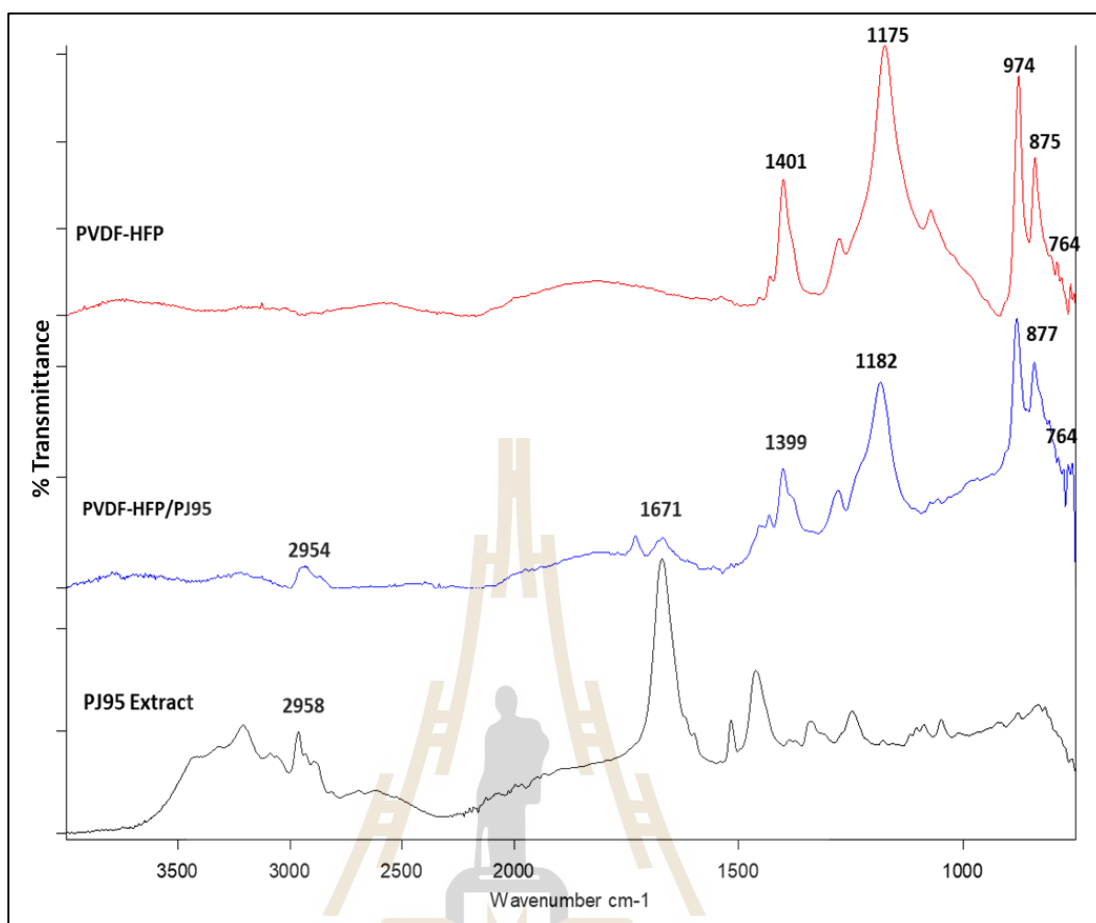


Figure 3.4 FTIR spectra of neat PVDF-HFP electrospun nanofibers compared to the PJ95 crude extract-loaded PVDF-HFP electrospun nanofibers.

3.4.3 Crude extract release study

The release behavior of PJ95 crude extract was performed by immersing the nanofiber disks in PBS and incubating at 37°C. The amount of released crude extract was measured every 6 h for a 48 h period using a spectrophotometer at 230 nm. This absorbance is the maximum absorbance of PJ95 crude extract. The rapid initial release of crude extract from the nanofibers was observed after 6 h of immersion, followed by

a slow release of crude extract. Finally, the maximum release of crude extract from the nanofibers was observed after 42 h of immersion.

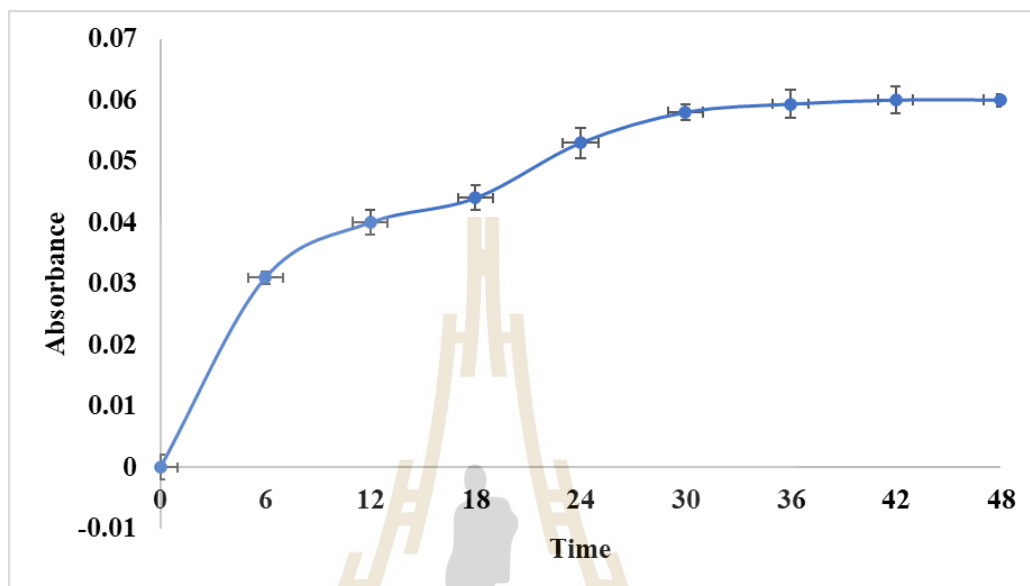


Figure 3.5 The crude extract release profile of PJ95 from PVDF-HFP electrospun nanofibers.

3.4.4 Antimicrobial activity analysis

The antibacterial activity of PVDF-HFP and PJ95 crude extract loaded PVDF-HFP electrospun nanofibers were tested against *S. aureus* TISTR 1466, *S. epidermidis* TISTR 518, MRSA DMST 20654, and *P. mirabilis* TISTR 100, using the disk diffusion method. A disk of PVDF-HFP electrospun nanofibers without PJ95 crude extract was used as a control. The bacteria were incubated at 37°C for 24 h. After incubation for 24 h, the inhibition zone of 7.6 ± 0.5 mm, 7.6 ± 1.1 mm, 12 ± 0.5 mm, and 13.6 ± 0.5 mm were observed against *P. mirabilis* TISTR 100, *S. epidermidis* TISTR 518, *S. aureus* TISTR 1466, and MRSA DMST 20654, respectively (Table 3.1).

In contrast, no inhibition zone was observed around the control nanofibers. This evidence proves that the released crude extract was responsible for inhibiting bacterial growth, not the PVDF-HFP fiber.

Table 3.1 Inhibition zone of PJ95 crude extract-loaded PVDF-HFP electrospun nanofibers against test pathogens.

Nanofibers	Inhibition zone (mm)			
	<i>P. mirabilis</i> TISTR 100	<i>S. epidermidis</i> TISTR 518	<i>S. aureus</i> TISTR 1466	MRSA DMST 20654
PVDF-HFP	0	0	0	0
PVDF-HFP/PJ95	7.6 ± 0.5*	7.6 ± 1.1*	12 ± 0.5**	13.6 ± 0.5**

n= 3, p<0.05

3.4.5 Indirect cytotoxicity analysis

To ensure the potential of PJ95 crude extract-loaded PVDF-HFP electrospun nanofibers as wound dressing, the non-toxic and biocompatible nanofiber are needed. Therefore, the investigation of PJ95 crude extract-loaded PVDF-HFP electrospun nanofibers cytotoxicity was performed against NIH-3T3 fibroblast cell line. Following the ISO 10993-5 standard, the NIH-3T3 cell lines were cultured on the extraction media containing PJ95 crude extract. The significant decrease in the cell viability when NIH-3T3 cells were observed on the incubation with the extracted medium of either PVDF-HFP (94%) or PJ95 crude extract loaded-PVDF-HFP nanofibers (87%) compared to the control (100%) (Figure 3.6). However, despite a decrease in cell viability of NIH-3T3 cell lines after treated with the extracted medium of the electrospun nanofibers, these nanofibers were still acceptable to be used as a wound dressing candidate.

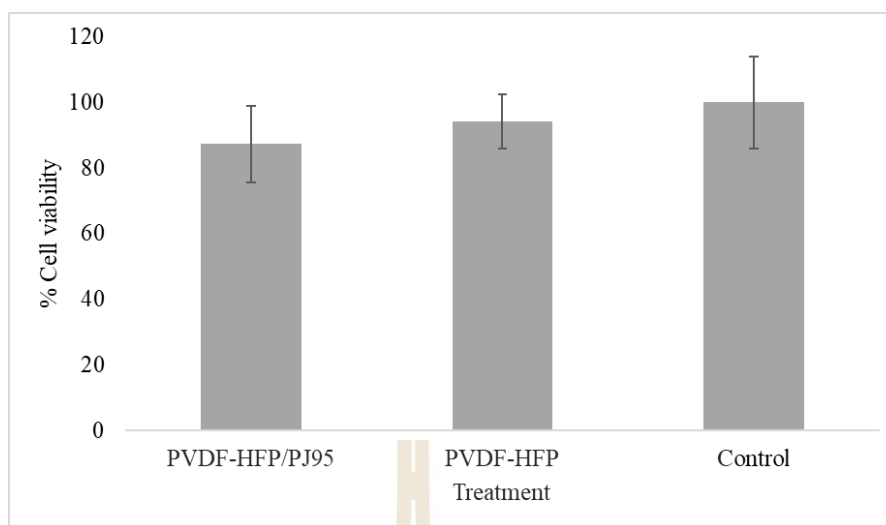


Figure 3.6 The cell viability of NIH-3T3 cell lines after treated with extracted medium from PJ95 crude extract-loaded PVDF-HFP and PVDF-HFP electrospun nanofibers (n=3, $p > 0,05$).

3.5 Discussions

Incorporating natural products and antibiotics with polymer to fabricate electrospun nanofibers as wound dressing represents an emerging area of interest. A very rare study has reported on the fabrication of electrospun nanofibers incorporated with crude extract of bacteria, especially *Streptomyces*. This study was investigating the incorporation of *Streptomyces* sp. PJ95 crude extract into electrospun PVDF-HFP nanofibers. The *Streptomyces* sp. PJ95 was chosen to be incorporated with the nanofibers because this isolate exhibit broad-spectrum antimicrobial activity against Gram-positive and Gram-negative pathogenic bacteria, including skin infection pathogenic bacteria used in this study. Before spinning, the PVDF-HFP polymer was dissolved in the acetone and DMF solvent with a ratio 1:1. The selection of solvent is important to produce smooth and bead-free nanofibers. The solvent for electrospinning

must be suitable to dissolve the polymers completely. Acetone and DMF were suitable for dissolving PVDF-HFP for electrospinning (Gizaw et al., 2018; Haider et al., 2018). Based on the SEM images, the average diameter of the nanofibers was decreased from $0.54\pm 0.05\ \mu\text{m}$ to $0.33\pm 0.06\ \mu\text{m}$ with the addition of PJ95 crude extract. There were several factors that could affect the size and morphology of nanofibers, including solution properties (concentration of polymer, solution viscosity, solution conductivity, surface tension, and solvent vapor pressure), the parameter for processing (distance between needle and collector, the flow rate of the polymer, and voltage), and ambient parameters (humidity and temperatures) (Ditaranto et al., 2018; Haider et al., 2018; Beachley and Wen, 2009). In the current study, the addition of PJ95 crude extract might decrease the solution viscosity. The decrease in solution viscosity resulted in less polymer unit per volume in the solution. In the end, the polymer chain tends to interact with the solvent, leading to a reduction in the chain entanglement among the polymer chains. The low viscosity of the polymer solution below the optimum concentration can cause the formation of droplets instead of fibers. In contrast, the high viscosity of the polymer solution causes the prohibition of the electrospinning process by the inability to maintain the flow of polymer solution to the tip of the needle (Deitzel et al., 2001; Haider et al., 2018; Sriyanti et al., 2018). This finding agreed with a previous study on the fabrication of PVDF-HFP electrospun by varying polymer concentrations from 15 to 10%. The viscosity of the polymer solution was decreased as polymers concentration decrease. Thus, the nanofiber's diameter was reduced from 500 to 100 nm, followed by the formation of beads caused by low viscosity (Lalia et al., 2013). Sriyanti et al. (2018) investigated the incorporation of various mangosteen pericarp extract (MPE) with PVP as a polymer. The nanofibers diameter decreased with an increase of MPE

concentration compared to the neat PVP nanofibers. On the other hand, Deitzel et al (2001) reported that the solution viscosity increase leads to increased fiber diameter.

The FTIR spectra of PVDF-HFP nanofibers show the α and β -phase of PVDF. This spectra profile was similar to the IR spectra of PVDF-HFP polymer reported by Priya and Suthanthiraraj (2013). In this study, the presence of IR spectra of α and β -phase were also detected on PJ95 crude extract loaded-PVDF-HFP nanofibers. Thus, according to the FTIR result indicated that the incorporation of crude extract did not affect the polymer structure. Two distinct IR spectra features of PJ95 crude extract corresponded to C-H and C=O stretching were also detected on the PJ95 crude extract-loaded PVDF-HFP nanofibers. This evidence proved that the crude extract was successfully loaded onto the PVDF-HFP nanofibers. The shifted peak of 1401 to 1399 that correspond to C-F stretching on the PJ95 crude extract-loaded PVDF-HFP nanofibers might occur because of incorporating crude extract into the nanofibers. Several characteristic peaks of crude extract were not detected in the PJ95 crude extract-loaded PVDF-HFP nanofibers, probably due to a small amount of the compound present in the nanofibers.

An optimal drug delivery system in wound dressing should release the antimicrobial agents in a selective and controlled way so that the wound follows the necessary healing process (Saghazadeh et al., 2019). The result of the crude extract release showed that rapid crude extract releases within 6 h after immersion. Later, the sustained release of the PJ95 crude extract continuously increased for 42 h of immersion. According to the obtained result, it was also known that the PJ95 crude extract can be maximally released from nanofiber until 42 h after immersion. The typical characteristic of polymeric electrospun nanofibers is the initial burst release,

leading to the distribution of drugs on the fiber surface (Gaharwar et al., 2014). The vancomycin initial burst release from the alginate/poly (ethylene oxide)/soy protein (SA/PEO/SPI) nanofibers was also observed after the first 4 h of immersion and followed by sustained release (Wongkanya et al., 2017). The release of the drug or antimicrobial agent from the electrospun nanofibers can be attributed to diffusion, polymer degradation, partitioning of the drug in polymers, and dissolution of the drug (Chou et al., 2015). In the current study, a diffusion is a possible option for crude extract release from the electrospun nanofibers. The controlled release of drugs from polymeric nanofibers can provide a suitable means of distributing the drug to the wound sites in a sustained manner for a long period without frequent dressing change. It might benefit to have reducing patient exposure to an excess of drugs at the wound site (Boateng et al., 2008; Saghazadeh et al., 2019).

The antimicrobial activity of PJ95-loaded PVDF-HFP electrospun nanofibers was also tested with several pathogenic bacteria that cause skin infection. In the current study demonstrated that the incorporation of PJ95 crude extract into the nanofibers inhibits *P. mirabilis* TISTR 100, *S. epidermidis* TISTR 518, *S. aureus* TISTR 1466, and MRSA DMST 20654 (Table 3.1). Chantasena and Nantapong (2016) reported that *Streptomyces* sp. PJ95 exhibit 99.8% similarity to *S. luteosporus* NBRC 14657^T and produced broad-spectrum antimicrobial agents which were active against several Gram-positive (*S. aureus* TISTR 1466, *Bacillus cereus* TISTR 687, *Bacillus subtilis* TISTR 008, *Staphylococcus epidermidis* TISTR 518, MRSA DMST 20654 and MRSA DMST 20651) and Gram-negative pathogenic bacteria (*Salmonella typhi* and *Proteus mirabilis* TISTR 100). Moreover, the *S. luteosporus* NBRC 14657^T known as a producer of thiolutin and indolmycin antibiotics (BacDive, 2019). Thiolutin is one of

the members of the pyrrothine class of natural antibiotics and act as inhibitors of DNA-dependent RNA polymerase (Olivia et al., 2001). On the other hand, indolmycin is an antibacterial drug that inhibits bacterial tryptophan-tRNA synthetase (Du et al., 2015). Therefore, the antimicrobial activity of PJ95 crude extract-loaded electrospun nanofibers might come from thiolutin and indolmycin. Thus, the PJ95 crude extract-loaded nanofibers offer roles for loading and releasing antimicrobial agents against skin infection pathogenic bacteria growth for wound dressing applications.

To simulate the condition of electrospun nanofibers application as wound dressing materials, the cytotoxicity evaluation was conducted using indirect cytotoxicity assay on the NIH-3T3 fibroblast cell lines. NIH-3T3 mouse fibroblast cell lines were chosen as tested cells for indirect cytotoxic activity because they play an essential role in wound healing process (Gurunathan et al., 2018). In the current study, the extracted medium from both electrospun nanofiber was toxic to the NIH-3T3 cell lines, indicated by the significant decrease of cell viability compared to the control. Although there was a decrease in the cells viability after cultured in the presence of media containing released crude extract, clearly, all the samples showed percentage of cell viability greater than 70%. According to ISO 10993-5:2009 about the biological evaluation of medical devices, the samples showing more than 70% in the relative cell viability were considered as biocompatible and non-toxic (Vatankhah, 2018). This acceptable value of cell viability percentage confirmed the negligible toxic potential of neat PVDF-HFP and PJ95 crude extract-loaded PVDF-HFP electrospun nanofibers.

The overall result of this study showed that the PJ95 crude extract-loaded PVDF-HFP was successfully fabricated using electrospinning. Additionally, PJ95 crude extract loaded into nanofibers could be sustained release over a period 42 h and provide

antimicrobial activity against *P. mirabilis* TISTR 100, *S. epidermidis* TISTR 518, *S. aureus* TISTR 1466, and MRSA DMST 20654. Therefore, the PJ95 crude extract-loaded PVDF-HFP nanofibers are a potential candidate for antimicrobial wound dressing.

3.6 References

- Álvarez-Paino, M., Muñoz-Bonilla, A., and Fernández-García, M. (2017). Antimicrobial polymers in the nano-world. **Nanomaterials**. 7(2): 1–44. <https://doi.org/10.3390/nano7020048>.
- BacDive. (2019). *Streptomyces luteosporus*. <https://doi.org/doi:10.13145/bacdive-16145.20191129.4.1>.
- Barka, E. A., Vatsa, P., Sanchez, L., Nathalie Gaveau-Vaillant, C. J., Klenk, H.-P., Clément, C., Ouhdouch, Y., and P. van Wezeld, G. (2016). Taxonomy, physiology and natural product of Actinobacteria. **American Society for Microbiology**. 80(1): 1–43. <https://doi.org/10.1128/MMBR.00019-15>.
- Beachley, V., and Wen, X. (2009). Effect of electrospinning parameters on the nanofiber diameter and length. **Materials Science and Engineering: C**. 29(3): 663–668. <https://doi.org/doi:10.1016/j.msec.2008.10.037>.
- Berdy, J. (2005). Bioactive microbial metabolites a personal view. **The Journal of Antibiotics**. 58(1): 1–26.
- Boateng, J. S., Matthews, K. H., Stevens, H. N. E., and Eccleston, G. M. (2008). Wound healing dressings and drug delivery systems: A review. **Journal of Pharmaceutical Sciences**. 97(8): 2892–2923. <https://doi.org/10.1002/jps.21210>.

- Chanhasena, P., and Nantapong, N. (2016). Biodiversity of antimicrobial-producing actinomycetes strains isolated from dry dipterocarp forest soil in Northeast Thailand. **Brazilian Archives of Biology and Technology**. 59(December): 1–11. <https://doi.org/10.1590/1678-4324-2016150674>.
- Chou, S., Carson, D., and Woodrow, K. (2015). Current strategies for sustaining drug release from electrospun nanofibers. **Journal of Controlled Release**. 28(Pt B): 584–591. <https://doi.org/10.1016/j.physbeh.2017.03.040>.
- Chou, S. F., and Woodrow, K. A. (2017). Relationships between mechanical properties and drug release from electrospun fibers of PCL and PLGA blends. **Journal of the Mechanical Behavior of Biomedical Materials**. 65: 724–733. <https://doi.org/10.1016/j.jmbbm.2016.09.004>.
- Deitzel, J., Kleinmeyer, J., Harris, D., and Beck Tan, N. (2001). Variability in the Ordovician acritarch *Dicrodiacrodium*. **Polymer**. 42: 261–272.
- Ditaranto, N., Basoli, F., Trombetta, M., Cioffi, N., and Rainer, A. (2018). Electrospun nanomaterials implementing antibacterial inorganic nanophases. **Applied Sciences**. 8(9). <https://doi.org/10.3390/app8091643>.
- Du, Y. L., Alkhalaf, L. M., and Ryan, K. S. (2015). In vitro reconstitution of indolmycin biosynthesis reveals the molecular basis of oxazolinone assembly. **Proceedings of the National Academy of Sciences of the United States of America**. 112(9): 2717–2722. <https://doi.org/10.1073/pnas.1419964112>.

- Fadhil, S., Marino, T., Makki, H. F., Alsally, Q. F., Blefari, S., Macedonio, F., Nicolò, E. Di, Giorno, L., Drioli, E., and Figoli, A. (2016). Novel PVDF-HFP flat sheet membranes prepared by triethyl phosphate (TEP) solvent for direct contact membrane distillation. **Chemical Engineering and Processing: Process Intensification**. 102: 16–26. <https://doi.org/10.1016/j.cep.2016.01.-007>.
- Fouda, M. M. G., El-Aassar, M. R., and Al-Deyab, S. S. (2013). Antimicrobial activity of carboxymethyl chitosan/polyethylene oxide nanofibers embedded silver nanoparticles. **Carbohydrate Polymers**. 92(2): 1012–1017. <https://doi.org/10.1016/j.carbpol.2012.10.047>.
- Gaharwar, A., Mihaila, S., Kulkarni, A., Patel, A., di Luca, A., Reis, R., Gomes, M., van Blitterswijk, C., Moroni, L., and Khademhosseini, A. (2014). Amphiphilic beads as depots for sustained drug release integrated into fibrillar scaffolds. **Journal of Controlled Release**. 187: 66–73. <https://doi.org/10.1016/j.jconrel.2014.04.035>.
- Gao, Y., Truong, Y. B., Zhu, Y., and Louis Kyratzis, I. (2014). Electrospun antibacterial nanofibers: Production, activity, and in vivo applications. **Journal of Applied Polymer Science**. 131(18): 9041–9053. <https://doi.org/10.1002/app.40797>.
- Gizaw, M., Thompson, J., Faglie, A., Lee, S. Y., Neuenschwander, P., and Chou, S. F. (2018). Electrospun fibers as a dressing material for drug and biological agent delivery in wound healing applications. **Bioengineering**. 5(1): 1–28. <https://doi.org/10.3390/bioengineering5010009>.

- Gurunathan, S., Qasim, M., Park, C., Yoo, H., Choi, D. Y., Song, H., Park, C., Kim, J. H., and Hong, K. (2018). Cytotoxicity and transcriptomic analysis of silver nanoparticles in mouse embryonic fibroblast cells. **International Journal of Molecular Sciences**. 19(11): 1–23. <https://doi.org/10.3390/ijms19113618>.
- Haider, A., Haider, S., and Kang, I. K. (2018). A comprehensive review summarizing the effect of electrospinning parameters and potential applications of nanofibers in biomedical and biotechnology. **Arabian Journal of Chemistry**. 11(8): 1165–1188. <https://doi.org/10.1016/j.arabjc.2015.11.015>.
- J, Y., Geng, J., Xing, Z., Shen, J., Kang, L., and Byun, H. (2010). Electrospinning of antibacterial Poly(vinylidene fluoride) nanofibers containing silver nanoparticles. **Journal of Applied Polymer Science**. 116(5): 668–672. <https://doi.org/DOI 10.1002/app.31632>.
- Jensen, J., and Proksch, E. (2009). The skin's barrier. **G Ital Dermatol Venerol**. 144(6): 689–700.
- Khan, A. R., Nadeem, M., Aqeel Bhutto, M., Yu, F., Xie, X., El-Hamshary, H., El-Faham, A., Ibrahim, U. A., and Mo, X. (2019). Physico-chemical and biological evaluation of PLCL/SF nanofibers loaded with oregano essential oil. **Pharmaceutics**. 11(8). <https://doi.org/10.3390/pharmaceutics11080386>.
- Khan, A. R., Xiangyang, S., Ahmad, A., and Mo, X. (2018). Electrospinning of crude plant extracts for antibacterial and wound healing applications: A Review. **SM J Biomed Eng**. 4(1): 1–8.
- Kurečić, M. (2013). Electrospinning : Nanofibre Production Method. **Tekstilec**. 56(1): 4–12.

- Lalia, B. S., Guillen-Burrieza, E., Arafat, H. A., and Hashaikeh, R. (2013). Fabrication and characterization of polyvinylidene fluoride-co-hexafluoropropylene (PVDF-HFP) electrospun membranes for direct contact membrane distillation. **Journal of Membrane Science**. 428(May): 104–115. <https://doi.org/10.1016/j.memsci.2012.10.061>.
- Mahajan, G., and Balachandran, L. (2015). Biodiversity in production of antibiotics and other bioactive compounds. **Advances in Biochemical Engineering /Biotechnology**. https://doi.org/10.1007/10_2014_268.
- Martins, A., Reis, R. L., and Neves, N. M. (2008). Electrospinning: Processing technique for tissue engineering scaffolding. **International Materials Reviews**. 53(5): 257–274. <https://doi.org/10.1179/174328008X353547>.
- Mohammadi, Z., Sharif Zak, M., Majdi, H., Mostafavi, E., Barati, M., Lotfimehr, H., Ghaseminasab, K., Pazoki-Toroudi, H., Webster, T. J., and Akbarzadeh, A. (2019). The effect of chrysin–curcumin-loaded nanofibres on the wound-healing process in male rats. **Artificial Cells, Nanomedicine and Biotechnology**. 47(1): 1642–1652. <https://doi.org/10.1080/21691401.2019.1594855>.
- Motealleh, B., Zahedi, P., Rezaeian, I., Moghimi, M., Abdolghaffari, A. H., and Zarandi, M. A. (2014). Morphology, drug release, antibacterial, cell proliferation, and histology studies of chamomile-loaded wound dressing mats based on electrospun nanofibrous poly(ϵ -caprolactone)/polystyrene blends. **Journal of Biomedical Materials Research - Part B Applied Biomaterials**. 102(5): 977–987. <https://doi.org/10.1002/jbm.b.33078>.

- Oliva, B., O'Neill, A., Wilson, J. M., O'Hanlon, P. J., and Chopra, I. (2001). Antimicrobial properties and mode of action of the pyrrothine holomycin. **Antimicrobial Agents and Chemotherapy**. 45(2): 532–539. <https://doi.org/10.1128/AAC.45.2.532-539.2001>.
- Pisani, S., Dorati, R., Chiesa, E., Genta, I., Modena, T., Bruni, G., Grisoli, P., and Conti, B. (2019). Release profile of gentamicin sulfate from polylactide-co-polycaprolactone electrospun nanofiber matrices. **Pharmaceutics**. 11(4). <https://doi.org/10.3390/pharmaceutics11040161>.
- Priya, W. M., and Suthanthiraraj, S. A. (2013). Electrochemical and FTIR studies of PVDF-HFP/(CF₃SO₃)₂Zn/Fe₂O₃ composite polymer electrolytes. **International Journal of Innovative Research in Science and Engineering**. ISSN (Online): 2347–3207. [http://ijirse.in/docs/ican14/ican42.pdf#search=%22Fe2O3 nanoparticles%22](http://ijirse.in/docs/ican14/ican42.pdf#search=%22Fe2O3%20nanoparticles%22).
- Ramakrishna, S., Fujihara, K., Teo, W. E., Yong, T., Ma, Z., and Ramaseshan, R. (2006). Electrospun nanofibers: Solving global issues. **Materials Today**. 9(3): 40–50. [https://doi.org/10.1016/S1369-7021\(06\)71389-X](https://doi.org/10.1016/S1369-7021(06)71389-X).
- Saghazadeh, S., Rinoldi, C., Schot, M., Kashaf, S. S., Derakhshandeh, H., Yue, K., and Swieszkowski, W. (2019). **HHS Public Access**. 402: 138–166. <https://doi.org/10.1016/j.addr.2018.04.008Drug>.
- Singleton, P. (2004). *Bacteria in biology, biotechnology and medicine* (6th edition). John Wiley.

- Song, K., Wu, Q., Qi, Y., and Kärki, T. (2017). Electrospun nanofibers with antimicrobial properties. In M. Afshari (Ed.), *Electrospun Nanofibers* (pp. 551–569). Woodheads Publishing. <https://doi.org/10.1016/B978-0-08-100907-9.00020-9>.
- Sripreechasak, P., Suwanborirux, K., and Tanasupawat, S. (2014). Characterization and antimicrobial activity of *Streptomyces* strains from soils in southern Thailand. **Journal of Applied Pharmaceutical Science**. 4(10): 24–31. <https://doi.org/10.7324/JAPS.2014.40105>.
- Sriyanti, I., Edikresnha, D., Rahma, A., Munir, M. M., Rachmawati, H., and Khairurrijal, K. (2018). Mangosteen pericarp extract embedded in electrospun PVP nanofiber mats: Physicochemical properties and release mechanism of α -mangostin. **International Journal of Nanomedicine**. 13: 4927–4941. <https://doi.org/10.2147/IJN.S167670>.
- Sundaramurthi, D., and Sethuraman, S. (2014). Electrospun nanofibers as scaffolds for skin tissue engineering. **Polymer Reviews**. 54(2): 348–376. <https://doi.org/10.1080/15583724.2014.881374>.
- Thongkrachang, N., Chanama, S., and Chanama, M. (2016). Inhibitory activity against pathogenic bacteria of *Streptomyces* isolated from natural soil resources. **Journal of Public Health and Development**. 14(3): 59–68.
- Unalan, I., Slavik, B., Buettner, A., Goldmann, W. H., Frank, G., and Boccaccini, A. R. (2019). Physical and Antibacterial Properties of Peppermint Essential Oil Loaded Poly (ϵ -caprolactone) (PCL) Electrospun Fiber Mats for Wound Healing. **Frontiers in Bioengineering and Biotechnology**. 7(November): 1–11. <https://doi.org/10.3389/fbioe.2019.00346>.

- Vatankhah, E. (2018). Rosmarinic acid-loaded electrospun nanofibers: In vitro release kinetic study and bioactivity assessment. **Engineering in Life Sciences**. 18(10): 732–742. <https://doi.org/10.1002/elsc.201800046>.
- Wang, X., Xiao, C., Liu, H., Huang, Q., Hao, J., and Fu, H. (2018). Poly(vinylidene fluoride-hexafluoropropylene) porous membrane with controllable structure and applications in efficient oil/water separation. **Materials**. 11(3). <https://doi.org/10.3390/ma11030443>.
- Wongkanya, R., Chuysinuan, P., Pengsuk, C., Techasakul, S., Lirdprapamongkol, K., Svasti, J., and Nooeaid, P. (2017). Electrospinning of alginate/soy protein isolated nanofibers and their release characteristics for biomedical applications. **Journal of Science: Advanced Materials and Devices**. 2(3): 309–316. <https://doi.org/10.1016/j.jsamd.2017.05.010>.
- Xu, X., Yang, Q., Wang, Y., Yu, H., Chen, X., and Jing, X. (2006). Biodegradable electrospun poly(l-lactide) fibers containing antibacterial silver nanoparticles. **European Polymer Journal**. 42(9): 2081–2087. <https://doi.org/10.1016/j.eurpolymj.2006.03.032>.
- Xue, J., Xie, J., Liu, W., and Xia, Y. (2017). Electrospun Nanofibers: New Concepts, Materials, and Applications. **Accounts of Chemical Research**. 50(8): 1976–1987. <https://doi.org/10.1021/acs.accounts.7b00218>.

CHAPTER IV

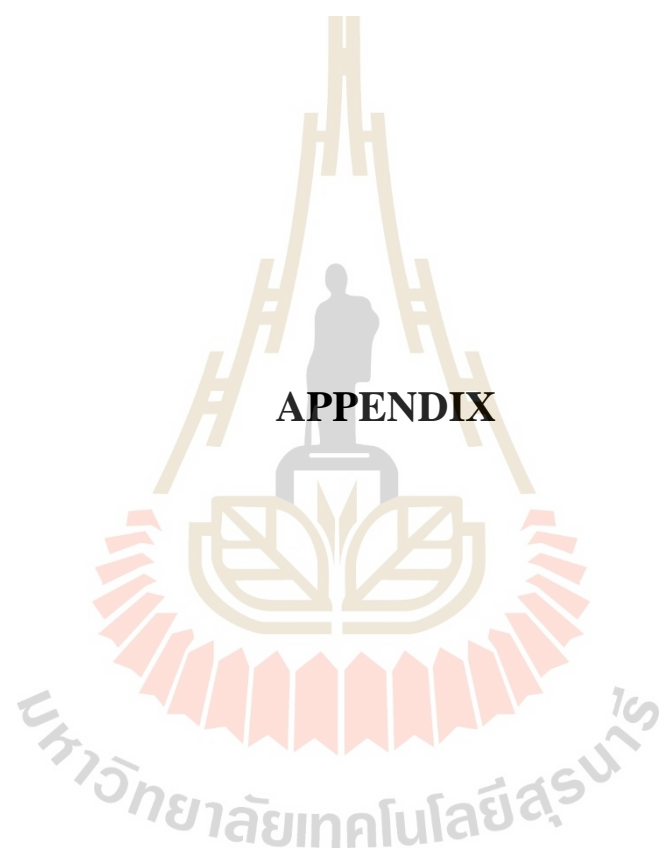
CONCLUSION

As a result of this research, the soil sample *Streptomyces* sp. SSUT88A was isolated from Sekaerat Research Environment Station, Thailand, and identified based on the 16s rRNA gene sequence. This isolate revealed high similarity to *Streptomyces chiangmaiensis* TA4-1^T. The *Streptomyces* sp. SSUT88A was used to synthesize AgNPs using intracellular and extracellular cell-free supernatant. The IS-AgNPs show a spherical shape with a diameter of 13,57 nm based on TEM observation. While the ES-AgNPs show a spherical shape with a diameter of 30,47 nm. Based on XANES and XRD study, the synthesized AgNPs are in the form of Ag⁰. The synthesized AgNPs provide different antimicrobial activity. The IS-AgNPs showed antimicrobial against all clinical isolate pathogens, while the ES-AgNPs only showed antimicrobial activity against MRSA DMST 20654. However, the IS-AgNPs exhibit high toxicity to NIH-3T3 cell lines than ES-AgNPs. Hence, the application of IS-AgNPs as antimicrobial agents needs to be careful, especially related to its cytotoxicity.

The *Streptomyces* sp. PJ95 was used to fabricate PVDF-HFP electrospun nanofibers via the electrospinning method. The crude extract of PJ95 and PVDF-HFP polymer was spin under 15 kV and distance 10 cm from the needle to the collector. The electrospun nanofiber's morphology is smooth and bead-free. The diameter of PVDF-HFP and PJ95 crude extract-loaded PVDF-HFP nanofibers are 0.54±0.05 μm and 0.33±0.06 μm, respectively. PJ95 crude extract-loaded PVDF-HFP nanofibers show

antimicrobial activity against skin infection pathogens *S. aureus* TISTR 1466, *S. epidermidis* TISTR 518, MRSA DMST 20654, and *P. mirabilis* TISTR 100. The indirect cytotoxicity analysis revealed that PJ95 crude extract-loaded PVDF-HFP nanofibers was considered as biocompatible and non-toxic. Therefore, PJ95 crude extract-loaded PVDF-HFP nanofibers are a potential candidate for wound dressing application.





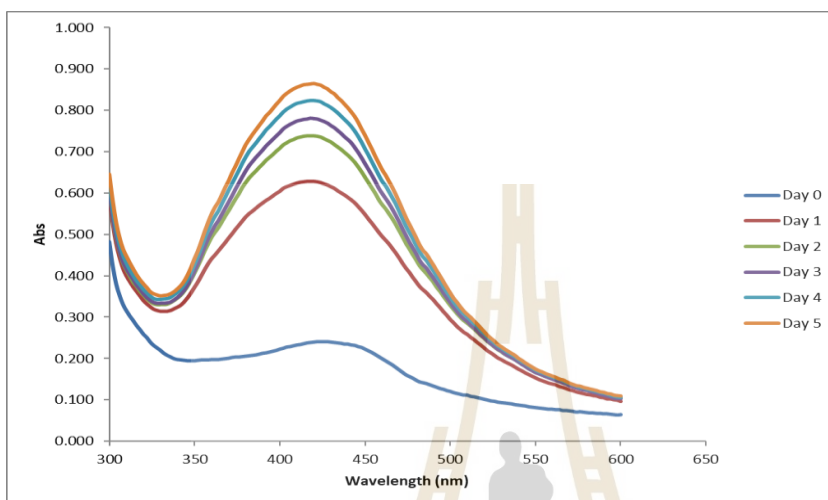
APPENDIX

ANTIMICROBIAL ACTIVITY OF SSUT88A BY PERPENDICULAR CROSS STREAK METHOD

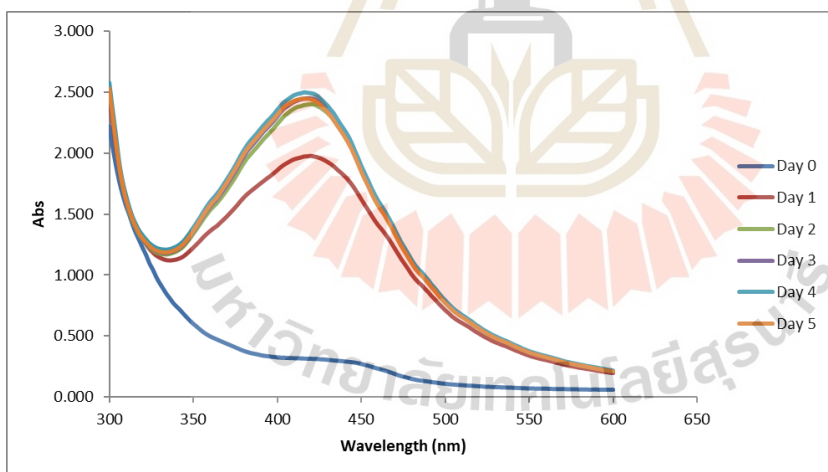
Test Pathogen	Inhibition zone (mm)
	<i>Streptomyces</i> sp. SSUT88A
<i>MDR A. baumannii</i>	8
<i>K. pneumoniae</i> 1617	0
<i>P. aeruginosa</i> N90PS	0
<i>E. coli</i> 8465	0
<i>S. aureus</i> ATCC29213	23
<i>S. aureus</i> TISTR1466	23
MRSA DMST20654	23
MRSA DMST20651	>30
<i>B. cereus</i> TISTR687	>30
<i>B. subtilis</i> TISTR008	>30
<i>S. epidermidis</i> TISTR518	>30
<i>S. typhi</i>	0
<i>P. mirabilis</i> TISTR100	0
<i>E. coli</i> TISTR 781	0

UV-VIS SPECTROSCOPY OF SYNTHESIZED AgNPs

Intracellular cell-free supernatant



Extracellular cell-free supernatant



CLINICAL ISOLATED PATHOGEN INFORMATION

Strains	Source	Susceptible	Drug resistant
<i>K. pneumoniae</i> (1617)	Sputum	Gentamycin	Ampicillin
			Amikacin
			Amoxicillin-Clavulanate
			Piperacillin-Tazabactam
			Cefoxitin
			Cefazolin
			Ceftriaxone
			Ceftazidime
			Cefepime
			Trimetroprim-Sulfamethoxazole
			Ciprofloxacin
			Levofloxacin
			Imipenem
			Ertapenem
Meropenem			
<i>E. coli</i> (8465)	Urine	Amikacin	Ampicillin
			Amoxicillin-Clavulanate
			Gentamycin
			Cefazolin
			Ceftriaxone

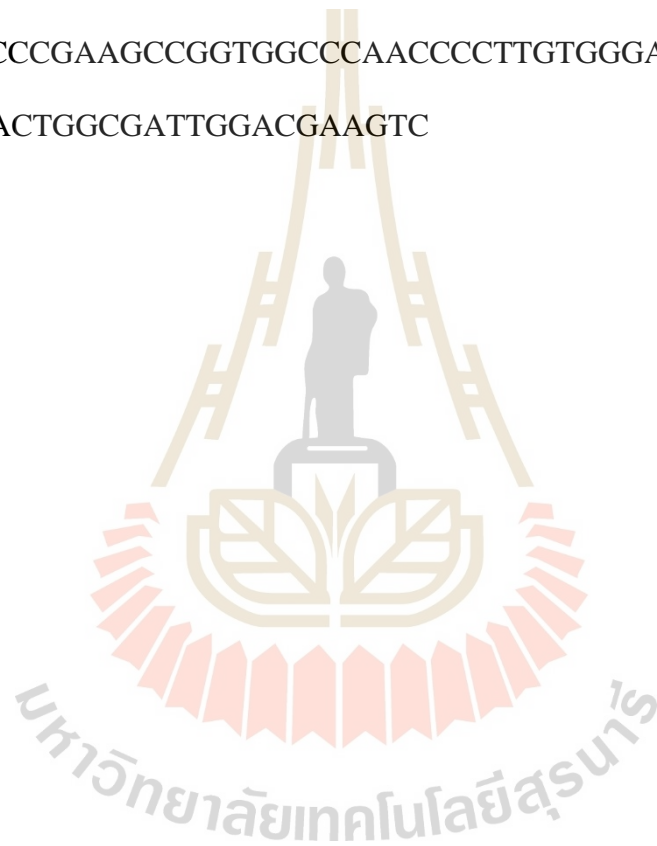
Strains	Source	Susceptible	Drug resistant
		Piperacillin- Tazabactam Cefoxitin Ceftazidime Imipenem Ertapenem Meropenem	Ciprofloxacin Levofloxacin Trimetroprim- Sulfamethoxazole
<i>A. baumannii</i> (MDR)	Sputum	Colistin (MIC=2.0)	Ampicillin-Sulbactam Piperacillin-Tazabactam Ceftazidime Ceftriaxone Cefepime Imipenem Meropenem Trimetroprim- Sulfamethoxazole Gentamycin Amikacin Ciprofloxacin Levofloxacin

SEQUENCES OF SOIL ISOLATED STREPTOMYCES

Streptomyces sp. SSUT88A

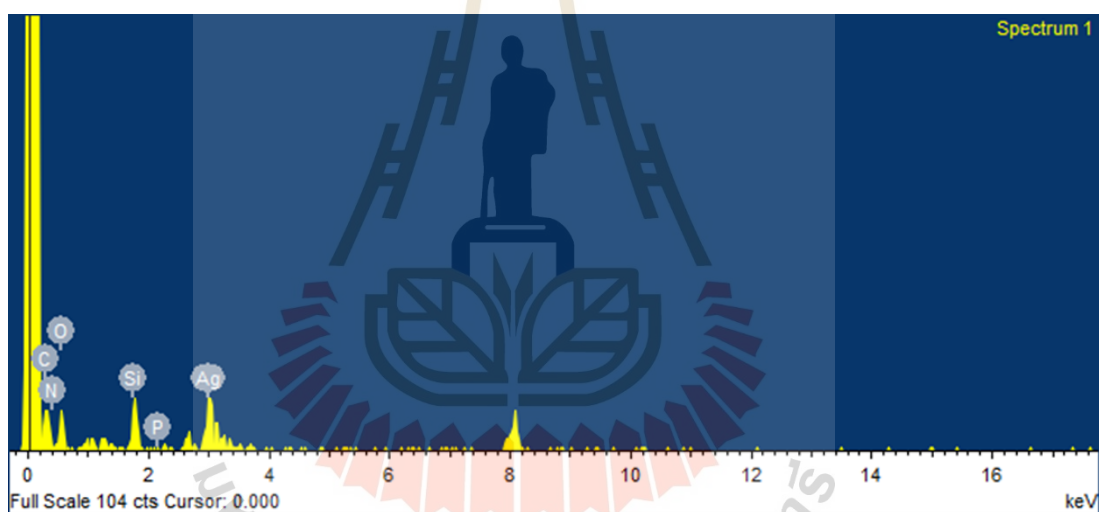
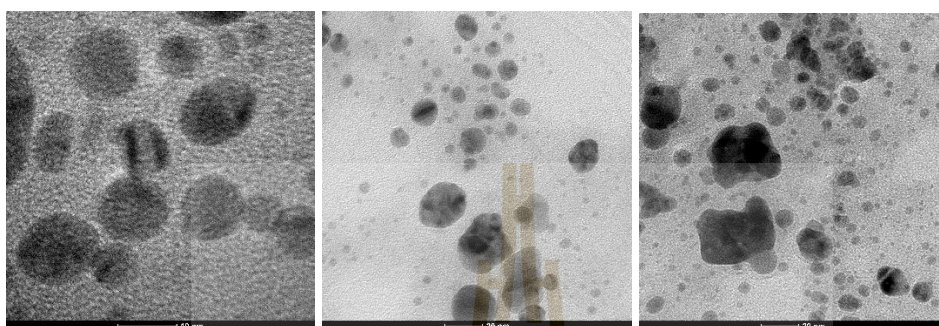
TGCAGTCGAACGATGAAGCCCTTCGGGGTGGATTAGTGGCGAACGGGTGA
GTAACACGTGGGCAATCTGCCCTGCACTCTGGGACAAGCCCTGGAAACGG
GGTCTAATACCGGATACGAGCCTCCGAGGCATCTTGGGGGTGGAAAGCT
CCGGCGGTGCAGGATGAGCCCGCGGCCTATCAGCTTGTTGGTGAGGTAAT
GGCTACCAAGGCGACGACGGGTAGCCGGCCTGAGAGGGCGACCGGCCA
CACTGGGACTGAGACACGGCCCAGACTCCTACGGGAGGCAGCAGTGGGG
AATATTGCACAATGGGCGCAAGCCTGATGCAGCGACGCCGCGTGAGGGAT
GACGGCCTTCGGGTGTAAACCTCTTTCAGCAGGGAAGAAGCGCAAGTGA
CGGTACCTGCAGAAGAAGCGCCGGCTAACTACGTGCCAGCAGCCGCGGTA
ATACGTAGGGCGCAAGCGTTGTCCGGAATTATTGGGCGTAAAGAGCTCGT
AGGCGGCTTGTCGCGTCGGTTGTGAAAGCCCAGGGCTTAACTCCGGGTCT
GCAGTCGATACGGGCAGGCTAGAGTTCGGTAGGGGAGATCGGAATTCCTG
GTGTAGCGGTGAAATGCGCAGATATCAGGAGGAACACCGGTGGCGAAGG
CGGATCTCTGGGCCGATACTGACGCTGAGGAGCGAAAGCGTGGGGAGCG
AACAGGATTAGATACCCTGGTAGTCCACGCCGTAAACGGTGGGCACTAGG
TGTGGGCAGCATTCCACGTTGTCCGTGCCGAGCTAACGCATTAAGTGCC
CCGCCTGGGGAGTACGGCCGCAAGGCTAAAACTCAAAGGAATTGACGGG
GGCCCGCACAAGCGGCGGAGCATGTGGCTTAATTCGACGCAACGCGAAG
AACCTTACCAAGGCTTGACATACGCCGAAACATCCAGAGATGGGTGCCC
CCTTGTGGTCGGTGTACAGGTGGTGCATGGCTGTCGTCAGCTCGTGTCTGTG
AGATGTTGGGTAAAGTCCCGCAACGAGCGCAACCCTTGTCCCGTGTGGCC

AGCAGGCCCTTGTGGTGCTGGGGACTCACGGGAGACCGCCGGGGTCAACT
CGGAGGAAGGTGGGGACGACGTCAAGTCATCATGCCCTTATGTCTTGGG
CTGCACACGTGCTACAATGGCCGGTACAATGAGCTGCGATGCCGTGAGGT
GGAGCGAATCTCAAAAAGCCGGTCTCAGTTCGGATTGGGGTCTGCAACTC
GACCCCATGAAGTCGGAGTCGCTAGTAATCGCAGATCAGCAGTGCTGCGG
TGAATACGTTCCCGGGCCTTGTACACACCGCCCGTCACGTCACGAAAGTC
GGTAACACCCGAAGCCGGTGGCCCAACCCCTTGTGGGAGGGAGCTGTCGA
AGGTGGGACTGGCGATTGGACGAAGTC



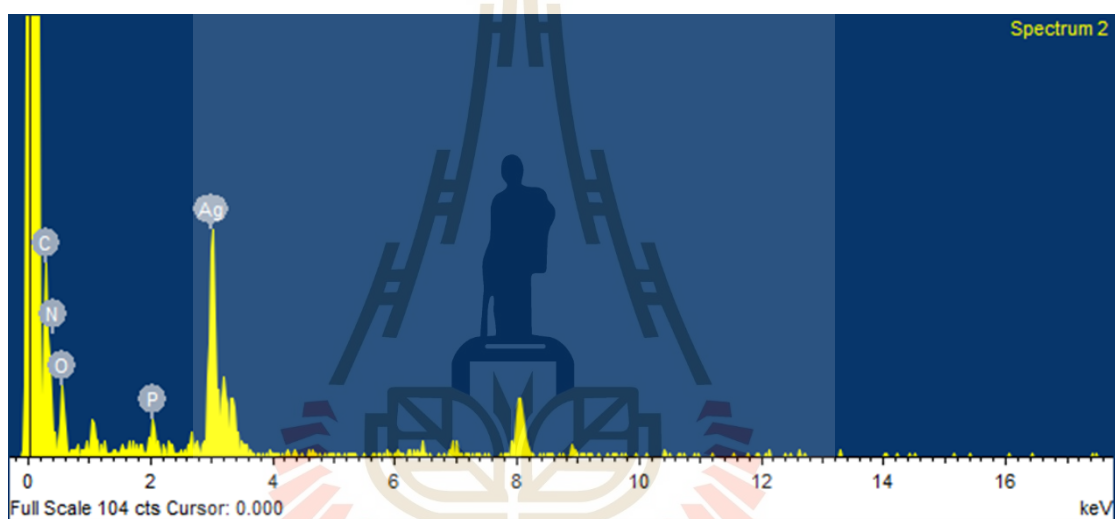
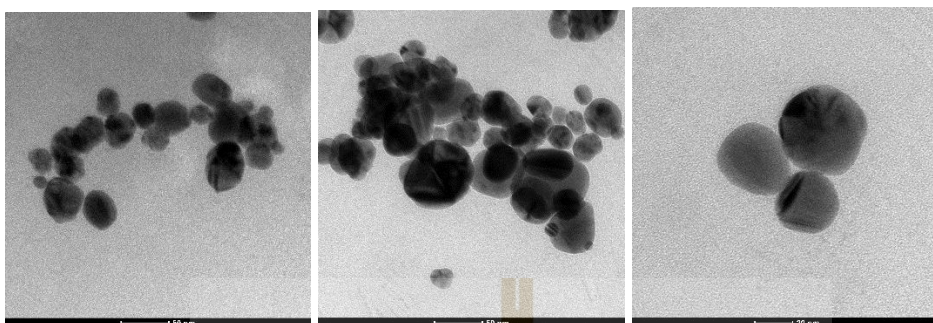
TEM IMAGE AND EDXRF OF SYNTHESIZED AgNPs

Intracellular AgNPs



Element	Weight%	Atomic%
C K	38.74	54.44
N K	21.17	25.51
O K	12.60	13.29
Si K	5.30	3.19
P K	0.25	0.14
Ag L	21.93	3.43
Totals	100.00	

Extracellular AgNPs



Element	Weight%	Atomic%
C K	28.19	54.95
N K	13.19	22.05
O K	7.27	10.64
P K	2.25	1.70
Ag L	49.09	10.66
Totals	100.00	

XRD RESULT OF SYNTHESIZED AgNPs

Intracellular AgNPs

Pattern: PDF 00-004-0783 Radiation: 1.54060 Quality: Indexed

Formula Ag Name Silver Name (mineral) Silver-3C, syn Name (common)		<table border="1"> <thead> <tr> <th>d</th> <th>2θ</th> <th>I fix</th> <th>h</th> <th>k</th> <th>l</th> </tr> </thead> <tbody> <tr><td>2.35900</td><td>38.117</td><td>100</td><td>1</td><td>1</td><td>1</td></tr> <tr><td>2.04400</td><td>44.278</td><td>40</td><td>2</td><td>0</td><td>0</td></tr> <tr><td>1.44500</td><td>64.427</td><td>25</td><td>2</td><td>2</td><td>0</td></tr> <tr><td>1.23100</td><td>77.475</td><td>26</td><td>3</td><td>1</td><td>1</td></tr> <tr><td>1.17960</td><td>81.539</td><td>12</td><td>2</td><td>2</td><td>2</td></tr> <tr><td>1.02150</td><td>97.891</td><td>4</td><td>4</td><td>0</td><td>0</td></tr> <tr><td>0.93750</td><td>110.501</td><td>16</td><td>3</td><td>3</td><td>1</td></tr> <tr><td>0.91370</td><td>114.928</td><td>12</td><td>4</td><td>2</td><td>0</td></tr> <tr><td>0.83410</td><td>134.889</td><td>13</td><td>4</td><td>2</td><td>2</td></tr> </tbody> </table>						d	2 θ	I fix	h	k	l	2.35900	38.117	100	1	1	1	2.04400	44.278	40	2	0	0	1.44500	64.427	25	2	2	0	1.23100	77.475	26	3	1	1	1.17960	81.539	12	2	2	2	1.02150	97.891	4	4	0	0	0.93750	110.501	16	3	3	1	0.91370	114.928	12	4	2	0	0.83410	134.889	13	4	2	2
d	2 θ	I fix	h	k	l																																																														
2.35900	38.117	100	1	1	1																																																														
2.04400	44.278	40	2	0	0																																																														
1.44500	64.427	25	2	2	0																																																														
1.23100	77.475	26	3	1	1																																																														
1.17960	81.539	12	2	2	2																																																														
1.02150	97.891	4	4	0	0																																																														
0.93750	110.501	16	3	3	1																																																														
0.91370	114.928	12	4	2	0																																																														
0.83410	134.889	13	4	2	2																																																														
Lattice: Cubic S.G.: Fm-3m (225)	Mol. weight = 107.87 Volume [CD] = 68.23 Dx = Dm = 10.5 l/lor = -1.000																																																																		
a = 4.08620 a/b = 1.00000 c/b = 1.00000	Z = 4																																																																		
Additional Patterns: See PDF 01-087-0597 Analysis: Spectrographic analysis indicated faint traces of Ca, Fe and Cu Color: Light gray metallic General Comments: Purity >99.999% Melting Point: 1233.6 K Opaque Optical Data: Opaque mineral optical data on specimen from Great Bear Lake, Canada: RR2Re=94.1, Disp.=16, VHN100=55-63, Color values .314, .321, 94.2, Ref : IMA Commission on Ore Microscopy QDF Sample Source or Locality: Sample obtained from Johnson Matthey Company, Ltd Temperature of Data Collection: Pattern taken at 300 K Unit Cell Data Source: Powder Diffraction																																																																			
Primary Reference Publication: Natl. Bur. Stand. (U. S.), Circ. 539 Detail: volume I, page 23 (1953) Authors: Swanson, Tatge.																																																																			
Radiation: CuK α 1 Wavelength : 1.54060 SS/FOM: 64.8 (0.0154,9)	Filter: F d-spacing:																																																																		

Extracellular AgNPs

Pattern: PDF 04-0783 Radiation: 1.54060 Quality: Indexed

Formula Ag		d	2θ	I fix	h	k	l
Name Silver		2.35900	38.117	100	1	1	1
Name (mineral) Silver-3C, syn		2.04400	44.278	41	2	0	0
Name (common)		1.44500	64.427	25	2	2	0
		1.23100	77.475	26	3	1	1
		1.17960	81.539	12	2	2	2
		1.02150	97.891	4	4	0	0
Lattice: Cubic		0.93750	110.501	15	3	3	1
S.G.: Fm-3m (225)		0.91370	114.928	12	4	2	0
Mol. weight = 107.87		0.83410	134.889	13	4	2	2
Volume [CD] = 68.23							
Dx =							
Dm = 10.5							
I/lor = 5.200							
a = 4.08620	Z = 4						
a/b = 1.00000							
c/b = 1.00000							
<p>Color: Light gray metallic Additional Pattern: See ICSD 64706 (PDF 01-087-0597) Sample Source Or Locality: Sample obtained from Johnson Matthey Company, Ltd General Comments: Purity >99.999% Analysis: Spectrographic analysis indicated faint traces of Ca, Fe and Cu Temperature Of Data Collection: Pattern taken at 27 C Optical Data: B=0.181 Melting Point: 960.6° General Comments: Opaque mineral optical data on specimen from Great Bear Lake, Canada: RR#2R#e=94.1, Disp.=16, VHN#1#0#0=55-63, Color values .314, .321, 94.2, Ref : IMA Commission on Ore Microscopy QDF</p>							
<p>Primary Reference Publication: Natl. Bur. Stand. (U.S.), Circ. 539 Detail: volume I, page 23 (1953) Authors: Swanson, Tatge.</p>							
Radiation: CuK α 1		Filter: F					
Wavelength : 1.54060		d-spacing:					
SS/FOM: 64.7 (0.0154,9)							

ZETA SIZER RESULT OF SYNTHESIZED AgNPs

The size distribution of intracellular AgNPs

Sample Details

Sample Name: intracellular AgNP 1

SOP Name: AgNP.sop

General Notes:

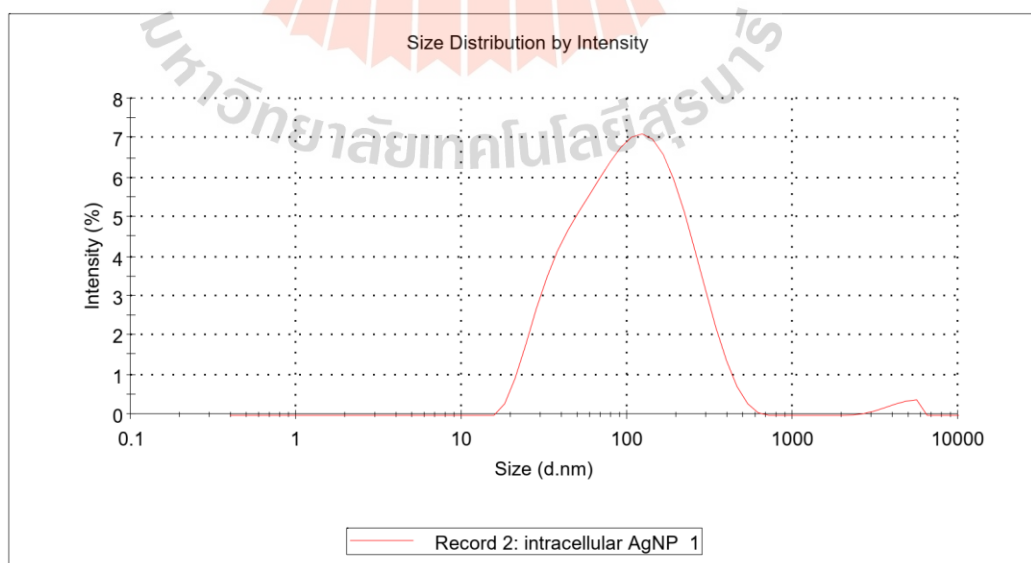
File Name: Aliya.dts	Dispersant Name: Water
Record Number: 2	Dispersant RI: 1.330
Material RI: 0.14	Viscosity (cP): 0.8872
Material Absorbtion: 0.000	Measurement Date and Time: Wednesday, August 26, 2020...

System

Temperature (°C): 25.0	Duration Used (s): 60
Count Rate (kcps): 237.1	Measurement Position (mm): 4.65
Cell Description: Low volume disposable sizing ...	Attenuator: 8

Results

	Size (d.nm):	% Intensity	Width (d.nm):
Z-Average (d.nm): 77.03	Peak 1: 126.9	98.6	92.30
PdI: 0.413	Peak 2: 4491	1.4	882.9
Intercept: 0.931	Peak 3: 0.000	0.0	0.000
Result quality : Good			



The size distribution of Extracellular AgNPs

Sample Details

Sample Name: extracellular AgNP 1

SOP Name: AgNP.sop

General Notes:

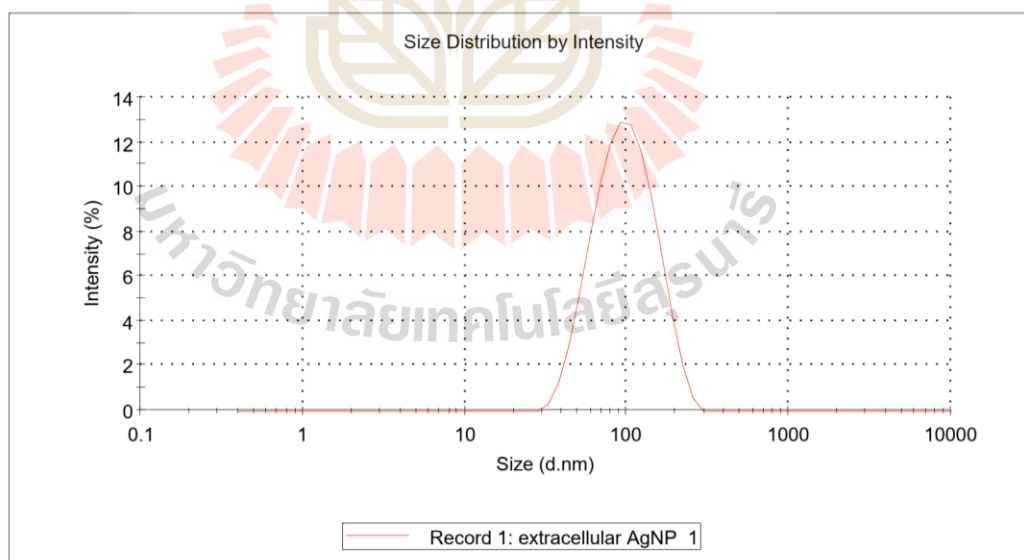
File Name:	Aliya.dts	Dispersant Name:	Water
Record Number:	1	Dispersant RI:	1.330
Material RI:	0.14	Viscosity (cP):	0.8872
Material Absorbtion:	0.000	Measurement Date and Time:	Wednesday, August 26, 2020...

System

Temperature (°C):	25.0	Duration Used (s):	60
Count Rate (kcps):	446.1	Measurement Position (mm):	4.65
Cell Description:	Low volume disposable sizing ...	Attenuator:	7

Results

	Size (d.nm):	% Intensity	Width (d.nm):
Z-Average (d.nm): 82.44	Peak 1: 103.8	100.0	43.24
Pdl: 0.196	Peak 2: 0.000	0.0	0.000
Intercept: 0.831	Peak 3: 0.000	0.0	0.000
Result quality: Good			



Zeta potential of intracellular AgNPs

Sample Details

Sample Name: intracellular AgNP 1

SOP Name: AgNP.sop

General Notes:

File Name: Aliya.dts Dispersant Name: Water
 Record Number: 3 Dispersant RI: 1.330
 Date and Time: Wednesday, August 26, 2020 10:... Viscosity (cP): 0.8872
 Dispersant Dielectric Constant: 78.5

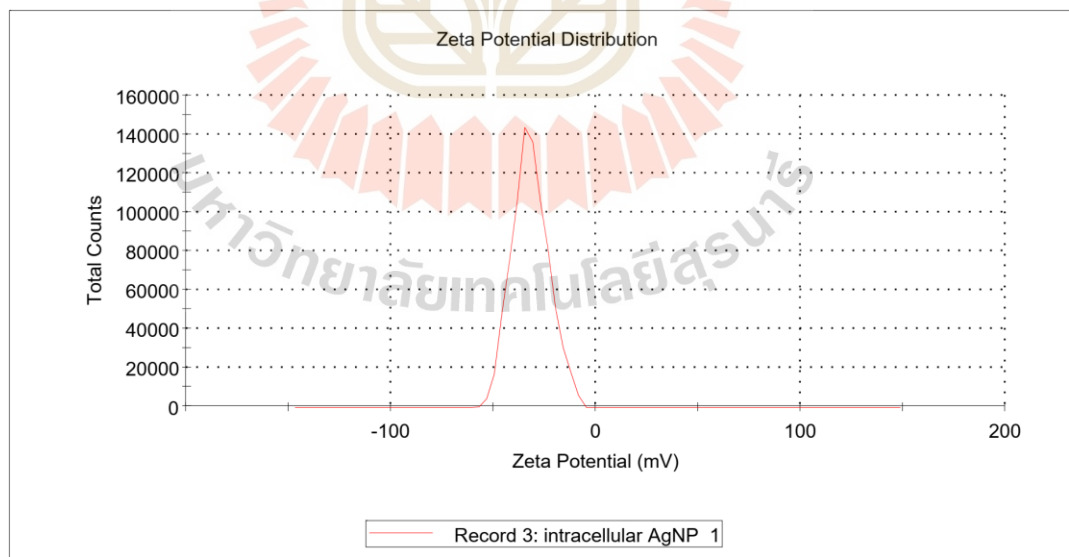
System

Temperature (°C): 25.0 Zeta Runs: 12
 Count Rate (kcps): 48.1 Measurement Position (mm): 2.00
 Cell Description: Clear disposable zeta cell Attenuator: 10

Results

	Mean (mV)	Area (%)	Width (mV)
Zeta Potential (mV): -32.0	Peak 1: -32.0	100.0	8.85
Zeta Deviation (mV): 8.85	Peak 2: 0.00	0.0	0.00
Conductivity (mS/cm): 0.0643	Peak 3: 0.00	0.0	0.00

Result quality : **Good**



Zeta potential of extracellular AgNPs

Sample Details

Sample Name: extracellular AgNP 1

SOP Name: AgNP.sop

General Notes:

File Name: Aliya.dts	Dispersant Name: Water
Record Number: 6	Dispersant RI: 1.330
Date and Time: Wednesday, August 26, 2020 10:...	Viscosity (cP): 0.8872
	Dispersant Dielectric Constant: 78.5

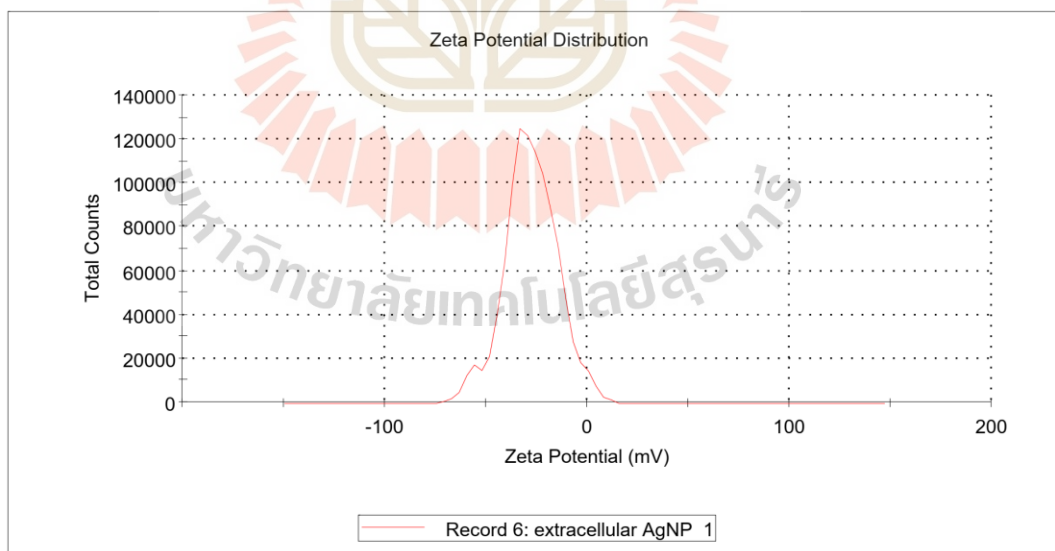
System

Temperature (°C): 25.0	Zeta Runs: 12
Count Rate (kcps): 95.3	Measurement Position (mm): 2.00
Cell Description: Clear disposable zeta cell	Attenuator: 10

Results

	Mean (mV)	Area (%)	Width (mV)
Zeta Potential (mV): -27.9	Peak 1: -26.7	94.9	11.9
Zeta Deviation (mV): 13.2	Peak 2: -57.1	5.1	4.47
Conductivity (mS/cm): 0.149	Peak 3: 0.00	0.0	0.00

Result quality : **See result quality report**



PREPARATION OF MEDIA AND REAGENTS

1. International *Streptomyces* Project 2 (ISP2) medium

Yeast extract	4 g
Malt extract	10 g
D-glucose	4 g
Agar	15 g
H ₂ O	1000 mL

2. 1 mM AgNO₃ solution

AgNO ₃ powder	0.017 g
H ₂ O	100 mL

3. Lysis buffer

1 mM Tris-HCl pH 8	40 mL
0,5 M EDTA	12 mL
5M NaCl	3 mL
10% SDS	10 mL
H ₂ O	35 mL

4. TBE buffer 10x

Tris base	108 g
Boric acid	55 g
EDTA	7.5 g
H ₂ O	up to 1000 mL

5. TE buffer

1M Tris-HCl	1 mL
0,5M EDTA	0.02 mL
H ₂ O	989.8 mL

6. PBS 1x

NaCl	8 g
KCl	0.20 g
Na ₂ HPO ₄	1.44 g
KH ₂ PO ₄	0.24 g
H ₂ O	up to 1000 mL

7. MTT Solution

MTT powder	2.50 mg
H ₂ O	5 mL

CURRICULUM VITAE

Name : Aliyatur Rosyidah

Date of Birth : August 17, 1990

Place of Birth : Malang, Indonesia

Education :

1. Bachelor's degree in Biology, Brawijaya University, Indonesia. May 28, 2012.
2. Master's degree in Biology, Brawijaya University, Indonesia. July 31, 2013.

Publications : -

Awards : -

Grant and Fellowships :

1. I-MHERE Student Grant from Ministry of Higher Education of Indonesia, 2010.
2. Fast track scholarship program for Master of Biology from Ministry of Higher Education of Indonesia, 2011.
3. SUT-Ph.D Scholarship for ASEAN.

Position and Place for Work : Junior Researcher, Indonesian Institute of Sciences (LIPI), Indonesia.